THE EFFECTS OF GRAIN SPHERICITY AND ROUNDNESS ON CRITICAL STATE PARAMETERS

A THESIS SUBMITTED TO
THE GRADUATE SCHOOL OF NATURAL AND APPLIED SCIENCES
OF
MIDDLE EAST TECHNICAL UNIVERSITY

BY

AHMET SEYİT AKSOY

IN PARTIAL FULFILLMENT OF THE REQUIREMENTS
FOR
THE DEGREE OF MASTER OF SCIENCE
IN
CIVIL ENGINEERING

SEPTEMBER 2024

Approval of the thesis:

THE EFFECTS OF GRAIN SPHERICITY AND ROUNDNESS ON CRITICAL STATE PARAMETERS

submitted by **AHMET SEYİT AKSOY** in partial fulfillment of the requirements for the degree of **Master of Science** i**n Civil Engineering, Middle East Technical University** by,

Prof. Dr. Naci Emre Altun
Dean, **Graduate School of Natural and Applied Sciences** _____

Prof. Dr. Erdem Canbay
Head of the Department, **Civil Engineering** _____

Prof. Dr. Kemal Önder Çetin
Supervisor, **Civil Engineering, METU** _____

Examining Committee Members:

Prof. Dr. Erdal Çokça
Civil Engineering, METU _____

Prof. Dr. Kemal Önder Çetin
Civil Engineering, METU _____

Assoc. Prof. Dr. Nejan Huvaj Sarıhan
Civil Engineering, METU _____

Assoc. Prof. Dr. Nabi Kartal Toker
Civil Engineering, METU _____

Prof. Dr. Berna Unutmaz
Civil Engineering, Hacettepe University _____

Date: 05.09.2024

I hereby declare that all information in this document has been obtained and presented in accordance with academic rules and ethical conduct. I also declare that, as required by these rules and conduct, I have fully cited and referenced all material and results that are not original to this work.

Name Last name : Ahmet Seyit Aksoy

Signature :

ABSTRACT

THE EFFECTS OF GRAIN SPHERICITY AND ROUNDNESS ON CRITICAL STATE PARAMETERS

Aksoy, S. Ahmet
Master of Science, Civil Engineering
Supervisor: Prof. Dr. Kemal Önder Çetin

September 2024, 155 pages

In this research study, the critical state parameters- specifically, the angle of critical state shearing resistance and the critical state loci in the void ratio vs. logarithmic effective stress domain- were experimentally assessed for five different silt and sand. The apparatus developed by Santamarina and Cho (2001) was modified to test Cine, Sile Silica, Tekirdag Silica and Aygaz Alluvial sands from Turkiye, along with Sabratah ilt from Libya to assess their critical state characteristics. To eliminate the need for fully saturating the sand samples, image processing techniques were utilized to facilitate the monitoring of volume changes when these samples were subjected to large strains, ensuring to reach critical state.

Particle shape characteristics—specifically, the sphericity (S) and roundness (R) of grains—were determined using a digital microscope with a 1600x zoom capability. Additionally, grain size distribution, void ratio limits, and specific gravity of the samples were evaluated. These test results, jointly with the data compiled from the literature, were used to assess critical state angle of shearing resistance and locus in the void ratio (e) vs. mean effective stress (p') domain.

Keywords: Critical state loci, Particle morphology, Angle of shearing resistance, Particle sphericity, Particle angularity

ÖZ

DANE KÜRESELLİK VE YUVARLAKLIĞININ KRİTİK DURUM PARAMETRELERİNE ETKİLERİ

Aksoy, S. Ahmet
Yüksek Lisans, İnşaat Mühendisliği
Tez Yöneticisi: Prof. Dr. Kemal Önder Çetin

Eylül 2024, 155 sayfa

Mevcut çalışma kapsamında kritik durum parametreleri -özellikle kritik durum kesme direnci açısı ve boşluk oranı ile logaritmik efektif gerilim düzlemindeki kritik durum lokasyonları- beş farklı silt ve kum için deneysel olarak değerlendirilmiştir. Santamarina ve Cho (2001) tarafından geliştirilen deney düzeneği, kritik durum özelliklerini değerlendirmek için Türkiye'den Çine, Şile Silis, Tekirdağ Silis ve Aygaz Alüvyonlu kumları ve Libya'dan gelen Sabratah siltini test etmek üzere değiştirildi. Büyük gerilmelere maruz kalan numulerin kritik duruma ulaşmaları sağlanmış, sonrasında numunede meydana gelen hacim değişimini bulmak için numuneleri tamamen doyurma ihtiyacını ortadan kaldırmak adına görüntü işleme teknikleri kullanılmıştır.

Parçacık şekli özellikleri -özellikle tanelerin küreselliği (S) ve yuvarlaklığı (R)- 1600x yakınlaştırma kapasitesine sahip bir dijital mikroskop kullanılarak belirlendi. Ek olarak, numunelerin tane boyutu dağılımı, boşluk oranı sınırları ve özgül ağırlığı değerlendirilmiştir. Elde edilen test sonuçları, literatürden derlenen verilerle birlikte, kritik durum kesme direnci açısı ve boşluk oranı (e) ile ortalama efektif gerilim (p') düzlemindeki kritik durum konumunu değerlendirmek için kullanılmıştır.

Anahtar kelimeler: Kritik durum lokasyonları, Parçacık morfolojisi, Kesme direnci açısı, Parçacık küreselliği, Parçacık yuvarlaklığı

To my family…

ACKNOWLEDGMENTS

The completion of this thesis would not have been possible without the generous help and support of many colleagues and friends.

First and foremost, I would like to express my deepest gratitude to my advisor, Prof. Dr. Kemal Önder Çetin, for his invaluable guidance, encouragement, patience, and support throughout my work. Thanks to his extraordinary motivation and belief in me, I was able to complete this thesis. The insights and mentorship he provided during this process have greatly contributed to my academic, professional, and personal growth, for which I am profoundly grateful.

I would also like to extend my heartfelt thanks to my colleagues and friends in the METU Geotechnical Engineering group, particularly Alaa As-Sayed, whose invaluable contributions during the initial stages of the experimental setup were crucial. I am also thankful to Ahmed Al-Suhaily, Moutasem Zarzour, Berkan Söylemez, Elife Çakır and Atasev Doğukan Taşbaşı for their unwavering support.

I would also like to express my sincere gratitude to Assoc. Prof. Burcu Güldür Erkal from Hacettepe University. Her invaluable contributions and expertise were immensely beneficial to my work, and I am truly thankful for her guidance.

My sincere appreciation goes to Kamber Bilgen and Ulaş Nacar for their technical expertise and invaluable assistance during the experiments.

Additionally, I would like to thank the Geodestek family for their support and the opportunities they provided. I extend my gratitude to Dr. Ali Anıl Yunatcı, Dr. Habib Tolga Bilge, and Uğur Çidem for their valuable contributions.

Finally, I wish to express my deepest love and appreciation to my family. I am sincerely grateful to my dear mother, Elif Aksoy, and my dear father, Kemal Aksoy, for their endless and unconditional love and support. I also want to thank my dear sisters, Şevval Aksoy and Zeynep Sena Aksoy. Knowing that they are always by my side gives me strength and confidence.

TABLE OF CONTENTS

LIST OF TABLES

TABLES

LIST OF FIGURES

FIGURES

LIST OF ABBREVIATIONS

ABBREVIATIONS

2D	Two-Dimensional
3D	Three-Dimensional
ASTM	American Society for Testing and Materials
CSL	Critical State Locus, Critical State Line
CS	Critical State
RD	Relative Density
FC	Fines Content
METU	Middle East Technical University
SEM	Scanning Electron Microscope
USCS	Unified Soil Classification System
SEM	Scanning Electron Microscop

LIST OF SYMBOLS

SYMBOLS

ε_v	Volumetric strain
ε_a	Axial strain
v	Specific volume
e	Void ratio
e_{max}	Maximum void ratio
e_{min}	Minimum void ratio
Δe	Change in void ratio
G_s	Specific gravity
D_{60}	60% of particles are finer than this size
D_{30}	30% of particles are finer than this size
D_{10}	10% of particles are finer than this size
D_{50}	Average grain size
C_u	Coefficient of uniformity
C_c	Coefficient of gradation
λ	Slope of the critical state line
ν	Poisson's ratio
Γ	Intercept of critical state line at 1 kPa
Φ'_{cs}	Angle of shearing resistance
R	Roundness

S	Sphericity
f_x	The distance between the camera's lens and its image sensor in x direction
f_y	The distance between the camera's lens and its image sensor in y direction
c_x	The optical center of the camera in x axis
c_y	The optical center of the camera in y axis
p'	Mean effective stress
$\bar{r}$	Arithmetic mean of radii of curvature fitting the grain’s protrusion
$r_{cir,min}$	Minimum circumscribable radius of particle
$r_{cir,max}$	Maximum inscribable radius
M_s	Mass of solids
V_{sp}	Volume of the specimen
V_s	Volume of soil
V_v	Volume of voids

CHAPTER 1

INTRODUCTION

1.1. Research Statement

The influence of grain shape on geomechanical behavior of granular materials has long been recognized in soil and geomechanics. Despite some research exploring the link between these two seemingly distinct characteristics, significant connections remain to be discovered. The correlation between critical state parameters and particle shape is a core aspect of granular material mechanics. This study delves into this relationship using a newly designed laboratory experiment concept along with interpretation and analysis within the framework of critical state soil mechanics (Sheffield and Wroth, 1968, Jerves and Kawamoto, 2016).

The conventional triaxial test and some other methods are used for the determination of critical state parameters; however, these experiments are time-consuming, and the test setups and procedures may require sophisticated systems and advanced knowledge in soil mechanics. For this reason, in order to determine the critical state loci for sandy soils, a simpler apparatus, which will be discussed in detail later in this thesis, was developed by Santamarina and Cho (2001), eliminating the need for using a confining chamber. However, this system requires full saturation of the sample under the suction applied by a vacuum pump, which may be quite challenging. To overcome this problem, image processing techniques were utilized to facilitate the monitoring of volume changes when sandy soil samples are subjected to large strains, ensuring to reach critical state.

With the advent of new computational techniques along with an increase in 3D reconstruction image processing that have allowed for better and more accurate

estimation of volume changes during large strain loading, a new system was developed to assess the loci of critical state by simplified laboratory testing on dry samples.

The test procedure can be easily implemented with simple equipments and is shown to produce repeatable and reliable results. The results obtained from the experiments were compared with the existing experimental test results available in the literature and it was observed that the inter and intra test result comparisons are robust and consistent with data in the literature.

Within the scope of this research study, simplified monotonic large strain loading tests carried out on 5 different sands, namely, Sabratah Silt, Cine Sand, Sile Silica Sand, Aygaz Alluvial Sand and Tekirdag Silica Sand, to investigate the role of their particle morphology on their critical state angle of shearing resistance and loci. Within the scope of the laboratory test program, the location of the critical state locus and the soil index test (minimum and maximum void ratio determination, grain size distribution and specific gravity determination) characteristics were determined for these 5 different silt and sand samples. The results were compared with existing literature.

1.2. Research Objectives

The research objectives of this study are described as follows;

1. To determine the critical state loci in logarithmic void ratio vs. logarithmic mean effective stress domain for five different sands.
2. To investigate the effects of grain size, shape and distribution characteristics on critical state characteristics of both angle of shearing resistance and critical state loci of these five samples through laboratory tests.

3. To compile a database from literature to investigate, the effects of grain size, shape and distribution characteristics on critical state characteristics through resulting database.

1.3. Scope of the Thesis

The thesis scope and outline are organized as follows:

Following this introduction, a comprehensive review of the available literature on the critical state mechanics of granular soils, focusing on critical state parameters and the aspects that affect these parameters.

Within Chapter 3, the detailed testing program, including descriptions of the test equipment, sample preparation techniques, and testing procedures is discussed.

The test results and their interpretation are presented in Chapter 4. By utilizing both existing literature data and the experimental results, the effects of grain shape and grain size distribution on the critical state parameters are analyzed, identifying correlations where applicable. Additionally, the test results are compared with those reported in the available literature.

In Chapter 5, the effects of particle shape, size and distribution parameters on critical state parameters were investigated by using the data obtained from the experimental results and the database in the literature. An optimum model was created for each critical state parameter by adopting maximum likelihood assessment framework.

Chapter 6 summarizes the conducted research studies and presents the main conclusions of the thesis. Additionally, recommendations are presented for future studies.

CHAPTER 2

LITERATURE REVIEW

2.1 Introduction

In this chapter, the critical state soil mechanics concept is explained in detail, focusing on how grain shape and size parameters influence the critical state locus in the e vs. logp' space. The laboratory experiments used to determine the critical state parameters are described, including the methodologies employed, the specific equipment used, and the types of samples tested. A comprehensive analysis of the advantages and disadvantages of these experimental approaches is provided to highlight the reliability and limitations of the findings.

Additionally, the modifications made to the procedure proposed by Santamarina and Cho (2001) are discussed. This includes a step-by-step outline of the changes implemented, the rationale behind these modifications, and their impact on the accuracy and efficiency of the procedure and results. Detailed explanations are provided on how grain shape parameters, such as sphericity and roundness, and the critical state angle are determined, incorporating both theoretical and practical perspectives.

2.2 Shear Straining Response of Sandy Soils

Sandy soils, due to their porous structure, facilitate the movement of pore water between grains. Consequently, under loading, the excess pore water pressure dissipates quickly, transferring the load to the soil particles. For this process to occur effectively, the loading rate must allow sufficient time for the excess pore water pressure to dissipate. This scenario is replicated in laboratory tests under drained

conditions (i.e. constant pore pressure). However, if the loading rate surpasses the rate at which excess pore pressure water can dissipate. The accumulation of pore water pressure can result in either negative or positive excess pore water pressures, depending on the soil's density and stress conditions. This type of loading is simulated in the laboratory using undrained tests (i.e. constant volume). The stress-strain and stress-volume change behaviors of "dense" and "loose" sand samples was illustrated in figure 2.1.

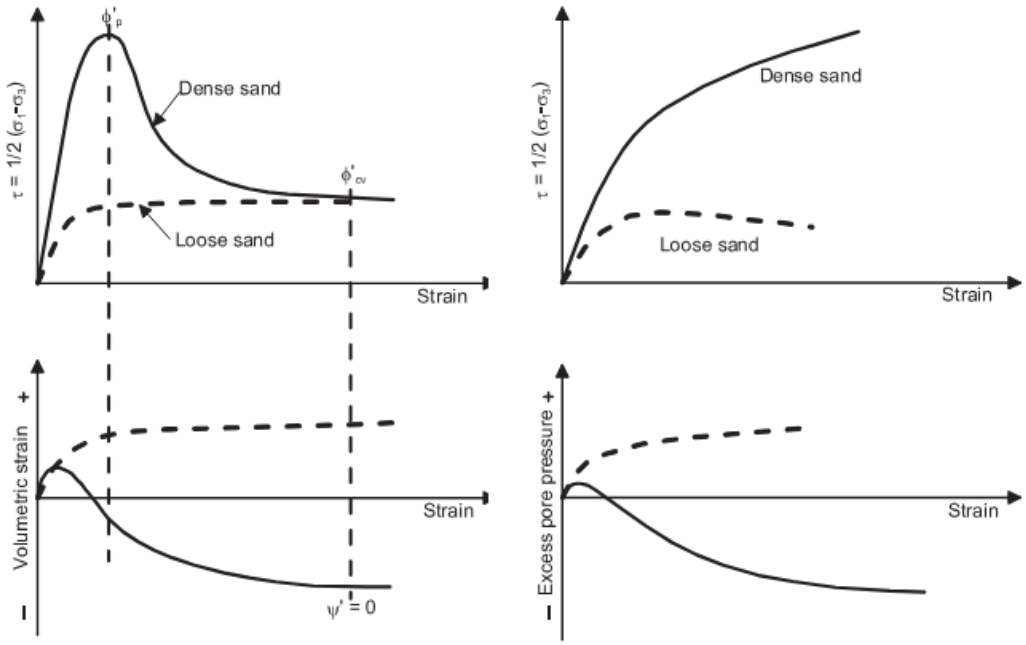

Figure 2. 1. Typical straining response of sands under drained and undrained loading (Andersen and Schjetnc, 2013)

"Dense" or "stiff" samples exhibit similar strain hardening behavior under undrained loading conditions, regardless of being fine or coarse-grained. Similarly, "loose" or "soft" samples under these conditions show strain softening behavior. This highlights that "dense"-"stiff" or "loose"-"soft" soils exhibit the same deformation behavior under similar conditions, irrespective of whether they are clay or sand.

In contrast, "dense" or "stiff" soil samples, which demonstrate strain hardening in undrained conditions, exhibit strain softening (loosening) in drained conditions. This indicates that soil structural behavior depends not only on material properties but also on drainage conditions, which are essentially loading boundary conditions.

As discussed above, the behavior of coarse-grained soils is controlled by their states relative to their critical state loci. The distance from the critical state locus governs if they behave in a dilative or contractive manner. The relationship between index and grain characteristics and their geomechanical response will be examined in detail in the following sections.

2.3 Critical State Concept

Sands subjected to shearing begin to contract or dilate based on their initial density and stress state. As shearing progresses, the sand samples reach a permanent state where no further volume or effective stress changes occur. The void ratio at this stage is known as the critical void ratio, and the relationship between the critical void ratio and effective stress defines the critical state locus (CSL) (Jefferies and Been, 2006).

The critical void ratio concepts for drained and undrained loading conditions was defined by Roscoe (1958). In drained tests, dense sands draw water into their pores, while loose sands expel water from their pores during shearing, resulting in changes of the void ratio. As stated earlier, the critical void ratio is the void ratio at the ultimate state, where shearing continues without any changes in void ratio.

In undrained tests, assuming that sand grains and pore water are incompressible, the volume of the specimen remains constant. Dense sands try to draw water that’s not available into their pores, creating negative pore pressure, while loose sands try to expel water that has no place to go from their pores, creating positive pore pressure during shearing. The critical void ratio is the void ratio at the ultimate state where shearing proceeds without any changes in effective stress. This means that the initial

void ratio, which remains constant during shearing, becomes the critical void ratio at this ultimate mean effective stress.

The critical void ratio remains unaffected by the initial void ratio or density at a given initial effective stress. Wroth and Bassett (1958), through simple shear tests on steel balls, found that when results were graphed, all samples converged to a similar void ratio at large strains, regardless of their initial conditions (Figure 2.2).

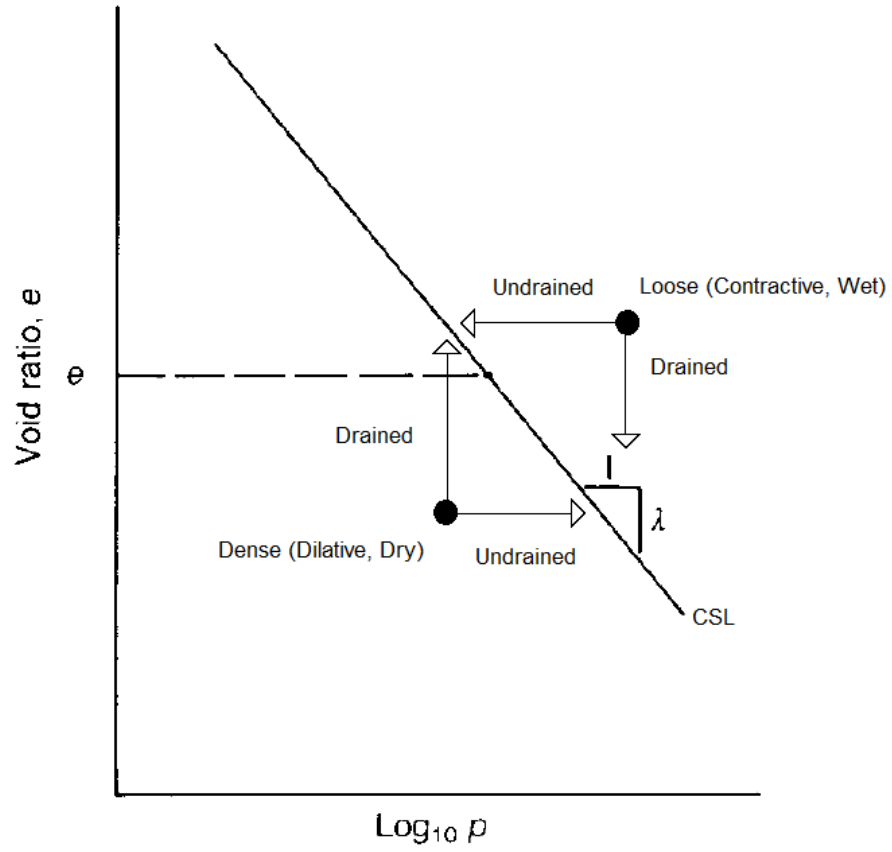

Figure 2. 2. Critical state line

Similarly, Stroud (1971) performed simple shear tests on sand at various stress levels. When the critical void ratio data for each stress level was plotted, it formed a straight line, known as the critical state line, which indicates that the critical void ratio decreases as effective stress increases (Figure 2.3).

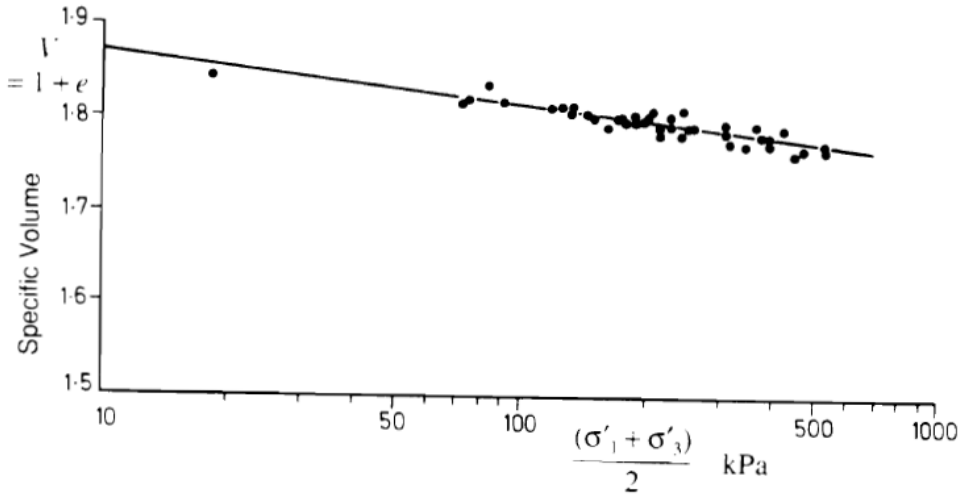

Figure 2. 3. Critical state line for simple shear tests performed on sand (after Stroud, 1971)

The relationship between the critical void ratio and effective stress necessitates the use of the critical state line rather than a singular critical void ratio. Schofield and Wroth (1968) connected specific volume and effective stress, categorizing sands as "wet" or "dry" based on their position relative to the critical state. The area above and to the right of the critical state is termed "wet" because a loose sand sample expels pore water, making the surrounding environment wetter. Conversely, the area below and to the left is termed "dry" because a dense sand sample absorbs water into its pores, creating a drier environment.

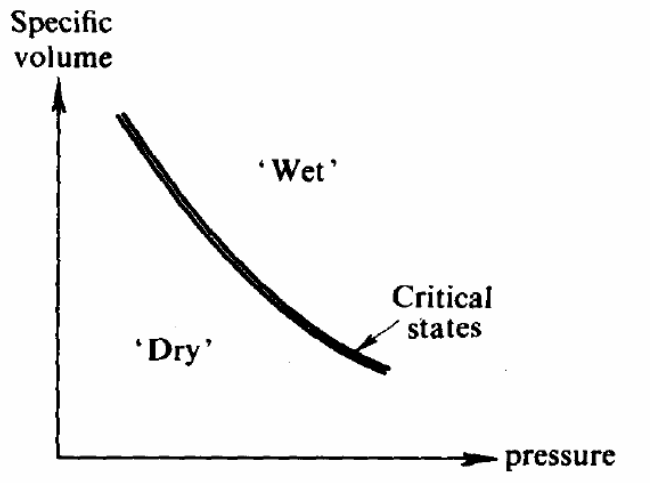

Figure 2. 4. Critical state (Schofield and Wroth, 1968)

Critical state is a key concept for accurately predicting soil behavior. All sands reach a common yield surface during continuous deformation, known as the critical state line, which combines the critical void ratio and effective stress. The initial position of a sand sample relative to this critical state line dictates how it will respond under stress.

At the critical state line, both dilation and contraction rates are zero (Houlsby, 1991). These changes occur as the sand sample moves toward the critical state. The initial distance between the sand sample's state and the critical state line indicates the amount of dilation or contraction that will happen during shearing. In figure 2.2 the slope of the critical state line is represented by λ, and Γ is the critical void ratio at p'=1 kPa, used as a reference for effective stress.

An important takeaway from figure 2.4 is that a sand sample with a particular density can exist on either side of the critical state line and display behavior typical of loose (wet) or dense (dry) sand, depending on the effective stress.

2.4 Simplified Critical State Test Procedure

Traditional triaxial testing is commonly employed to ascertain critical state parameters, but it is often labor-intensive and entails significant costs, making it less practical for routine geotechnical applications. To address this issue, Santamarina and Cho introduced a simplified testing procedure designed specifically for determining the critical state line in sandy soils. This method, which is also part of this thesis study, employs an innovative approach that incorporates image processing techniques. This procedure utilizes a straightforward testing setup that allows for easier sample preparation and testing compared to conventional triaxial tests. It involves preparing loose, homogeneous sandy soil samples to ensure consistent sample density and structure for accurate measurements.

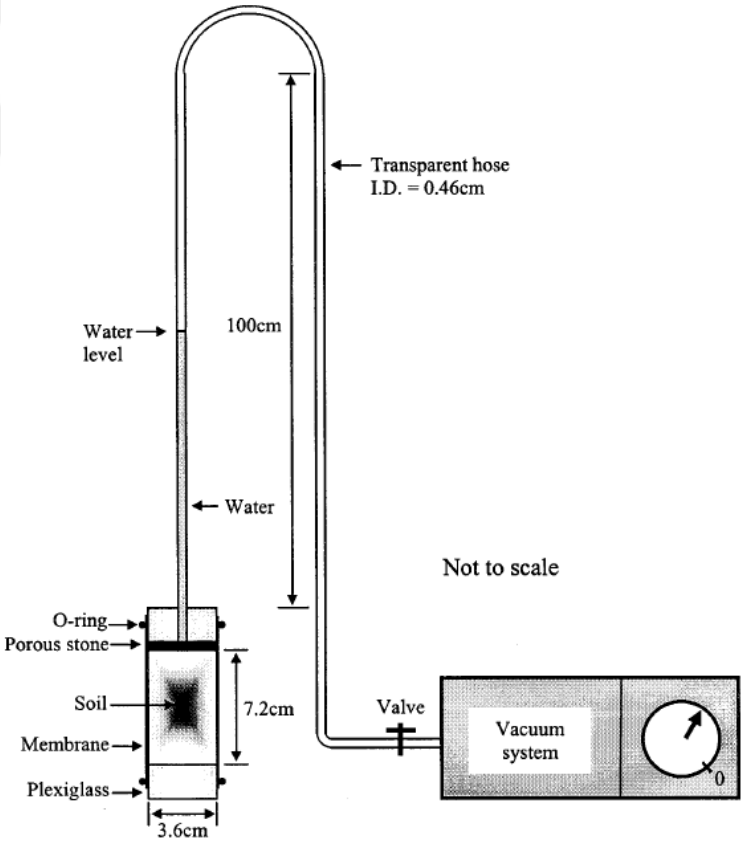

Figure 2. 5. Device and experimental setup used for the simple CS test (Santamarina and Cho, 2001)

The test employs a saturated sample, which is subjected to high strains under various pressure levels, allowing for precise calculations of volume change and, consequently, the void ratio. In this way, this method facilitates the determination of the critical state locus of the sample, confidently indicating that it has reached the critical state, all within the e-log p' space. The equipment used for the system and the installation schematic are shown in figure 2.5.

To validate the reliability of this simplified procedure, results are presented that compare the critical state parameters obtained through this method with those derived from conventional triaxial tests, as illustrated in figure 2.6, 2.7 and 2.8. The comparison demonstrates a strong correlation between the critical state parameters acquired via the proposed method and those obtained through triaxial testing. However, the study also identifies certain limitations that must be considered.

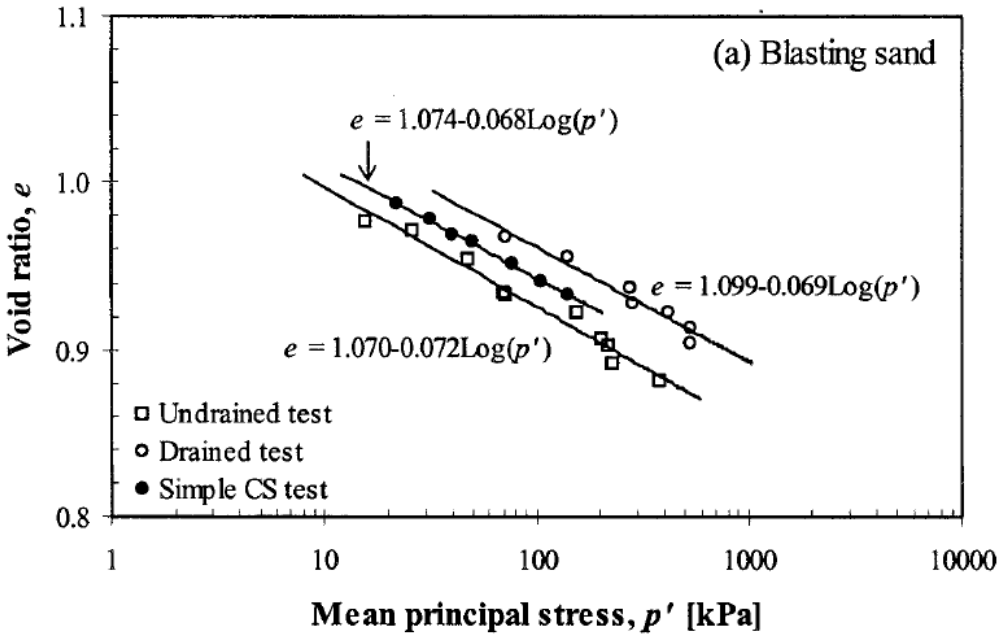

Figure 2. 6. Comparison between simple CS test results and triaxial test results for Blasting sand (Santamarina and Cho, 2001)

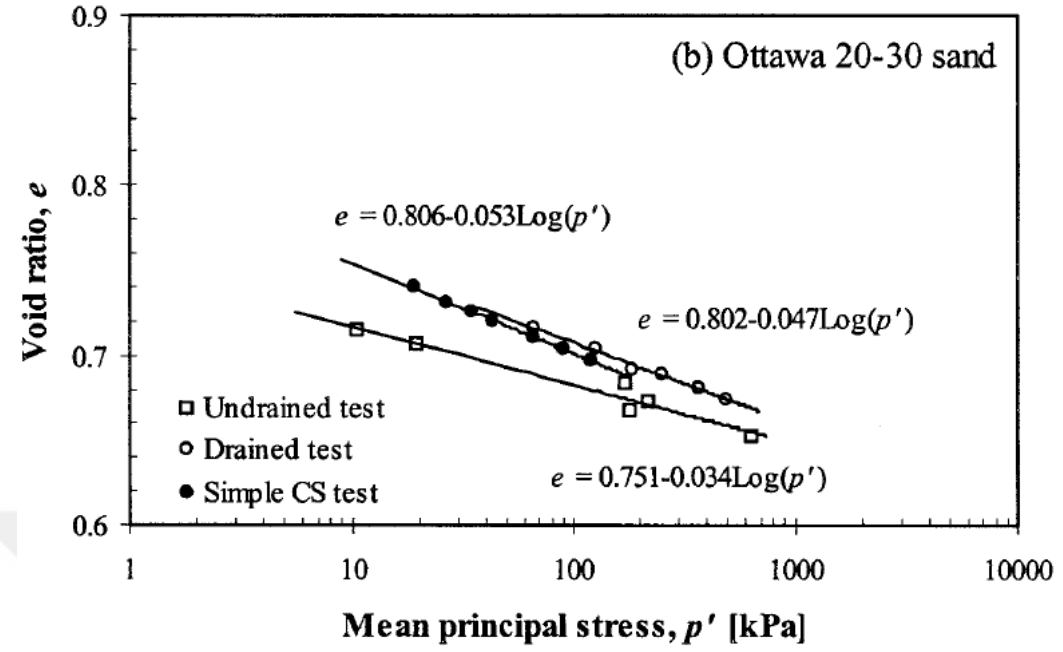

Figure 2. 7. Comparison between simple CS test results and triaxial test results for Ottawa 20-30 sand (Santamarina and Cho, 2001)

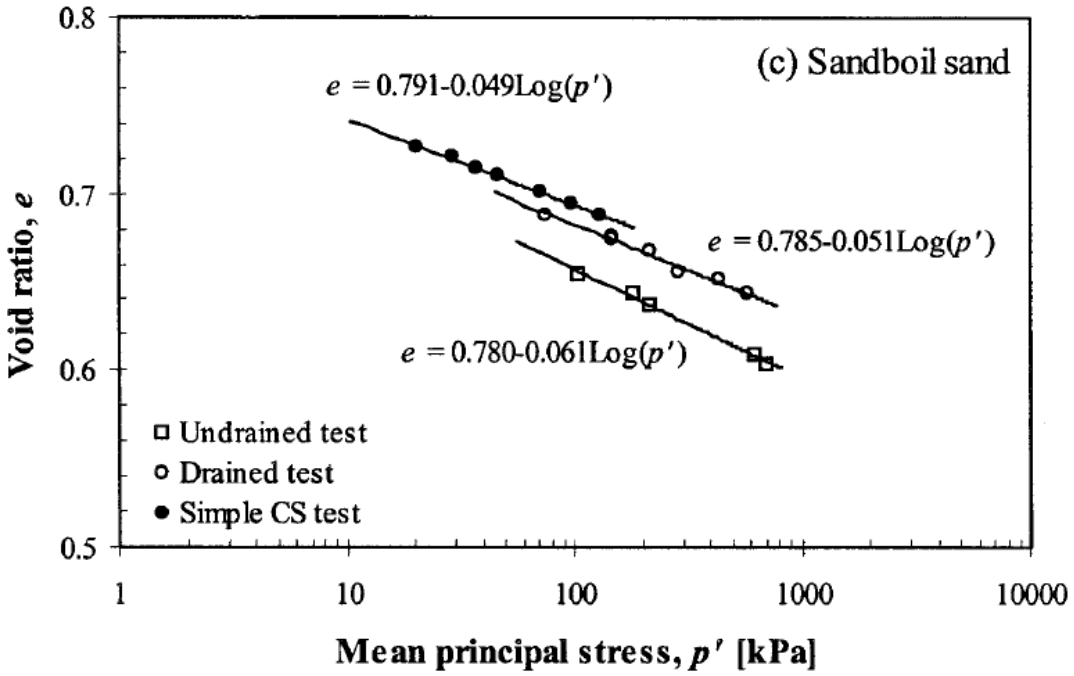

Figure 2. 8 . Comparison between simple CS test results and triaxial test results for Sandboil sand (Santamarina and Cho, 2001)

Despite its reliability, certain limitations were acknowledged, such as the need for further validation across a wider range of soil types and conditions to establish universality. In summary, the simplified critical state test procedure proposed by Santamarina and Cho in 2001 presents an innovative and practical alternative for determining critical state parameters in sandy soils, providing a valuable tool for geotechnical engineers.

It is crucial to recognize that the simple CS test data tend to align more closely with the critical state line derived from drained, loose, and homogeneous specimens. This contrasts with the more conventional method, which relies on undrained loading of loose specimens. The difference between these two approaches highlights the significance of drainage conditions in influencing test outcomes, particularly in scenarios involving loose materials. The drained condition, in particular, offers a clearer representation with the simple critical state behavior compared to the undrained method (Santamarina and Cho, 2001).

2.5 Shape Parameters

This study aims to explore the relationship between grain morphology—specifically, sphericity and roundness—and critical state (CS) parameters, such as the slope (λ) and intercept (Γ) of the critical state line in the e-log(p') domain, as well as the critical state angle of shearing resistance (ϕ'_{cs}). Sphericity and roundness are selected as the key morphological parameters due to their common use in geotechnical research. Sphericity (S) is widely utilized to describe particle shape, with various definitions based on measurements of particle dimensions taken from two-dimensional (2D) projections (Tickell 1931; Wadell 1935; Krumbein and Sloss 1951; Santamarina and Cho 2004; Altuhafi et al. 2013). The specific definition applied in this research is presented in Equation 2-1.

$$S = \frac{r_{in,max}}{r_{cir,min}} \qquad \text{Eqn. 2-1}$$

In Equation 2-1, $r_{in;max}$ is the maximum inscribable radius and $r_{cir;min}$ is the minimum circumscribable radius of a given particle. Roundness is defined as given in Equation 2-2.

Roundness is a parameter that expresses the sharpness of the grain. In contrast to the straightforward calculation of sphericity (S), roundness (R), as defined by Wadell in the early 1930s, is much more complex to determine through basic image analysis. Wadell described R as the ratio between the average radius of curvature at a particle's corners and the radius of the largest possible inscribed circle. Wadell's original method for determining roundness involves significant manual work. Each corner of a particle's outline is matched against transparent templates to identify the largest circle that can fit within the corner. Although this process is labor-intensive and subjective, the procedure is still widely used today (Santamarina & Cho, 2004; Mitchell & Soga, 2005; Cho et al., 2006; Bareither et al., 2008; Chapuis, 2012; Cabalar et al., 2013; Shin & Santamarina, 2013).

Calculating Wadell roundness involves pinpointing each particle's corners and assessing their sharpness. In manual approaches, this process relies on subjective judgment and intuition to identify the corners, as demonstrated in figure 2.9.

$$R = \frac{\bar{r}}{r_{cir,min}} \qquad \text{Eqn. 2-2}$$

In Equation 2-2, where $\bar{r}$ is the arithmetic mean of radii of curvature fitting the grain's protrusion.

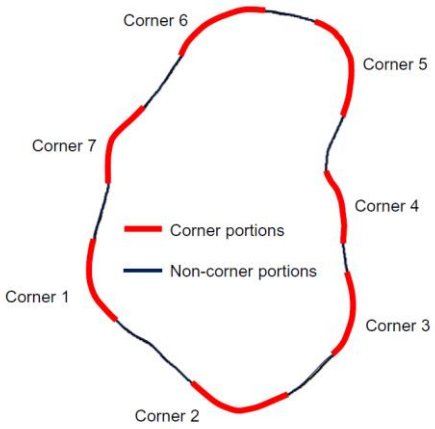

Figure 2. 9. Corner and non-corner portions of a particle outline (Zheng and Hryciw, 2015)

In the 1950s, reference charts featuring particle shapes were introduced to simplify the estimation of Wadell's roundness by allowing for visual comparison with particles observed under a microscope. Three key charts were developed for this purpose by Krumbein (1941), Powers (1953), and Krumbein & Sloss (1963).

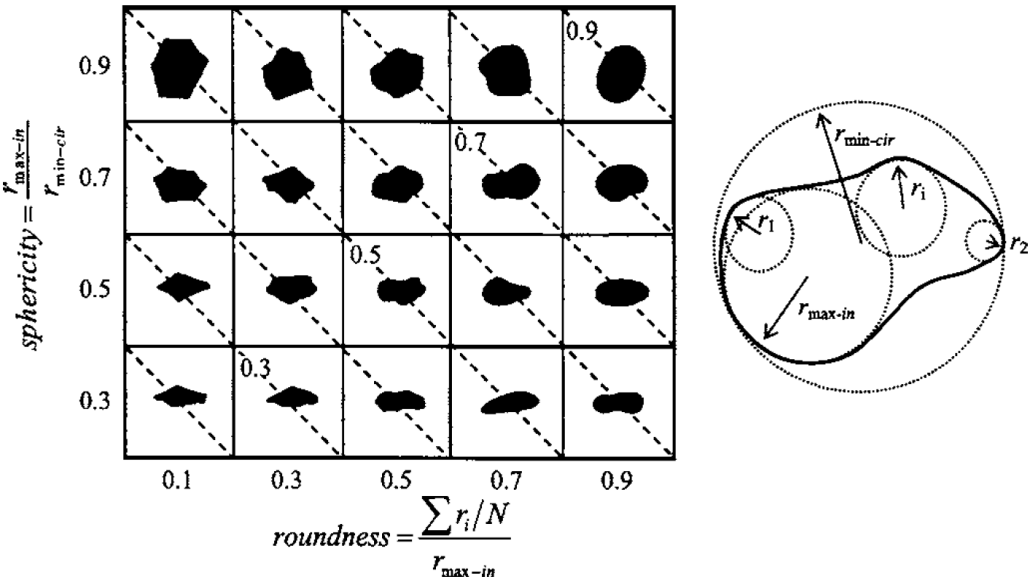

Figure 2. 10. article shape determination—sphericity S and roundness R chart. (modified from Krumbein and Sloss, 1963)

Although these charts are more subjective than Wadell's original template-based method, they remain widely used in fields like geotechnical engineering, soil science, agriculture, powder engineering, pavement engineering, and geology.

In this study, sphericity and roundness are determined by analyzing individual grains under a digital microscope and comparing their geometry to the 2D figures provided in the chart shown in figure 2.10. The roundness (R) and sphericity (S) values for the grains were then calculated using the method refined by Cho, Dodds, and Santamarina (2006), which builds on the original approach by Krumbein and Sloss (1963).

2.6 Image Based 3D Reconstruction

3D reconstruction refers to the process of capturing the shape and appearance of real objects or environments and creating a three-dimensional digital model from that data. It is widely used in fields such as computer vision, medical imaging, architecture, entertainment and civil engineering purposes.

This method uses multiple 2D images taken from different angles. These images are then analyzed by software algorithms to extract depth information and build a 3D model. Techniques like photogrammetry and Structure from Motion (SfM) are examples of this approach.

2.6.1 Photogrammetry

Photogrammetry is the way to obtain solid information about physical objects and environments through the process of recording, measuring, and interpreting photographic images. In this context, the images are used to derive 3D spatial information.

Process is explained as below:

- Multiple images of an object or environment are captured from different angles.
- Key features, such as edges or unique textures, are detected in these images.
- Corresponding features between different images are matched.
- The software uses these matches to compute the relative position of the cameras.
- A 3D point cloud is generated from the matched points, which is then used to create a mesh.
- The mesh is textured using the images to create a realistic model.

2.6.2 Camera Calibration

Within the scope of the study, the chessboard calibration method was used to calibrate the camera used to take 2D photographs for 3D reconstruction. Chessboard calibration is a common method used in computer vision to estimate the parameters of a camera, including its intrinsic and extrinsic properties. Calibration helps correct distortions in images, especially lens distortions, and allows for accurate 3D scene understanding.

In single-camera calibration, the camera's intrinsic parameters (like focal length, optical center, and distortion coefficients) and extrinsic parameters (like the camera’s orientation and position relative to the chessboard) are estimated.

2.6.3 Intrinsic Parameters

These define the internal characteristics of the camera and how it transforms 3D objects into 2D images. Important intrinsic parameters include:

- Focal Length (fx, fy): The distance from the camera's lens to its image sensor, determining the scale of the image captured.
- Principal Point (cx, cy): he optical center of the camera, generally located near the center of the image frame, indicating where the camera's lens axis intersects the image plane.
- Distortion Coefficients: These correct for lens distortions such as:
    - Radial Distortion: Causes straight lines to appear curved, commonly seen with wide-angle lenses.
    - Tangential Distortion: A type of optical distortion that arises when the camera's lens and sensor are misaligned, causing straight lines to appear slightly skewed or curved, particularly toward the edges of the image.

2.6.4 Extrinsic Parameters

These define the camera's position and orientation in the world or relative to the calibration object (chessboard). The main components are:

- Rotation Matrix (R): Describes the camera's rotation relative to the world.
- Translation Vector (T): Describes the camera's position relative to the world or the chessboard.

2.6.5 Chessboard Pattern

A chessboard (or checkerboard) with known dimensions is used because its corners form an easily detectable grid, allowing the algorithm to precisely locate the pattern

points. The squares are typically black and white, forming a pattern of alternating colors. Each corner represents a point in 3D space, which is used in the calibration process.

2.6.6 Calibration Process

- Print a chessboard pattern with known square dimensions (e.g., 9x6 grid of squares) on a flat surface. Ensure that the square sizes are measured precisely since the physical dimensions of the squares are important for accuracy.
- Take multiple images of the chessboard from different angles and distances using the camera you want to calibrate. These images should cover various perspectives to ensure the algorithm can accurately estimate both intrinsic and extrinsic parameters. The more diverse the images, the better the calibration.
- Use an algorithm to detect the inner corners of the chessboard squares in each image. In MATLAB, the Zhang's Calibration Algorithm is primarily used for camera calibration. Zhang's method is based on capturing multiple images of a planar chessboard pattern from different angles. The algorithm then uses the known structure of the chessboard (i.e., known 3D coordinates of corners) and the detected 2D coordinates in the images to compute the camera's intrinsic and extrinsic parameters. Zhang's method simplifies the calibration process by using the properties of a flat, planar pattern like a chessboard.
- Since the dimensions of the chessboard are known, the positions of the corners can be mapped in a 3D coordinate system (assuming the chessboard lies on the z=0 plane). These are the world coordinates.
- Using a method such as least squares minimization, the algorithm computes the camera parameters (both intrinsic and extrinsic) by minimizing the reprojection error. The reprojection error is the difference between the observed 2D points (in the images) and the projected 3D points (from the

chessboard) onto the image plane, given the camera's intrinsic and extrinsic parameters.

- Once the intrinsic parameters (focal length, principal point, and distortion coefficients) are estimated, they can be used to undistort the images. This step corrects for the distortions caused by the lens, producing a more accurate representation of the scene.

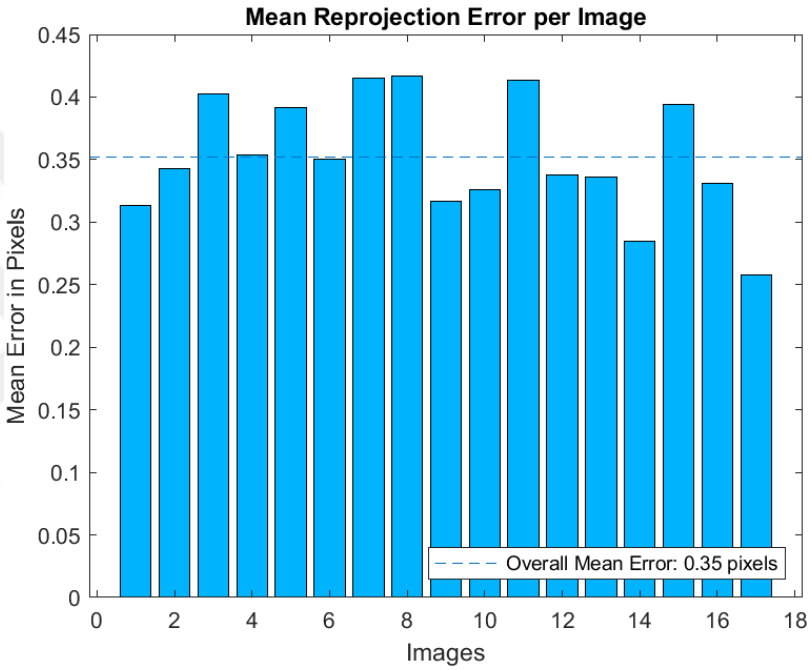

Figure 2. 11. Mean reprojection error values obtained from each calibration photograph within the scope of the study

In the last step, calibration can be refined by adjusting the parameters to minimize the reprojection error further (Figure 2.11). More images of the chessboard from various angles can improve the accuracy.

CHAPTER 3

LABORATORY TESTING PROGRAM AND PROCEDURES

3.1 Introduction

In this chapter, the laboratory testing program and testing procedures are explained. The experimental study was carried out on 5 different silt and sand samples: Sabratah Silt, Cine Sand, Sile Silica Sand, Aygaz Alluvial Sand and Tekirdag Silica Sand. The laboratory testing program consists of soil index tests, modified simplified critical state tests (Santamarina, 2001) performed to determine the critical state angle of shearing resistance and critical state locus. Large strain levels need to be achieved to reach critical state. At the same time, in order to avoid localization problems at large strain levels, each sample have to be prepared loose, and additional care must be taken during the preparation of loose samples.

Indeed, it seems that the best method to obtain the critical state parameters is to use homogeneous loose specimens subjected to drained shear (Santamarina & Cho, 2001). Based on this principle, specimens are prepared at 25% to 35% relative density during the experiment. A 5cm diameter mold is used while preparing the specimen. While preparation dry deposition will be used. In the experiments carried out at different pressure levels for the same sample, the specimen volume is kept constant (same mold and caps), and the mass of the sample was kept constant by weighing at each level, thus the density could be adjusted in a controlled manner.

$$RD = \frac{e_{max} - e}{e_{max} - e_{min}} \qquad \text{Eqn. 3-1}$$

3.2 Soil Index Testing and Particle Morphology

For the five different silt and sand samples tested, index properties including specific gravity (G_s), minimum void ratio (e_{min}), maximum void ratio (e_{max}), and gradation were determined. To ascertain the specific gravity (G_s), three specimens were prepared and tested in accordance with ASTM D854-14. The average G_s of the specimens is presented in the Table 3.1. The detailed results of all tests are provided in Appendix A.

Table 3. 1. Grain size distribution characteristics and specific gravity proporties of tested samples

Parameter	Sabratah Silt	Cine Sand	Sile Silica Sand	Aygaz Sand	Tekirdag Silica Sand
USCS	-	SP	SP	SP-SM	SP
D_{60}	-	0.46	0.50	0.30	0.54
D_{10}	-	0.12	0.20	0.09	0.33
D_{30}	-	0.26	0.33	0.18	0.44
Coefficient of Uniformity, C_u	-	3.83	2.50	3.33	1.64
Coefficient of Gradation, C_c	-	1.2	1.1	1.2	1.1
Specific Gravity, G_S	2.683	2.645	2.677	2.684	2.558
Fines Content (%)	63.31	0.07	0.01	7.04	0.03

The maximum void ratio (e_{max}) is estimated following the ASTM D4254-16 standard. The value obtained by the relevant laboratory procedure represents the loosest state of a cohesionless, free-draining soil. The oven-dried sample was placed in a container of known volume, and the maximum void ratio of the soil was determined to minimize soil compaction by preventing swelling and particle

segregation. The volume of the container was measured, and the volume of solids and voids were calculated to obtain void ratio. The minimum void ratio (e_{min}) is determined similarly by placing the oven-dried sample in three layers. For each layer, vibration was applied for a certain period of time with the help of a vibrating device and layer compression was also applied. Experiments for the determination of e_{max} were conducted three times, while those for e_{min} were conducted twice. The values obtained for 5 different silt and sand samples are presented in the Table 3.2.

Table 3. 2. The void ratio limits and range for 5 different silt and sand samples

	Sabratah Silt	Cine Sand	Sile Silica Sand	Aygaz Sand	Tekirdag Silica Sand
e_{max}:	1.339	0.889	0.706	0.934	0.818
e_{min}:	0.740	0.516	0.538	0.544	0.580
e_{max}-e_{min}	0.599	0.373	0.168	0.390	0.238

The gradation of five different sand samples was determined through a series of laboratory tests conducted in accordance with ASTM D6913/6913M-17. This standard outlines procedures for particle size distribution (grading) analysis using sieving methods that are critical to understanding the granular composition of sands.

The results of the gradation (grain size distribution) for five different sands, namely Sabratah Silt, Çine Sand, Şile Silica Sand, Aygaz Alluvial Sand and Tekirdag Silica Sand, are presented in Table 3.1. The analysis included determining key parameters such as the uniformity coefficient (C_u), coefficient of curvature (C_c), and the effective sizes (D_{10}, D_{30}, D_{60}). Following the gradation analysis, it was found that the sample from Sabratah used in the experiment was classified as silt rather than sand according to the unified soil classification system (USCS). Çine Sand has D_{10}, D_{30}, and D_{60} values of 0.12 mm, 0.26 mm, 0.46 mm, respectively, with a C_u value of 3.83 and a C_c value of 1.2, also indicating that it is a poorly graded sand (SP). Sile Silica Sand has D_{10}, D_{30}, and D_{60} values of 0.20 mm, 0.33 mm, 0.50 mm respectively, with a Cu value of 2.50 and a Cc value of 1.1, classifying it as poorly graded sand (SP).

For Aygaz Sand, the D_{10}, D_{30}, and D_{60} values are 0.09 mm, 0.18 mm, 0.30 mm, respectively, with a Cu value of 3.33 and a Cc value of 1.2, classifying it as SP-SM. These parameters, crucial for characterizing the soil. Gradation curves and additional data are presented in the following section.

The sphericity, S and roundness, R of the sand grains were determined using a 1600x electronic microscope. For each sample, a minimum of 10 to 15 grains were selected randomly for testing purposes to obtain representative results. The image of each grain was captured using an electronic microscope and then transferred to custom desktop software for further analysis. In the software, maximum inner circle, minimum outer circle and inner maximum inscribable circles were drawn to scale to evaluate the shape properties of the grain. To ensure the accuracy of the measurements, simple calibrated printed paper was used for calibration purposes. This calibration was performed using an application that converts pixel measurements to micrometers, allowing precise scaling. Using this calibrated system, the gross dimensions of each sand particle were also accurately measured. This detailed analysis facilitated the determination of sphericity and roundness of sand grains and provided valuable information about the morphological properties. The results, including the calculated sphericity and roundness values for each sample, are presented and average value for each soil sample tabulated in the Chapter 4, highlighting the differences in particle shape and texture between different silt and sand samples. A sample of grains is shown in figure 3.1.

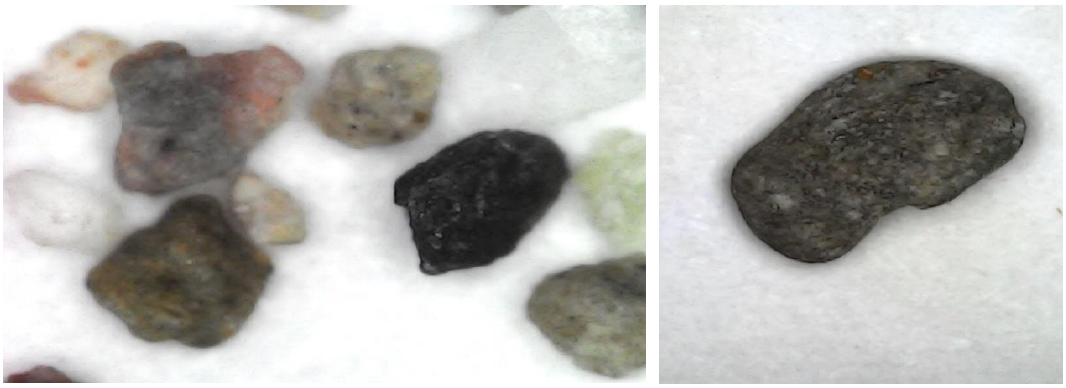

Figure 3. 1. View of Cine sand particles under a 1600x electronic microscope

The electronic microscope not only facilitated detailed geometric measurements, but also allowed visualization of the mineralogical composition of sand grains. Minerals such as quartz and mica, which are commonly found in sands, can be clearly identified. However, it is important to note that no detailed mineralogical analysis was conducted within the scope of this study.

3.3 Modified Simple Critical State Testing

3.3.1. Introduction

The assessment of the critical void ratio of sands has been a topic of extensive debate and research since Casagrande's pioneering work in 1936. The critical state was defined by Roscoe et al. (1958) as the condition in which a soil deforms continuously under increasing shear strains while maintaining a constant stress level and void ratio. The critical void ratio decreases as the mean effective stress increases. This relationship between the critical void ratio and mean effective stress is known as the critical state locus (CSL). The CSL, which represents the soil's state, is typically illustrated as a line in the void ratio (e) versus logarithmic mean principal effective stress (p') plane. Since Casagrande first proposed the concept of a critical void ratio

in 1936, developing reliable methods to accurately determine the critical state line (CSL) has proven challenging (Been, 1991).

Several methods have been employed over the years to study and validate the critical state concept for sand. Ring shear tests (Negussey et al. 1988) and direct shear tests (Oyenuga and Tisot 1989) were conducted to confirm the uniqueness of the critical state across different types of sands. However, employing these tests to measure the critical state can present challenges, as the stress state within a ring or direct shear sample cannot be fully defined (Chu, 1995).

Alternatively, triaxial tests used to verify the critical state concept. Studies using triaxial tests were published by Been et al. (1991). This approach is favored because critical state strength can be attained with a relatively low amount of global strain (Been et al. 1991; Lee 1995). However, dilative-drained tests, as well as both contractive and dilative undrained tests, are susceptible to localization. This can cause the measured global void ratio to differ from the local void ratio in the shear band where significant strains occur. Consequently, the most effective method for obtaining critical state parameters seems to be using homogeneous loose specimens subjected to drained shear. Additionally, this test method is not affected by incomplete saturation. Nonetheless, it requires application of large shear strains on samples. Achieving the critical state can pose challenges for experimental design due to the required large strain levels. Although relatively low strains are sufficient to alter the network of interparticle forces, a micro-scale view of the problem indicates that strains exceeding 30 to 50% are necessary for simple shear testing. This ensures that particles have a high probability of exchanging neighbors, thereby attaining the unique fabric conditions associated with the critical state. Such strain levels are not attainable in triaxial testing. Drained tests, in particular, demonstrate that the critical state may not be reached at the conventionally preferred 20% strain limits. Conversely, undrained tests are complicated by poroelastic effects and localization issues. Despite these challenges, the conventional triaxial test continue to be widely used for determining the locus of critical states in the e-p'-q space. For simplicity, the critical state line can be represented by its 2D projection on the e-log p' space,

represented by critical state parameters of slope λ and intercept Γ. Multiple tests are often conducted to account for experimental variability. This time-consuming and complex process has somewhat limited the application of critical state soil mechanics. However, problems regarding the measurement of the critical state for sand remain unresolved. To overcome the difficulties in measuring the critical states of sand, a relatively new testing method, simple critical state test procedure has been proposed by Santamarina and Cho (2001). Moreover, within the scope of this study, the simple procedure developed by Santamarina and Cho (2001) was modified, to eliminate the need for fully saturating the sand samples. In this way, a new experimental methodology has been suggested in assessing the critical state locus. The modified simple test procedure is proposed in the next section.

3.3.2. Modified Simple Critical State Test

The critical state locus, typically represented on the 2D void ratio - mean effective stress axes, is considered semi-logarithmic for soils in most existing studies, at least from an engineering perspective.

$$e_c = \Gamma - \lambda \ln (p_c^{'}) \qquad \text{Eqn. 3-1}$$

In this context, Γ and λ are accepted as intrinsic soil properties. It is important to be cautious with quoted values of λ, as both base-10 logarithms and natural logarithms are used in the literature. Natural logarithms are more convenient for constitutive modeling, while base-10 logarithms are typically used for plotting experimental data (Been and Jefferies, 2006). In this study, they are differentiated by two different notations of λ and λ_{10} (=2.303λ). The parameter Γ the void ratio value for p′=1 kPa. The validity of representing the Critical State Locus (CSL) by a line is simply as choice of a reference frame and does not rely on a semi-log approximation. It is merely a modeling detail.

First of all, it would be appropriate to repeat the definition of the critical state as the situation in which the soil "continues to deform at constant stress and constant void ratio" (Roscoe, Schofield and Wroth, 1958). Because the entire purpose of the modified test procedure is based on the assumption that the sample reaches a critical state under axial strain exceeding 40% in the drained condition (no further volume change occurs under displacement). After the sample reaches the critical state, its volume and therefore the void ratio (the sample used in the test is a completely oven-dry sample) is calculated by photogrammetry and 3D reconstruction method. Mathematically, this behavior can be expressed as the cessation of the variation of q, p′ and specific volume (ν) therefore void ratio (e), with the relevant unit deformation, as given by Equation 3-2.

$$\frac{dp'}{d\varepsilon_q} = \frac{dq}{d\varepsilon_q} = \frac{dv}{d\varepsilon_q} = 0 \qquad \text{Eqn. 3-2}$$

However, this statement alone is not sufficient to prove that the critical state has been reached. To distinguish the critical state from the 'instantaneous' critical state, which can be described as a quasi-steady state, the 'change of change' must also subside. This condition also requires that the second derivatives of the variables p'-q-ν reach zero. To illustrate some of the details of test interpretation, the behavior of a loose sample under drained condition is shown in figure 3.2 (Been et al, 1991). In drained tests on loose samples, although it requires more than 20% axial strain for critical conditions to become established, the soil eventually reaches the critical state, which is then very easy to identify. The modified critical state test methodology presented within the scope of the study was also built accordingly. For each experiment, under drained conditions, the final volume (void ratio) of the sample was calculated under axial strains exceeding 40% by allowing the volume of the sample to change. The stages of the experiment are briefly summarized below.

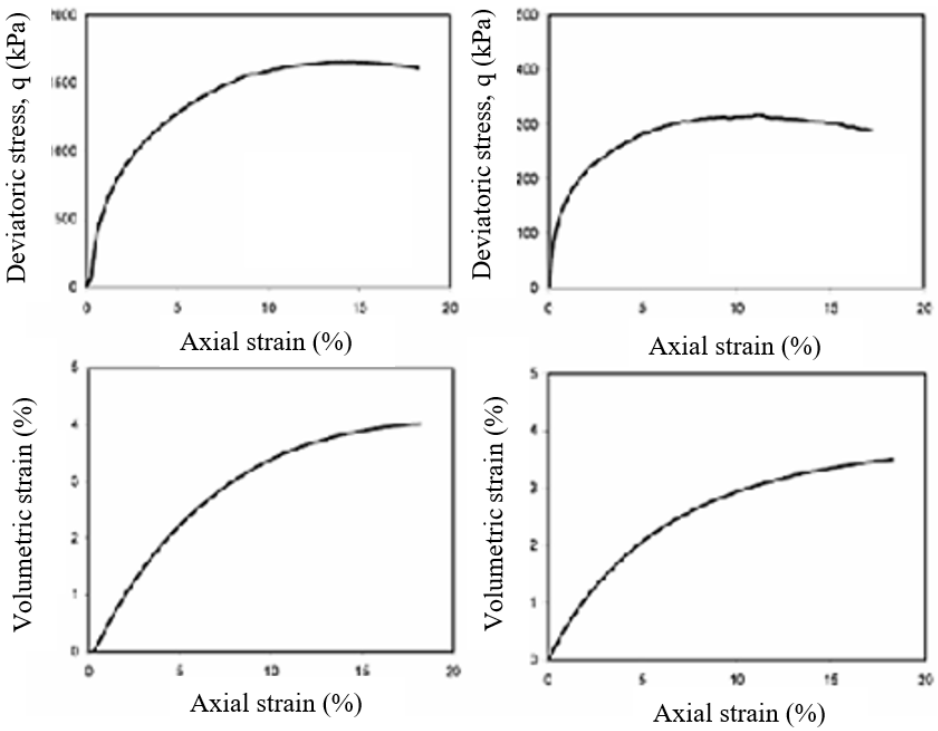

Figure 3. 2. Examples of drained triaxial tests on loose samples reaching critical state (Been, 1991)

- Uniform samples should be prepared in a loose state (the operator should aim for the loosest void ratio in the first stage and then samples should be prepared to approximately achieve that void ratio).
- Since the test will be carried out on completely dry samples taken out of the oven, no saturation will be carried out.
- After the sample has been prepared, a vacuum pump must be used to reach the relevant pressure level. This vacuum pump must have a regulator valve to apply the desired pressure. The pressure level must be increased for each test level.
- A system that can apply high axial strain should be used. (For this purpose, a hydraulic load frame was used within the scope of the study.)
- After the sample is subjected to high axial stresses, it must be reformed in shape for volume calculation. (this can be done by hand)

- The procedures required to deal with each of these issues are explained in the following stages of the study.

The high pressures used in undrained tests are both inappropriate for most commercial triaxial equipment and often cause grain crushing. In the modified simple test procedure, tests are performed at lower confining stress levels that will not trigger particle crushing and selected as p'<80 kPa. Often the sample is loaded to axial strain levels exceeding 40%. The usefulness of the modified simple critical state test becomes apparent when plotting the steady state void ratio and mean effective stress states to estimate the CSL.

3.3.3. Experimental Apparatus

The method presented here is a modified version of simple critical state testing proposed by (Santamarina and Cho, 2001). It enables accurate measurement of all necessary parameters and requires minimal, low-cost components that are readily available in most geotechnical laboratories.

The following components are needed:

- Vacuum pump,
- Thin latex membrane (with markings on - 0.4mm thick membrane was used during experiments-),
- Two caps (Aluminum caps are used within the scope of the test, plexiglass caps can also be used),
- Four O-rings (two for bottom, two for top),
- Mold,
- A porous stone.
- Silicone hose and valve
- Tripod and camera,
- A suitable background and marked base on which to place the sample,
- A simple stepper motor and control system to rotate the sample.

- Precision scale,
- A computer to run software to be used for volume calculations.
- Hydraulic jack (with a diameter of 4.75cm and a stroke length of approximately 10 cm was used)

The cap with the porous stone is connected with the hose to the vacuum system, which is used to apply effective confinement.

3.3.4. Sample Preparation

At the beginning, before starting the experiments soil grains remaining from the previous experiment were removed from the caps and membrane with the help of a brush and swab. Since the sample is not saturated during the experiment, there is no need to boil the porous stone before every test, but it is boiled occasionally to ensure its permeability. Before starting the experiment, all parts used in the test (pedestal and top cap, membrane, o-ring and valve) except the sand are weighed on a sensitive scale. Thanks to this measurement, the weight of the sample to be used in the experiment will be measured and obtained later. After all the parts are ready, the latex membrane is placed on the pedestal. Immediately after the latex membrane is fitted on the pedestal, two o-rings are placed in the grooves on the pedestal. Additionally, a mold normally used in the preparation of triaxial specimens is used to ensure that the membrane takes the correct shape while preparing the specimen. In this way, specimens with similar densities can be prepared with the same method during each experiment. The mold is placed on the pedestal, around the membrane. During specimen preparation external holder etc. is not needed.

While filling the sample into the mold the dry deposition method was used, oven dried sand was filled in a cone shaped funnel with a 7 mm spout opening, which traversed over the specimen mold in a circular motion, as illustrated in figure 3.3, slowly from almost zero height. Since the aim is to prepare the specimen in the loosest state, no compaction or tapping by hitting the side of the mold was applied.

After the mold is filled to the brim (in order to prevent necking between the cap and the specimen when vacuum is applied, compaction can be applied very lightly from the top with the help of a stick) excess sand is removed and top cap is placed. After the top cap is placed, two o-rings are placed over the membrane in a similar manner, corresponding to the grooves on the cap.

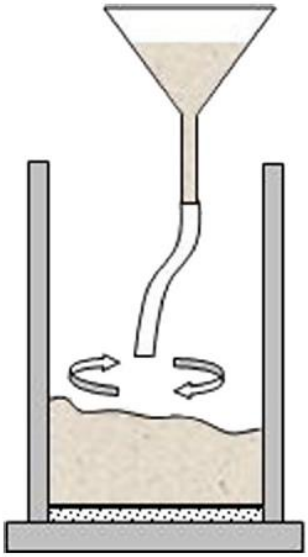

Figure 3. 3. Dry deposition method for sample preperation (Santana and Candeias, 2018)

While the specimen is in the mold, the hose connected to vacuum is attached to the valve in the pedestal, without disturbing the loose state of the specimen or moving the mold. The vacuum pressure under which the spcimen will be tested is applied with the help of the regulator, and the mold is removed while connected to the vacuum and the setup is made ready for testing.

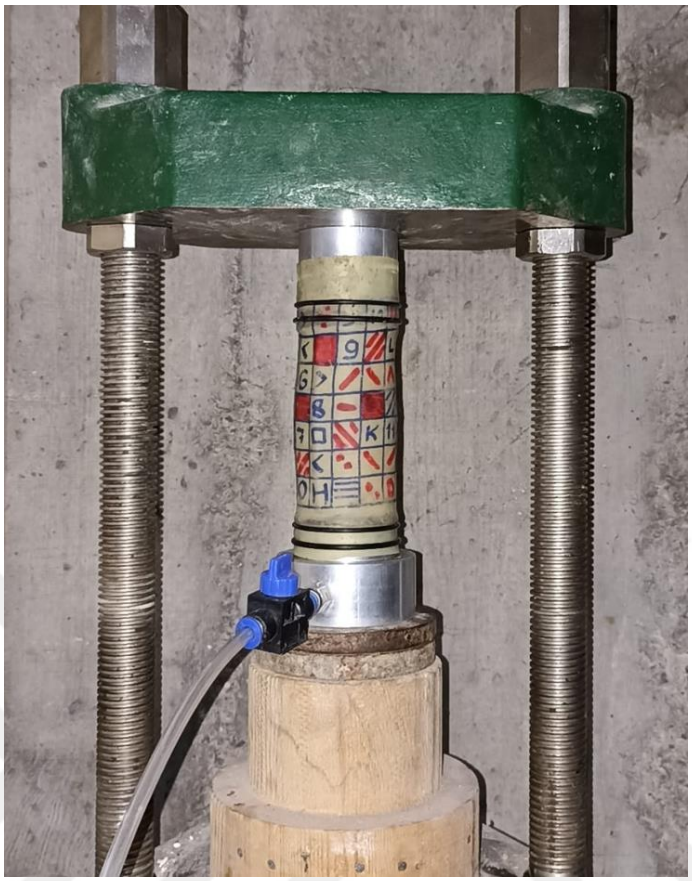

Figure 3. 4. A soil sample ready to be axially loaded by the jack

3.3.5. Test Procedure – Image Processing & 3D Reconstruction

After the sample was prepared, the membrane is checked for any leaks, excessive wrinkles or deformities while still under vacuum. While under vacuum, the sample is placed under a hydraulic jack to subject it to axial deformation. The jack is advanced until the top cap touches the load frame, ensuring there is no gap left. At this point, the length of the specimen is measured using a ruler. The heights of the caps, which are known, are subtracted from the total height to obtain the height of the specimen, providing information about the axial deformation to be applied. Based on the measured height, the sample is deformed by applying axial force with the jack while maintaining vacuum pressure. After applying axial strain of up to 40%, the valve on the pedestal, which is connected to the vacuum, is closed, and the

sample is removed from the jack. Once the hose is removed from the valve, the sample is weighed on a precision scale before proceeding with the volume measurement. The weight of the sand used is determined by subtracting the weight of the previously measured apparatus from the total weight.

Figure 3. 5. Sample with over 40% axial deformation

After these processes are completed, the specimen is brought to the designated area for volume measurement. Since the specimen volume will be determined digitally using the photogrammetry method, the specimen is reshaped by hand while taking photographs to capture images of every surface and eliminate folds in the membrane caused by deformation. This ensures that all points on the membrane are captured in the photo frame, which is crucial for creating an accurate 3D model. After the specimen is reshaped, it is placed centrically in the area to be photographed.

Specimen photographs were taken using a Canon camera. A tripod was employed to ensure the camera's stability and to achieve the desired angle for each photograph. Similarly, a green background is used in photogrammetry to take photographs of the specimen because it enhances the visibility of the specimen details, facilitating accurate 3D reconstruction. The green color provides high contrast against most objects, making it easier to distinguish the model from the background. Additionally, digital cameras are more sensitive to green light, capturing sharper and clearer images essential for precise reconstruction. Green background also reflects light evenly, creating a uniform backdrop that simplifies isolating the model during post-processing. This technique aligns with standard visual effects practices, ensuring compatibility with software optimized for green background removal, thereby streamlining the entire photogrammetry workflow.

Figure 3. 6. View of marked membrane and reshaped sample

In this study, the accuracy and detail of 3D modeling were significantly enhanced by employing a technique involving random shapes in two distinct colors, blue and red, on the membrane used for the tests. These contrasting colors created identifiable reference points and unique patterns on the model's surface, aiding the photogrammetry software recognizing and distinguishing various parts of the model. The clear, high-contrast features provided by the blue and red shapes facilitated the software in tracking the model's spatial orientation and surface texture from different angles. Through this method, the complex details and geometry of the model were accurately captured and recreated. Moreover, issues with uniform textures and surfaces, which can pose challenges for software distinction, were mitigated with these colored markers. Consequently, the overall precision and quality of the 3D model were enhanced, resulting in more reliable and detailed reconstructions in the study.

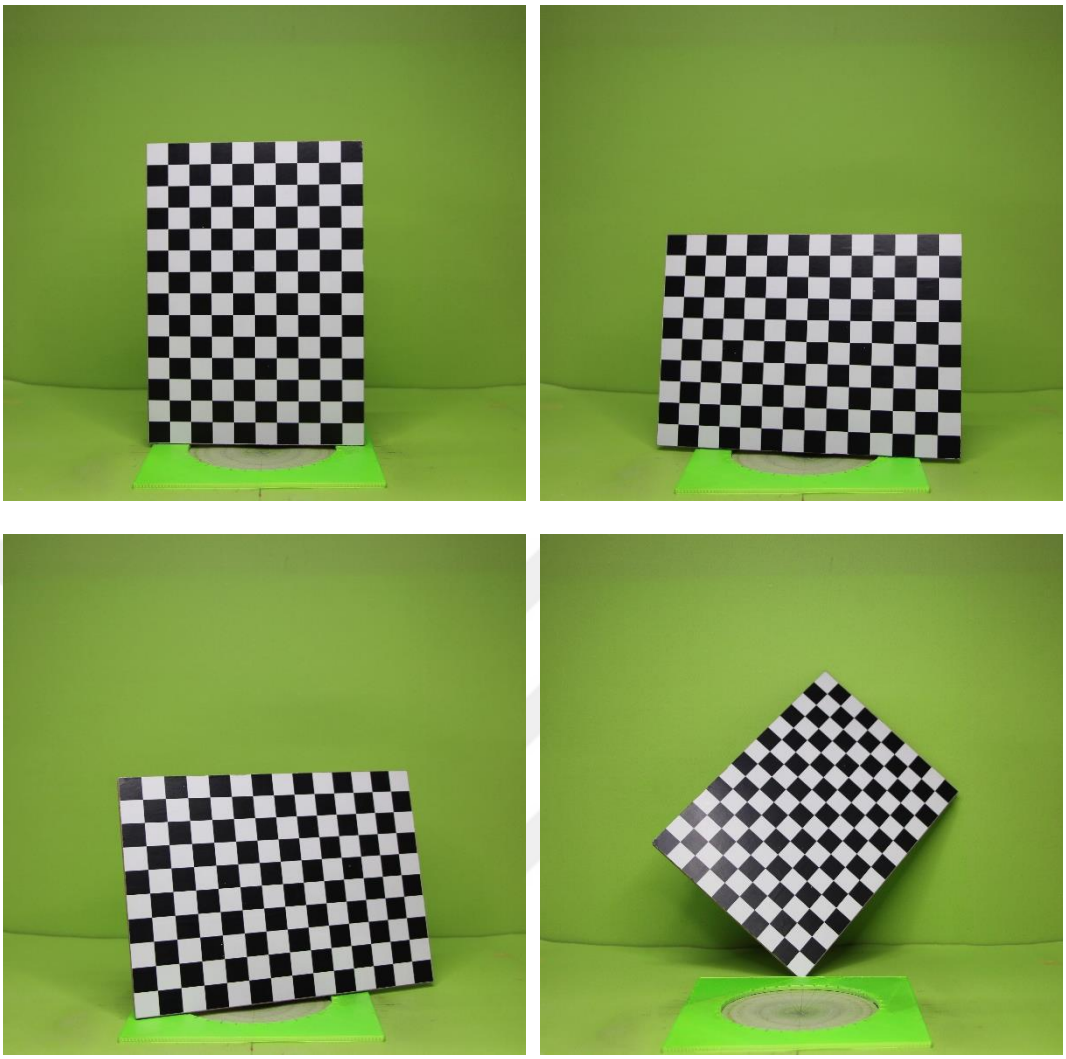

Figure 3. 7. Chessboard calibration images used for camera distortion correction

The camera intended for the test was calibrated beforehand using a method called “Chessboard Camera Calibration”, aiming to ensure more accurate results. Chessboard camera calibration is a crucial step in the photogrammetry and 3D reconstruction processes. It involves capturing images of a chessboard pattern from various angles and distances shown in figure 3.7 using the camera that will be used in subsequent imaging tasks. By analyzing these images, the camera's unique parameters, such as focal length, key point and lens distortion coefficients, can be accurately determined (Table 3.3). This calibration is necessary because it allows removing distortions present in the images and ensures that measurements and calculations based on these images are accurate. In photogrammetry, precise

measurements of object dimensions and spatial relationships rely on distortion-free images. Similarly, in 3D reconstruction, accurate camera calibration ensures that reconstructed models faithfully represent real-world objects.

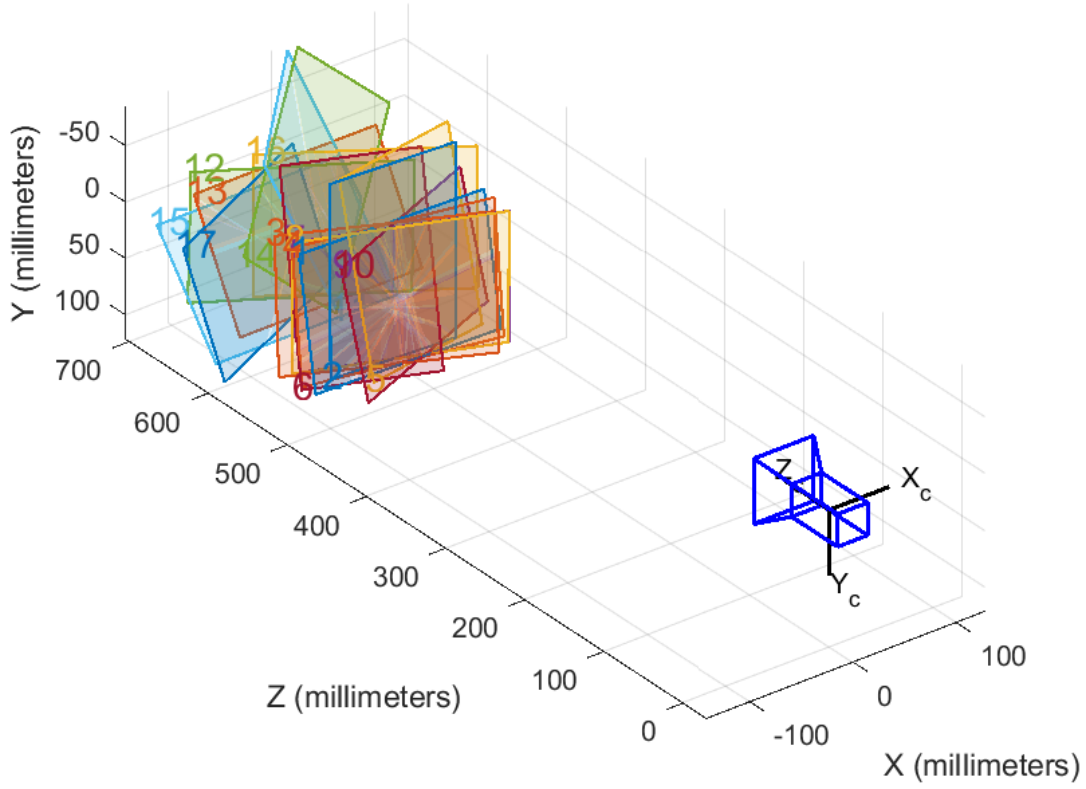

Figure 3. 8. Extrinsic parameters visualization

Table 3. 3. Intrinsic properties of the camera used in distortion correction

Focal length (pixels):	[5706.2564 +/- 2.7025 5704.0305 +/- 2.5448]
Principal point (pixels):	[2609.6937 +/- 1.1570 1705.2447 +/- 2.0362]
Radial distortion:	[-0.1091 +/- 0.0022 0.2277 +/- 0.0249]

Chessboard camera calibration therefore serves as a fundamental step to guarantee the reliability and precision of subsequent photogrammetric and 3D reconstructions. In the study, the Matlab Camera Calibrator application was employed for the purpose of chessboard camera calibration. This application offers a user-friendly interface for

the calibration process, allowing researchers to easily capture images of the chessboard pattern from different viewpoints and distances using their camera setup (Figure 3.8).

Figure 3. 9. Uncorrected and distortion-corrected versions of the same photo

The Matlab Camera Calibrator then utilizes advanced algorithms to automatically detect the corners of the chessboard pattern in the images and estimate the intrinsic parameters of the camera. By extracting and incorporating these parameters into the program itself, the photographs taken during the experimental setup can be internally calibrated within the software, ensuring precise and distortion-free images for subsequent analysis in photogrammetry and 3D reconstruction operations. This integrated approach streamlines the calibration process and enhances the overall accuracy and reliability of the imaging system.

Figure 3. 10. Chessboard calibration images used for camera distortion correction

After all these steps are followed and the camera is positioned at the correct angle, the sample is rotated every 10° and 36 photographs are taken for a total of 360° as shown in figure 3.10.

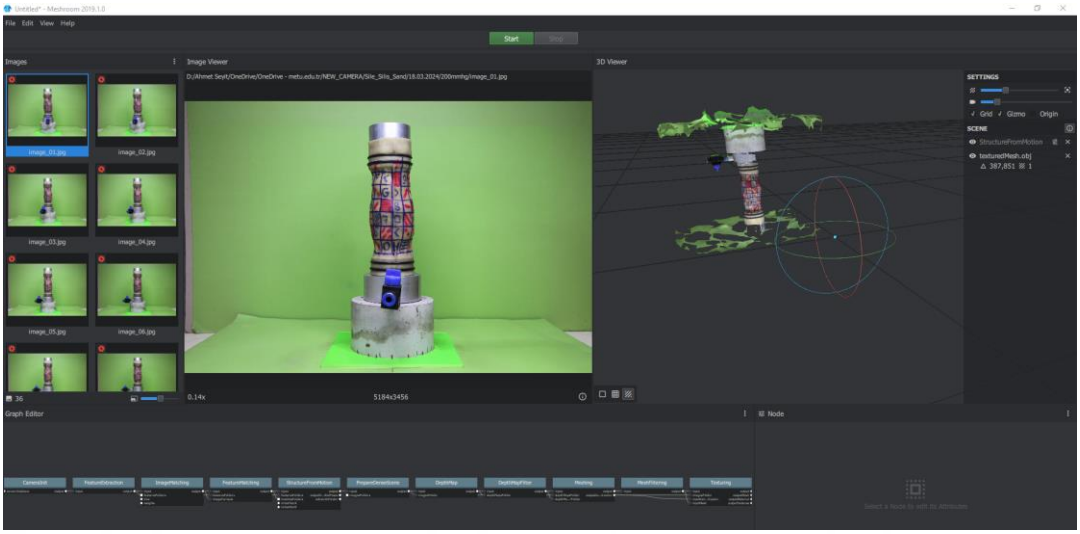

Figure 3. 11. Interface of Meshroom program

This process is followed separately for each pressure level, and in one set of experiment, 5 separate 3D reconstruction operations are performed on a total of 210 photographs at 5 different pressure levels on the same specimen. The device saves photos instantly to an external SD card. Once the experiment is concluded, all photos are transferred to a computer via the SD card. In MATLAB, the photos undergo rearrangement to remove distortion based on the camera's parameters. Subsequently, the 36 photos obtained for each pressure level are uploaded to Meshroom, an open-source software. After making necessary program adjustments in Meshroom, a 3D textured mesh of the sample in object (.obj) format is created and exported. This textured mesh is then imported into Blender, another open-source software. In Blender, various basic operations are performed on the sample to calculate its volume using the application's capabilities. The procedures performed are summarized step by step below.

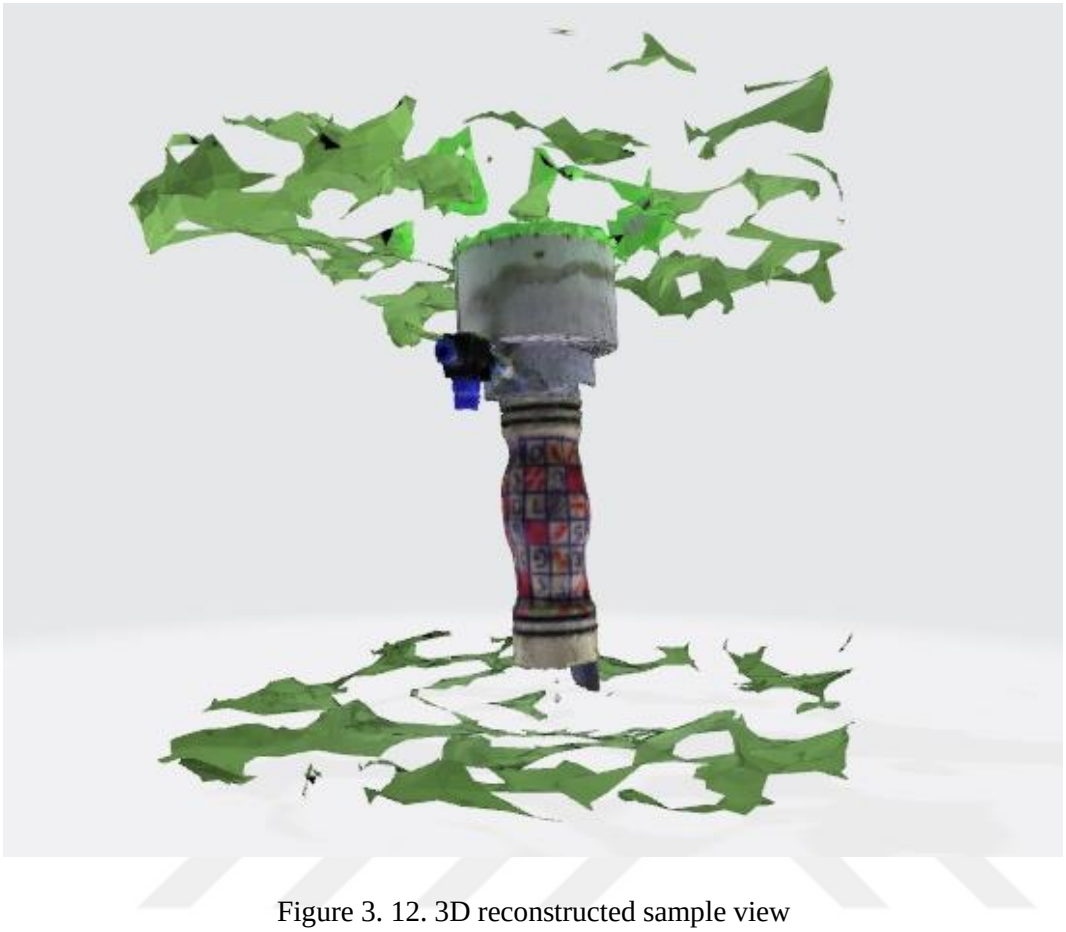

Figure 3. 12. 3D reconstructed sample view

Before explaining the operations performed in Blender, the method and algorithm used by Blender to calculate volume is briefly explained.

Blender primarily relies on algorithms like Poisson Surface Reconstruction when converting point clouds into watertight meshes for volume calculation. The process of turning a point cloud into a watertight mesh is typically done in multiple steps:

1. **Point Cloud Processing**: Initially, the point cloud is cleaned and sometimes down sampled. Blender may use built-in filters to remove noise or outliers.
2. **Poisson Surface Reconstruction:** This is one of the most widely used algorithms for generating a watertight mesh from a point cloud. It works by interpreting the points as samples from an implicit function, then solving a Poisson equation to create a surface that fits the points. This method ensures

the surface is smooth and watertight, which is essential for volume calculations.

3. **Post-Processing:** After initial surface generation, Blender may apply smoothing, remeshing, or decimation to improve the quality of the mesh. This can include converting non-manifold edges into a solid (watertight) structure, which is crucial for accurate volume calculations.

Blender first ensures that the 3D mesh is represented as a series of triangles (a triangular mesh). If the mesh isn't triangulated already, it may automatically convert any polygonal faces (quads or n-gons) into triangles for the volume calculation. For volume calculation to be accurate, the mesh must be watertight, meaning there should be no holes or gaps in the mesh. If the mesh is non-manifold (has open edges or disconnected parts), Blender's volume calculation will either fail or produce inaccurate results.

Tetrahedral decomposition is the key algorithm used for calculating the volume. This method breaks the mesh down into a series of tetrahedrons (pyramids with triangular bases) by connecting the vertices of the triangles to a common reference point (usually the origin of the mesh’s coordinate system). Once the volume of each tetrahedron is calculated, Blender sums up all the individual tetrahedron volumes to get the total volume of the mesh.

In summary, Blender uses a form of tetrahedral decomposition or a similar geometric approach to compute the volume of watertight meshes. This method ensures accuracy as long as the mesh is closed and properly oriented.

At the beginning of the steps explained, first of all the model is initially imported into Blender as a point cloud, indicating it hasn't yet formed a watertight mesh, which is necessary for volume calculation.

- To achieve this, a section with pre-established dimensions is identified on the imported textured mesh. For this purpose, the base of the specimen is chosen. A precise section is then cut and removed from the 3D model of the

base in the software. This extracted section is made watertight (solid) using the remesh function.

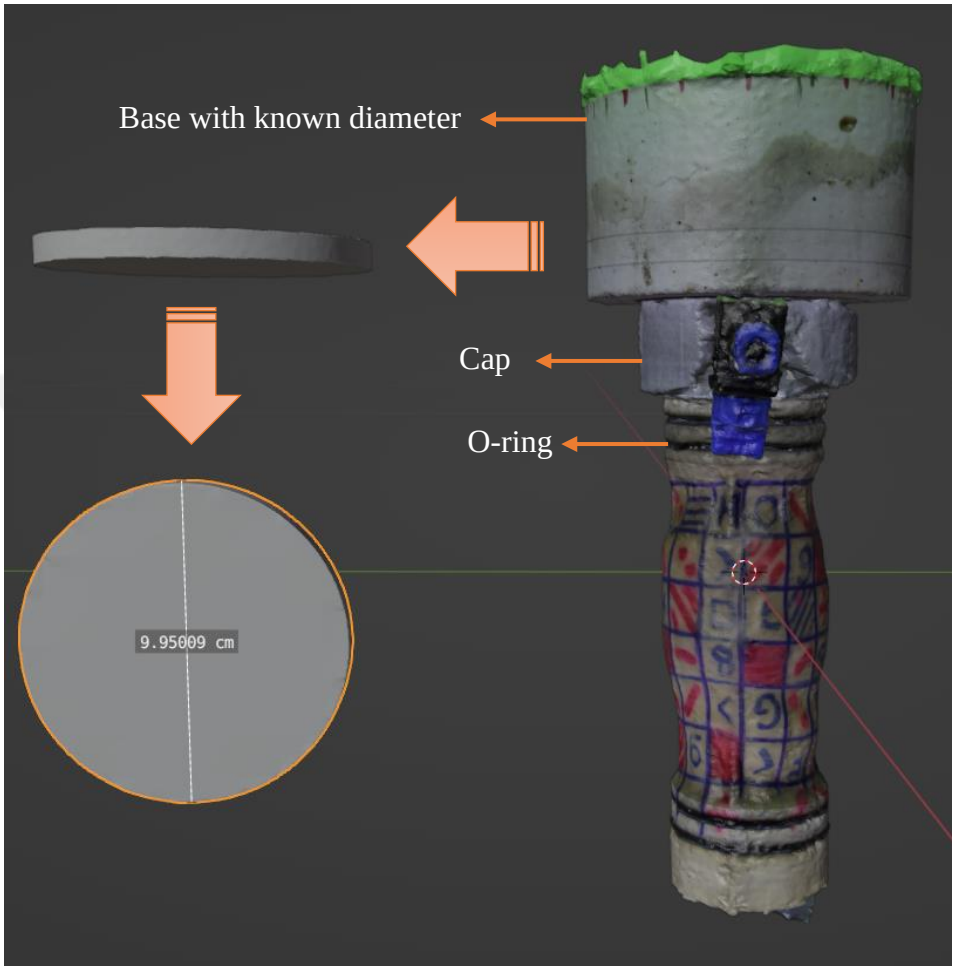

Figure 3. 13. A precise section taken from the base with a known diameter of 9.95 cm used for calibration

- Next, the diameter and dimensions corresponding to the x and z axes of this 3-dimensional circular object are extracted from the model. To ensure accuracy, the actual size of the object is measured with a sensitive micrometer. A scale factor is then derived by dividing the size measurement from the program to the actual size. This scale factor is applied as input to calibrate the 3D model.

- Following calibration, the 3D model is trimmed from specific reference points on the bottom and top caps, leaving only the sample intact. The first o-rings on the caps serve as reference points to cut the sample for consistency. These o-rings are situated in a groove positioned 5.5 mm below the cap top surface and remain fixed in their positions.

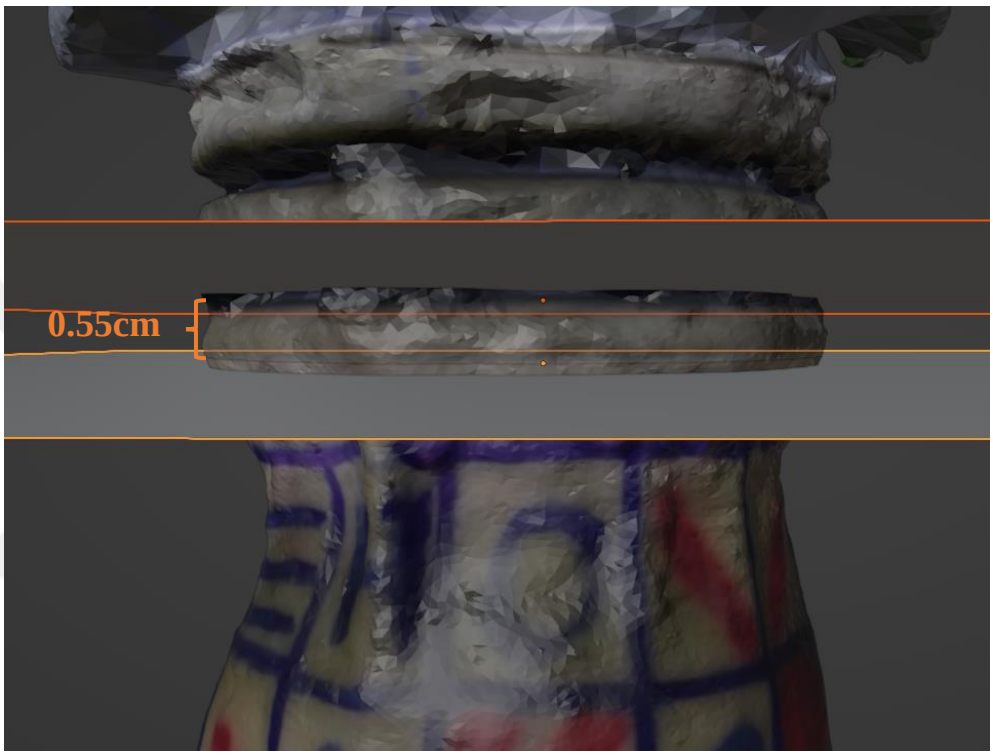

Figure 3. 14. O-ring and offset plate used as reference to take the cross-section of the sample

- Planes are assigned to these reference points, which are then shifted up and down by 5.5mm (previously calibrated). The model is cut along these shifted planes, distinguishing the sample from the cut pieces. The remaining piece now represents a 3D calibrated model of the membrane plus specimen.

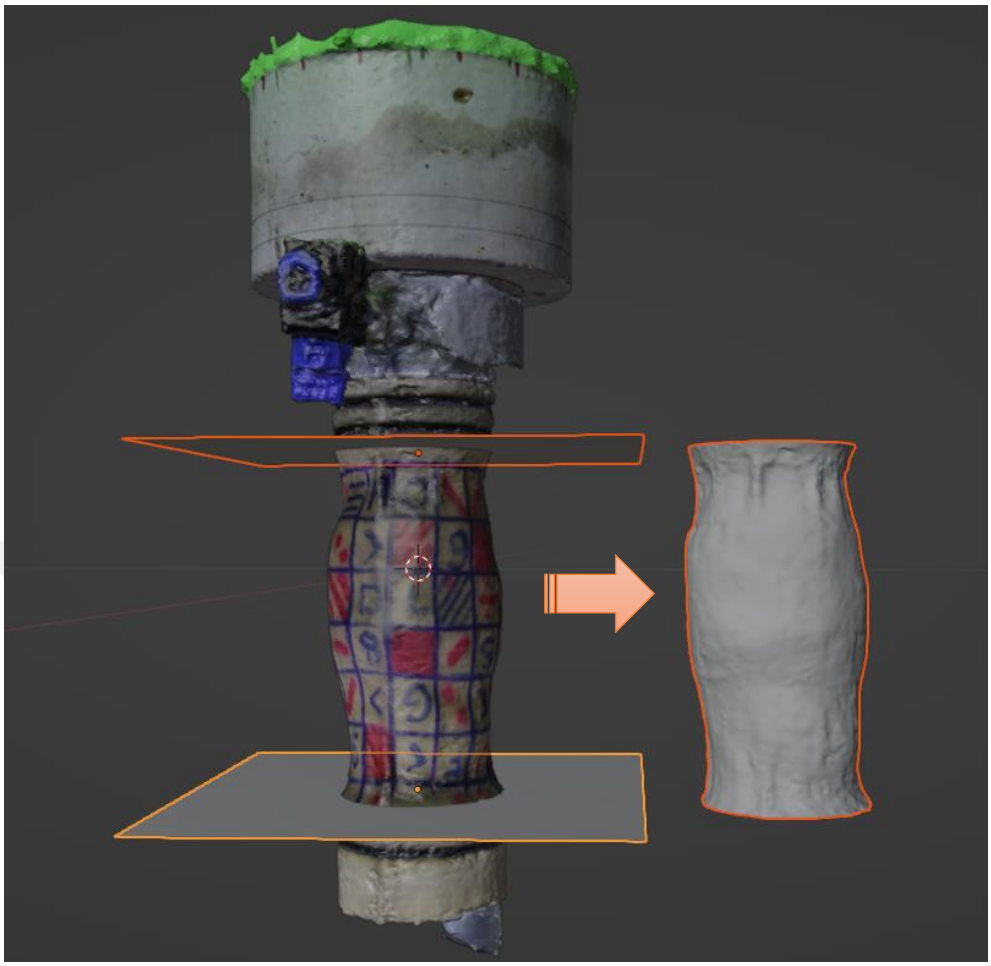

Figure 3. 15. Reference plates assigned to the bottom and top caps and the cut sample

- Subsequently, the separated specimen is converted into a watertight mesh using the remesh function. Finally, utilizing the volume calculation function within the program, the volume of the specimen is determined.

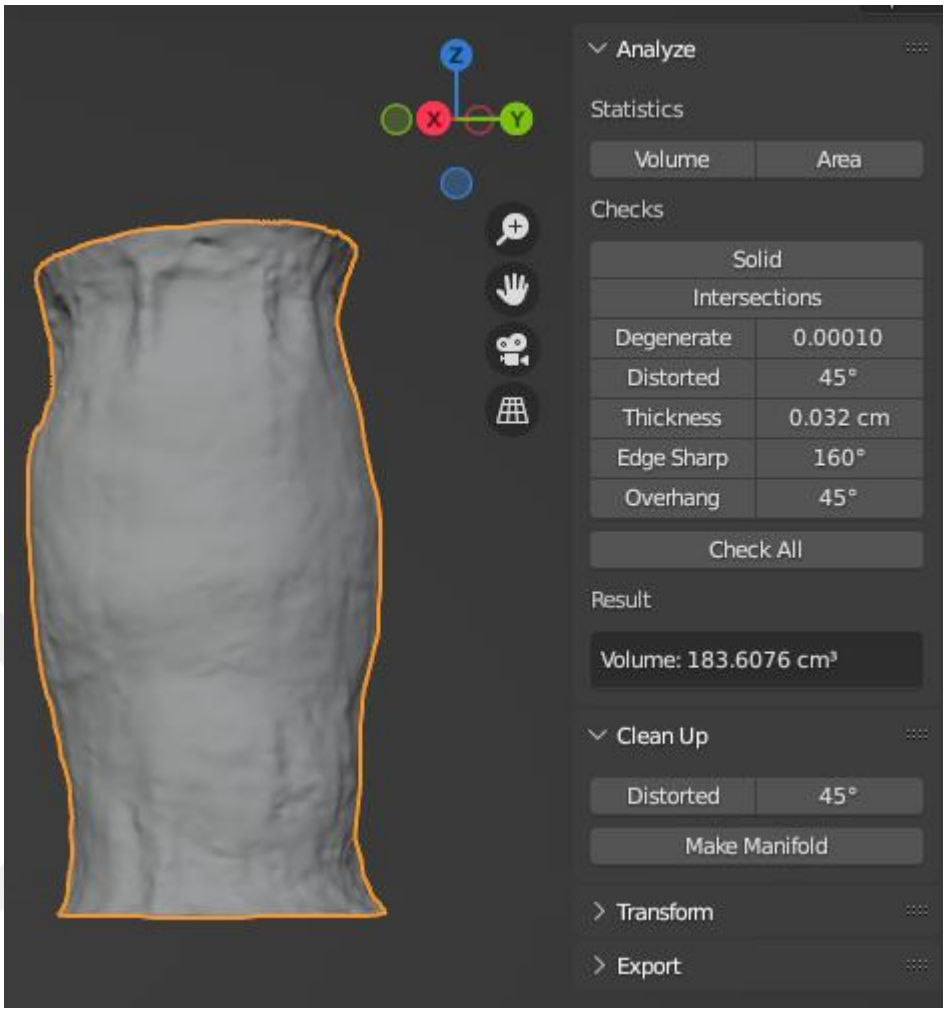

Figure 3. 16. Sample made into a watertight mesh and volume calculation

After all these operations, the following values are obtained for each pressure level:

- M_s: Mass of solids (mass of sand)
- V_{sp}: Volume of the specimen (deformed volume of the specimen with the membrane)

The specific gravity of the specimen is used to determine the exact volume of the solids, V_s (solid volume).

With this information, the void ratio for that pressure level can be calculated: (V_{sp} - V_s)/ V_s (void volume divided by solid volume).

Furthermore, the applied effective pressure information, denoted as p', is obtained from the control unit connected to the vacuum device.

Using these data, the void ratios at the relevant pressure level can be plotted in e-log p' space, thus determining the position of the critical state line.

3.3.6. Angle of Shearing Resistance at the Critical State

To determine the critical state angle of shearing resistance, the methodology outlined in Santamarina and Cho (2001), which is illustrated in figure 3.18 was followed. A plexiglass container with dimensions of 10x20x50 cm was prepared. The sample was poured into the container along with water, filling it to capacity, and the container's mouth was closed by a plate. Afterward, the container was rotated beyond 60°, it was then gradually brought back to vertical. Care was given to minimize excessive movement or shaking during this process to prevent water oscillation.

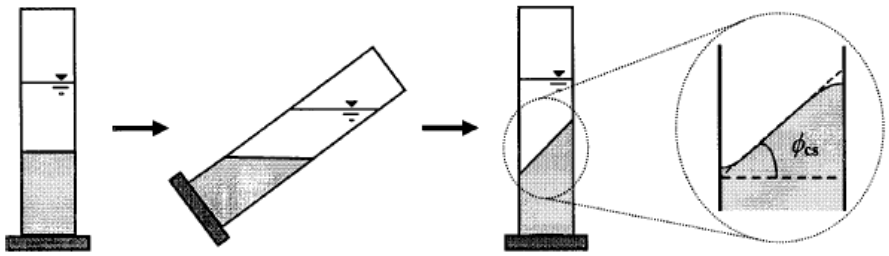

Figure 3. 17. Simplified method to determine the critical state angle of shearing resistance (Santamarina and Cho, 2001)

This test is performed while the sample is submerged water because the sample is poured slowly into the water and the aim is to settle in the loosest form. Once the water stabilized and the sand grains settled, the slope formed by the sand grains from the steepest location was measured, allowing for the determination of the critical state angle of shearing resistance, as shown in figure 3.17.

Figure 3. 18. Critical state angle of shearing resistance experiment performed on Sile Silica sand

While finding the angle of shearing resistance, a photograph looking at the container from the front is taken and a triangle is created with the help of a scaled background and with the help of scaled straight lines the angle is obtained.

CHAPTER 4

TEST RESULTS AND THEIR INTERPRETATIONS

4.1. Introduction

In this chapter, the results of modified simplified critical state tests results are presented and compared with available literature. Besides, laboratory test results for angle of shearing resistance and grain shape are presented for Sabratah Silt, Cine Sand, Sile Silica Sand, Aygaz Alluvial Sand and Tekirdag Silica Sand. Moreover, to investigate the grain size effect on critical state parameters, D_{50}, and C_u values are evaluated. For the grain shape parameters, roundness and sphericity are investigated. Their impacts on the mechanical behavior of the soils are also studied for understanding the soil's structural properties and behavior under different loading conditions. By comparing these findings with existing literature, the aim is to validate the results and contribute to the broader knowledge in soil mechanics and geotechnical engineering from a critical state soil mechanics perspective. The effects of grain size and shape will be investigated in more detail in Chapter 5.

4.2. Modified Simple Critical State Tests and Their Results

In the critical state framework, the parameters, slope (λ_{10}), and intercept (Γ_1, void ratio at p'=1 kPa) of the critical state locus are considered intrinsic properties that remain constant regardless of the soil's state or the boundary conditions it experiences (Yang and Luo, 2015). These values are anticipated to represent the characteristics of the constituent particles, including grain size, distribution, and shape. At this stage, a key question arises: Do the grain size and shape parameters measured at the microscopic level impact the behaviour of the sample at macroscopic scale?

In order to answer this question, an experimental program was prepared consisting of laboratory tests at both macro and micro scale. It cannot be concluded that solely grain size and distribution or only shape parameters influence the intrinsic properties of the soil at critical state. Therefore, experiments were conducted considering both factors. In Chapter 5, an attempt will be made to establish a correlation using both micro and macro data obtained from new laboratory tests and data from available literature.

Five different silt and sand samples were used in laboratory experiments as presented in Table 4.1. On the micro-scale, particle shape was precisely measured using an electronic microscope with 1600x zoom capabilites and roundness and sphericity parameters were calculated separately for each grain which were selected randomly to represent the soil under consideration. On the macro-scale, new modified simplified test procedures, which were discussed in Section 3, were used to assess the critical state locus in the e-log(p′) space and demonstrate that the particle shape and grain size can influence it.

In Table 4.1, the average grain size (D_{50}), coefficient of uniformity (C_u), maximum void ratio (e_{max}), minimum void ratio (e_{min}), roundness (R), sphericity (S), angle of shearing resistance (ϕ'_{cs}), CSL slope (λ_{10}), CSL intercept (Γ_1) parameters of the samples are summarized.

Table 4. 1. Experimental data results

Sample	$D_{50\ (mm)}$	C_u	**R**	**S**	e_{max}	e_{min}	ϕ'_{cs} (°)	Γ_1	λ_{10}
Sabratah Silt			0.48	0.64	1.339	0.74	31.0	1.108	0.0503
Cine Sand	0.38	3.83	0.28	0.58	0.889	0.516	33.0	0.876	0.0490
Sile Silica Sand	0.435	2.5	0.37	0.60	0.706	0.538	33.5	0.644	0.0109
Aygaz Alluvial Sand	0.235	3.33	0.24	0.60	0.934	0.544	31.2	0.884	0.0400
Tekirdag Silica Sand	0.51	1.61	0.25	0.60	0.818	0.580	33.5	0.763	0.0174

As widely known in geotechnical engineering, all soils reach critical state (CS) at high strain levels, regardless of their initial void ratios and stresses, and the drainage conditions adopted during the tests. In the modified simple CS experiments, the volumetric compression of the sample under increasing loads leading to grain rearrangement to form a stable structure which exhibits no further volume change. Consistently, as stresses increase, the data points nearly align with a single straight trendline in the e – log(p') space. The slopes of these best-fit lines were found to vary. Differences in grain shape and size properties led to changes in the slope and intercept of the critical state line.

As discussed by Mesri and Vardhanabhuti (2009), in some fine-grained soil types with a fibrous structure, such as peat, the volumetric decrease produced by the resettlement of grains may also due by bending, twisting, or even compression of the grains themselves. However, due to the stress levels reached in our experiments, which are less than 100 kPa, it is not expected that the grains themselves will experience bending, twisting, or crushing. Therefore, there is no volumetric decrease due to crushing of particles in our experiments. For all soil types, the sample structure evolving to a higher unit weight with increasing compression is possible with the resettlement of the grains after the sliding. Rotational movement triggered after the frictional resistance between the grains has been overcome.

First, on the macro-scale, the behavior of the sample at the same density under different pressure levels is illustrated in the e – log(p') in figure 4.1. The critical state parameters were subsequently obtained. Resulting CS loci are shown in figure 4.2 to figure 4.6.

Contrary to the common simplification and assumption of linearity frequently encountered in the literature, numerous experimental studies show that CS behavior is not linear in the e-log(p') plane.

Note that the experiments in this study were conducted at low stress levels and critical state locus will exhibit a linear behavior, hence grain damage leading to fracture may not be the cause of this slightly nonlinear response. In this context, consistent with eqn. 4-1, assuming that the CS locus is linear, Γ_1 and λ_{10} parameters were evaluated.

$$e = \Gamma_1 + \lambda_{10} \cdot log_{10}(p') \qquad \text{Eqn. 4-1}$$

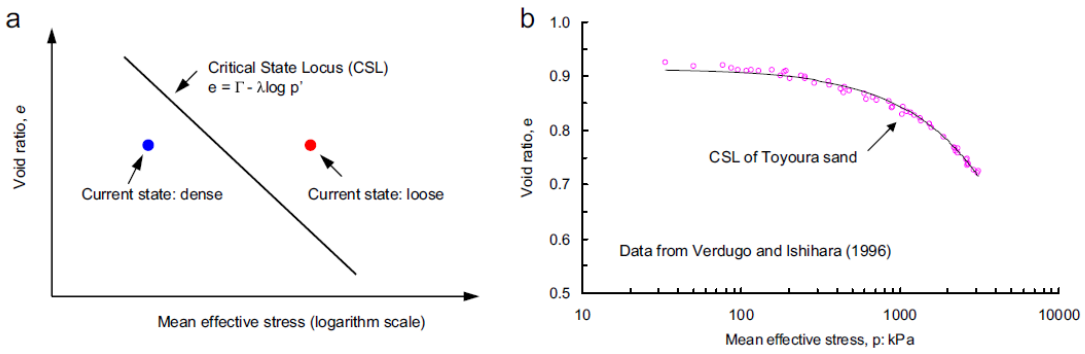

Figure 4. 1. Representation of critical states: (a) in e- log(p') plane as a straight line; (b) in e- log(p') plane as curved line (Yang and Luo, 2015).

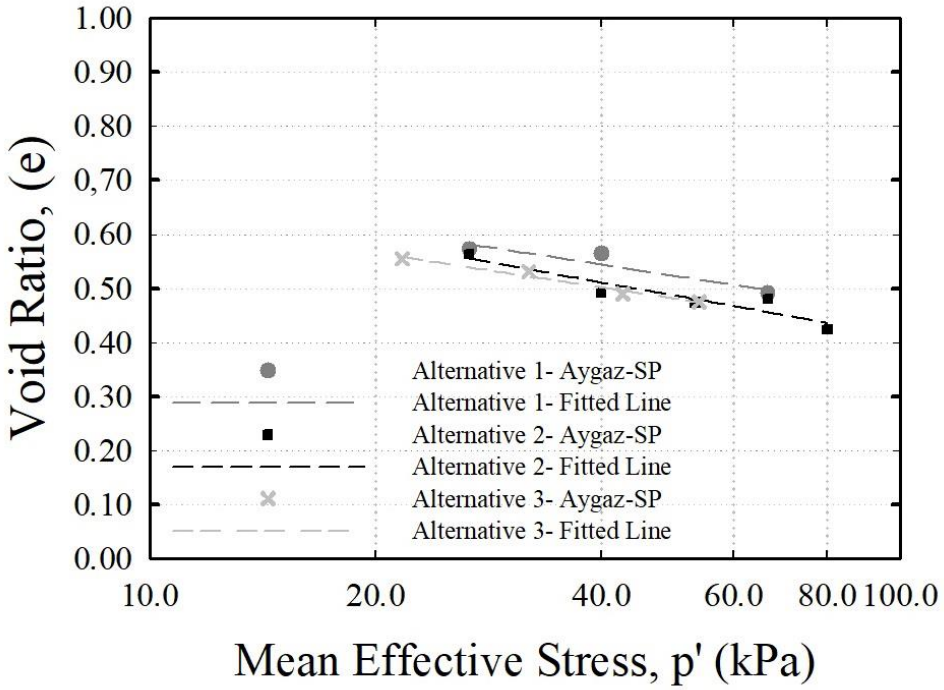

Figure 4. 2. The modified simple CS test results of Aygaz Alluvial Sand

Table 4. 2. The CS test results of Aygaz Alluvial Sand

Test Label	**Γ_1**	**λ_{10}**
Alternative 1- Aygaz SP	0.884	0.040
Alternative 2- Aygaz SP	0.910	0.047
Alternative 3- Aygaz SP	0.841	0.040

Among the presented results, each data set corresponds to a separate experiment. Among the tests conducted at consistent pressure levels, those three test exhibiting the highest R^2 value in the linear regression analysis were chosen as the most representative. The R^2 value, a key indicator of how well the data fits the linear model, was used to determine the accuracy and reliability of each test.

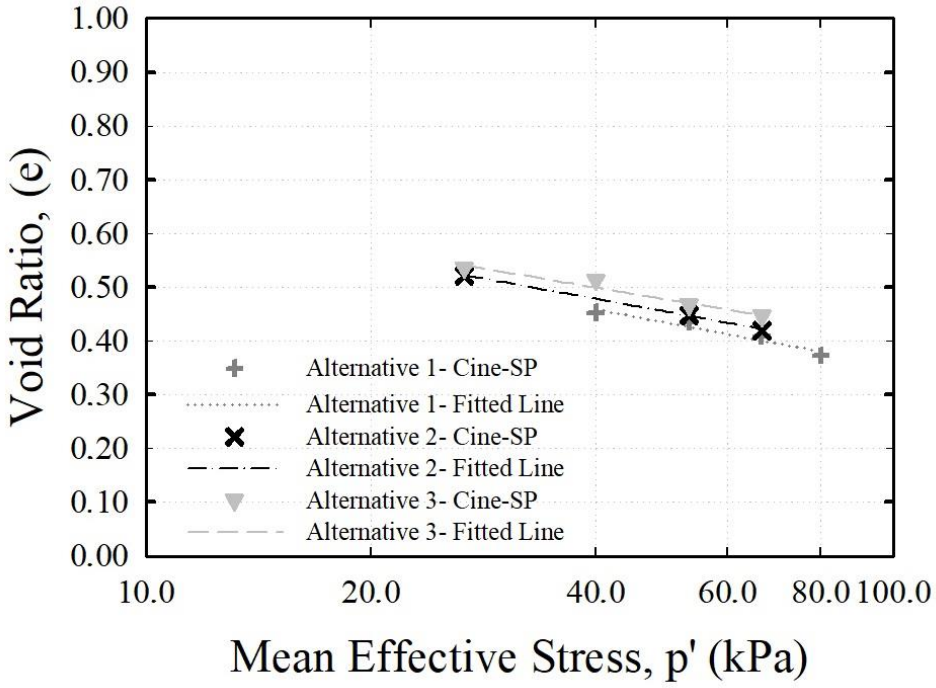

Figure 4. 3. The modified simple CS test results of Cine Sand

Table 4. 3. The CS test results of Cine Sand

Test Label	Γ_1	λ_{10}
Alternative 1- Cine SP	0.876	0.049
Alternative 2- Cine SP	0.884	0.048
Alternative 3- Cine SP	0.875	0.044

In the results shown, each alternative test result represents a separate experiment. Out of all the experiments conducted, the best 3 experimental results and parameters are presented. From these, Alternative 1 was selected as the best fit in the linear regression analysis to represent the critical state parameters for Cine Sand.

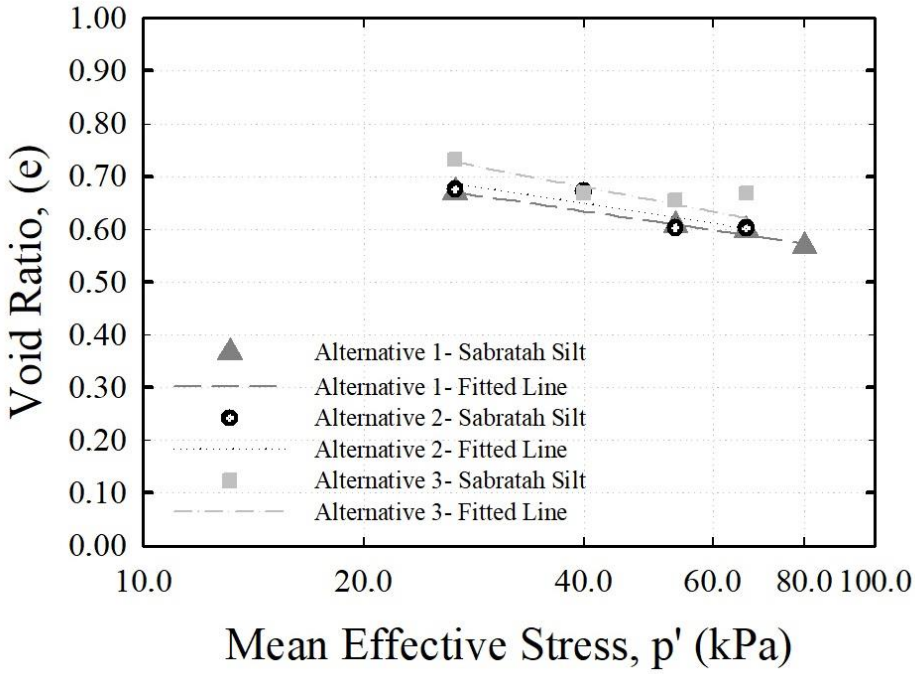

Figure 4. 4. The modified simple CS test results of Sabratah Silt

Table 4. 4. The CS test results of Sabratah Silt Sand

Test Label	**Γ_1**	**λ_{10}**
Alternative 1- Sabratah Silt	0.933	0.039
Alternative 2- Sabratah Silt	0.962	0.040
Alternative 3- Sabratah Silt	1.108	0.050

Among all the experiments conducted, the best three results and their parameters are highlighted. From these alternatives, Alternative 3 was selected as the best fit in the linear regression analysis to represent the critical state parameters for Sabratah Silt.

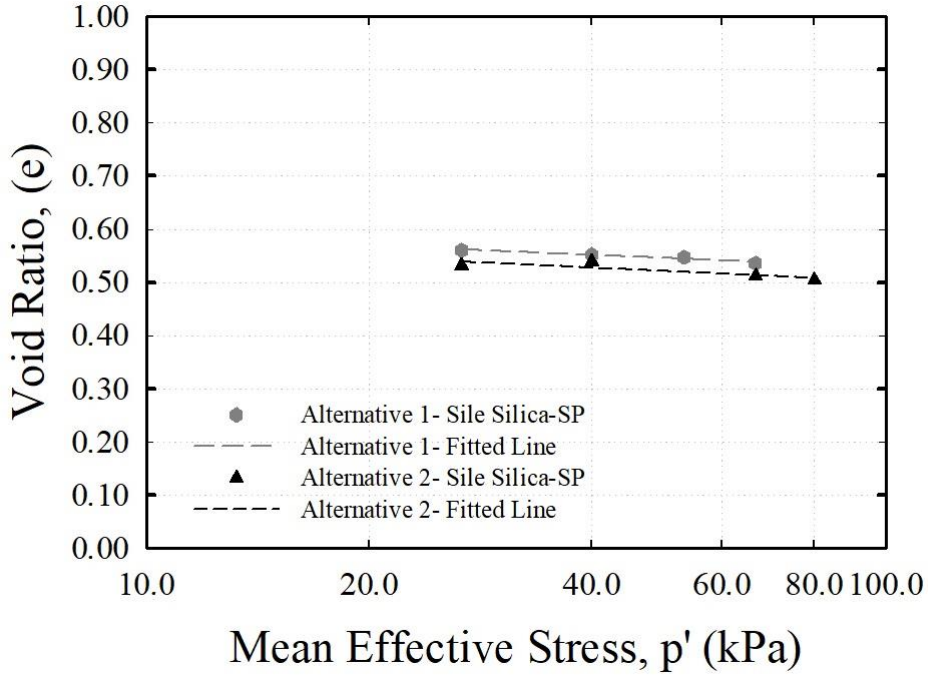

Figure 4. 5. The modified simple CS test results of Sile Silica Sand

Table 4. 5. The CS test results of Sile Silica Sand

Test Label	**Γ_1**	**λ_{10}**
Alternative 1- Sile Silica	0.655	0.011
Alternative 2- Sile Silica	0.642	0.012

Among the two experiments performed on Sile Silica Sand, Alternative 1 was selected as the best fit in the linear regression analysis to represent the critical state parameters for Sile Silica Sand. The experimental results and parameters are presented in Table 4.5.

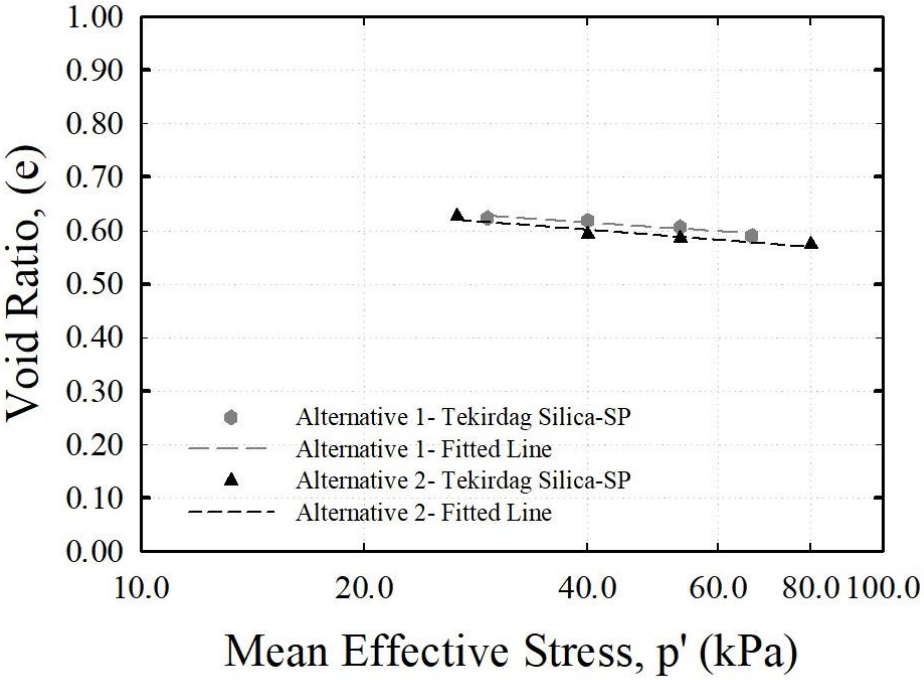

Figure 4. 6. The modified simple CS test results of Tekirdag Silica Sand

Table 4. 6. The CS test results of Tekirdag Silica Sand

Test Label	**Γ_1**	**λ_{10}**
Alternative 1- Cine SP	0.763	0.017
Alternative 2- Cine SP	0.772	0.020

Among the 2 experiments performed on Tekirdag Silica Sand, Alternative 1 was selected to represent the critical state line, and parameters as the best fit in the linear regression analysis. The experimental results and parameters are presented in Table 4.6.

As discussed earlier, all soils reach critical state at high strain levels and the adopted simple CS test procedures fulfill this requirement by reaching axial strain levels of approximately 40 to 50 %. These high strain levels guarantee reaching critical state. In the experiments, samples were prepared as loose as possible. figure 4.7 shows the dense and loose samples after large strains. As shown in this figure loose samples do not exhibit stain localization response. The potential for particle breakage was not an issue due to low confining stresses (<100 kPa), which is significantly lower than the stress level required for particle crushing. Verdugo and Ishihara (1996) conducted triaxial tests on Toyoura sand and reported that particle crushing starts at confining stresses exceeding 4 MPa.

(a) (b)

Figure 4. 7. Deformed shape of samples: (a) Dense sample with shear band formation, (b) loose sample showing bulging response

The applied effective pressure, denoted as p', is obtained from the control unit connected to the vacuum device. At this stage, as a validation step, an additional test was conducted on a sample with the highest λ_{10} value, where the volume changes were relatively more significant.

In the standard test procedure, after the sample is deformed using a hydraulic jack under vacuum, the jack is removed without disconnecting the vacuum, and the valve is closed, leaving the sample exposed only to vacuum pressure to maintain constant effective stress.

After closing the valve, the shape of the sample is slightly adjusted by hand to eliminate shadow effects and capture photos using the photogrammetric method, after which the volume calculation is initiated. At this point, the question arises: does the sample's volume change during reshaping in its final state? If so, an additional test was performed to assess the effect of this change on the critical state position.

In this additional validation test, the sample was similarly deformed using the jack under vacuum. Once deformed, it was reshaped by hand without disconnecting the vacuum. Just before taking the photo for volume calculation, the valve was closed, ensuring that only vacuum pressure was applied to the sample in its final state. The results of this experiment, conducted on Sabratah silt, along with the relevant parameters, are presented as alternative 4 in figure 4.8 and table 4.7.

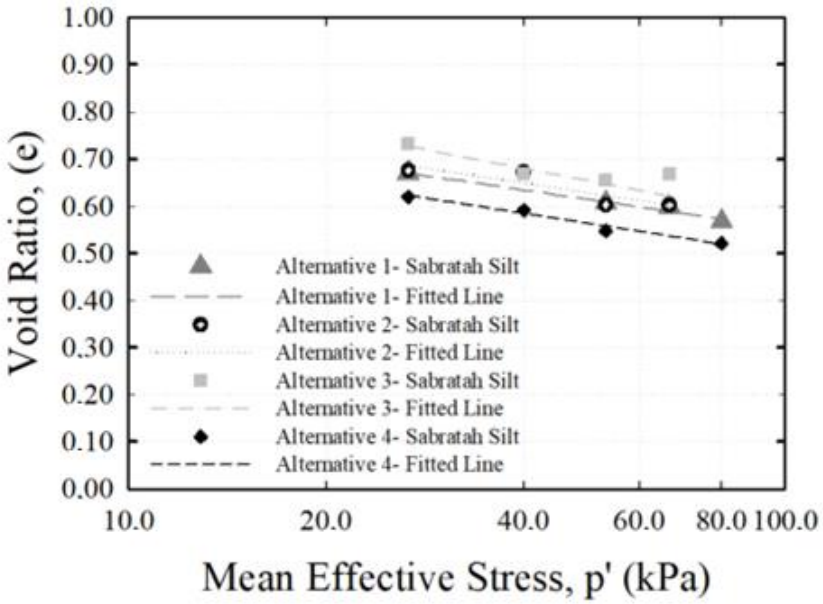

Figure 4. 8. The modified simple CS test results of Sabratah Silt

Table 4. 7. The CS test results of Sabratah Silt

Test Label	**Γ_1**	**λ_{10}**
Alternative 1- Sabratah Silt	0.933	0.039
Alternative 2- Sabratah Silt	0.962	0.040
Alternative 3- Sabratah Silt	1.108	0.050
Alternative 4- Sabratah Silt	0.931	0.041

In previous experiments conducted, once the sample was confirmed to have reached the critical state, it was removed from the hydraulic jack under vacuum, and the valve was closed. During the subsequent reshaping process, in accordance with the critical state definition, it was assumed that the sample, having reached the critical state, would not exhibit any change in volume despite increased deformations. Therefore, the volume was calculated on the basis that no volume change occurred. In the final condition, the average effective stress was determined directly from the control unit.

4.3. Tests for CS Angle of Shearing Resistance

To obtain the angle of shearing resistance at CS, the method proposed by Santamarina and Cho (2001) was utilized. The angle of shearing resistance was checked for repeatability. The test procedure was applied in a specially manufactured transparent container, which was specifically chosen for its visibility. This procedure was used for all silt and sand samples. After placing the container in an upright position, a frontal photograph was taken. The angle of repose was then measured by scaling the photograph and using the scaled lengths.

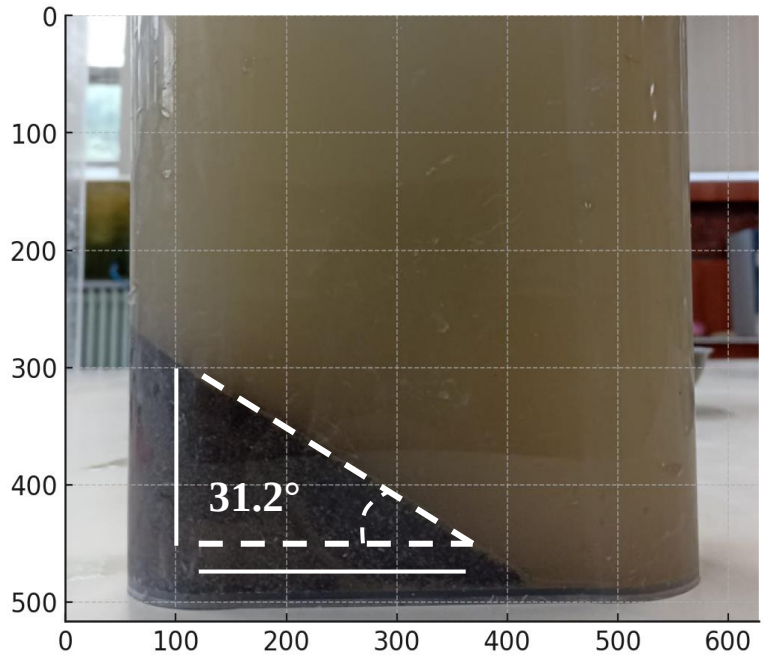

Figure 4. 9. CS Angle of shearing resistance test results of Aygaz Alluvial Sand (ϕ'_{CS} = 31.2°)

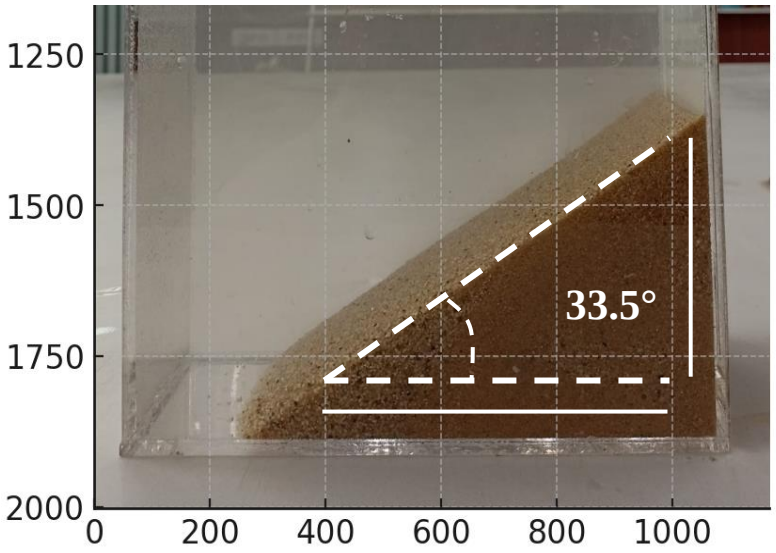

Figure 4. 10. CS Angle of shearing resistance test results of Sile Silica Sand (ϕ'_{CS} = 33.5°)

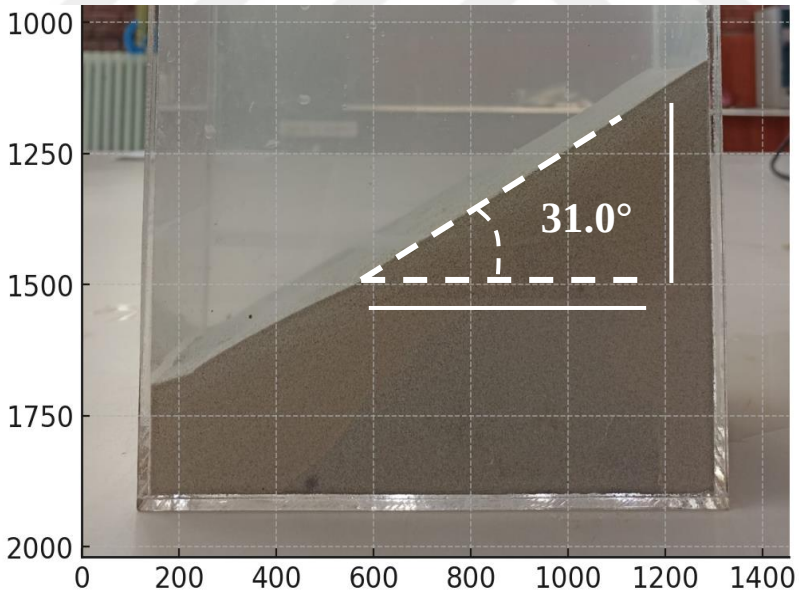

Figure 4. 11. CS Angle of shearing resistance test results of Sabratah Silt (ϕ'_{CS} = 31.0°)

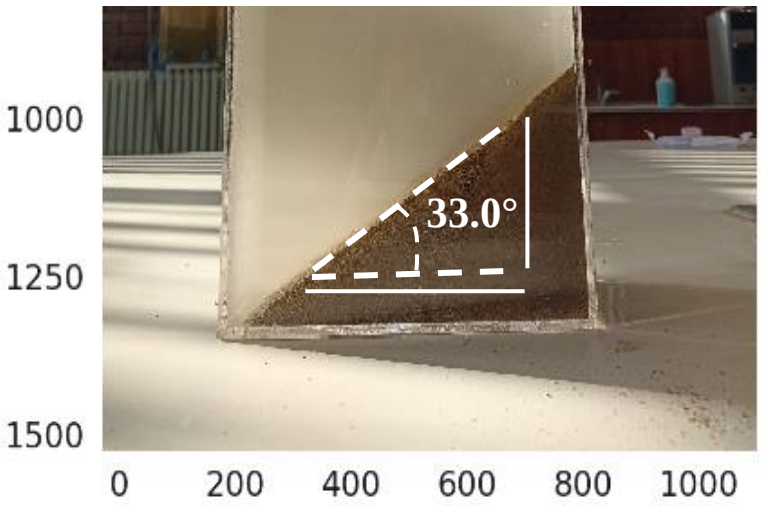

Figure 4. 12. CS Angle of shearing resistance test results of Cine Sand (ϕ'_{CS} = 33.0°)

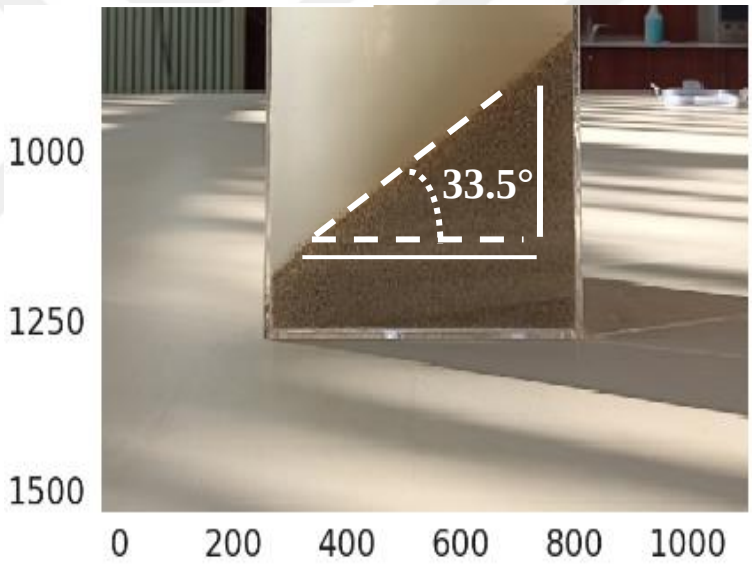

Figure 4. 13. CS Angle of shearing resistance test results of Tekirdag Silica Sand (ϕ'_{CS} = 33.5°)

The results obtained from the experiments for 5 different silt and sand samples are presented in Table 4.7.

Table 4. 8. The results of CS angle of shearing resistance

Sample Type	ϕ'_{CS}
Aygaz Alluvial Sand	31.2°
Cine Sand	33.0°
Sabratah Silt	31.0°
Sile Silica Sand	33.5°
Tekirdag Silica Sand	33.5°

4.4. Tests to Evaluate Particle Shape Parameters

Figure 4. 14. Electronic microscope

An electronic microscope with a zoom capacity of 1600x was used to examine the shape parameters. The images were transferred to a computer and processed using a desktop application. A general view of the magnified particles, obtained with the microscope, is presented in figure 4.14.

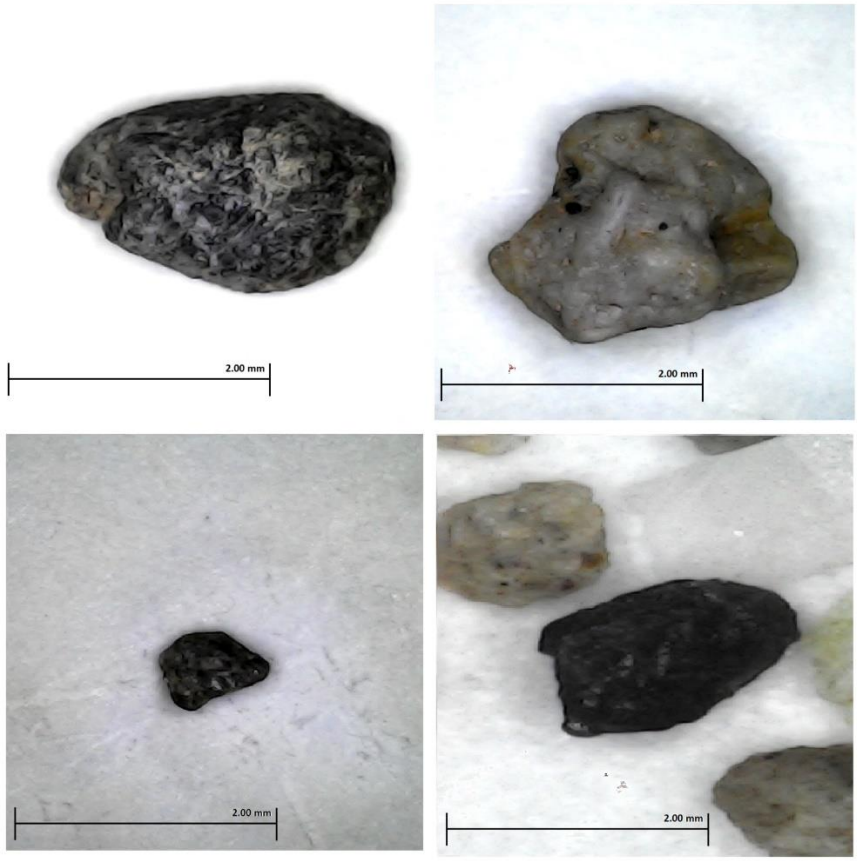

Figure 4. 15. Magnified microscopic vies of Cine Sand grains

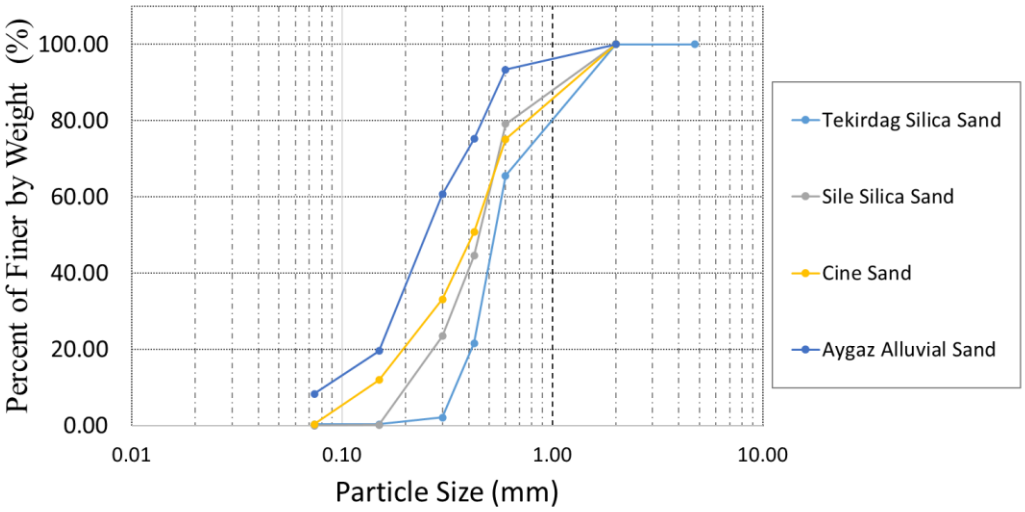

Figure 4. 16. Grain size distribution curves

The grain size distribution curves of the sand samples used in the experiment are given in figure 4.16 After processing the grain images, the roundness (R) and sphericity (S) parameter values representing the sample grains were determined by following the methodology proposed by Cho, Dodds and Santamarina (2006). This technique is a refinement of the original method by Krumbein and Sloss (1963). These parameters are illustrated in figure 4.14, which includes a plot and a particle shape determination chart (as proposed by Krumbein and Sloss (1963)) for visual inspection. The R and S values of each examined grain from the same sample are then represented as a scatter plot in the R-S plane. The arithmetic mean (i.e. centroid) of all values of the same sample is then calculated as the characteristic R and S of that sample.

An example visual and optical measurements of various radii for particle, and the S and R values for all examined grains are shown on separate pairs of figures for each sample (Figures 4.18 to 4.27).

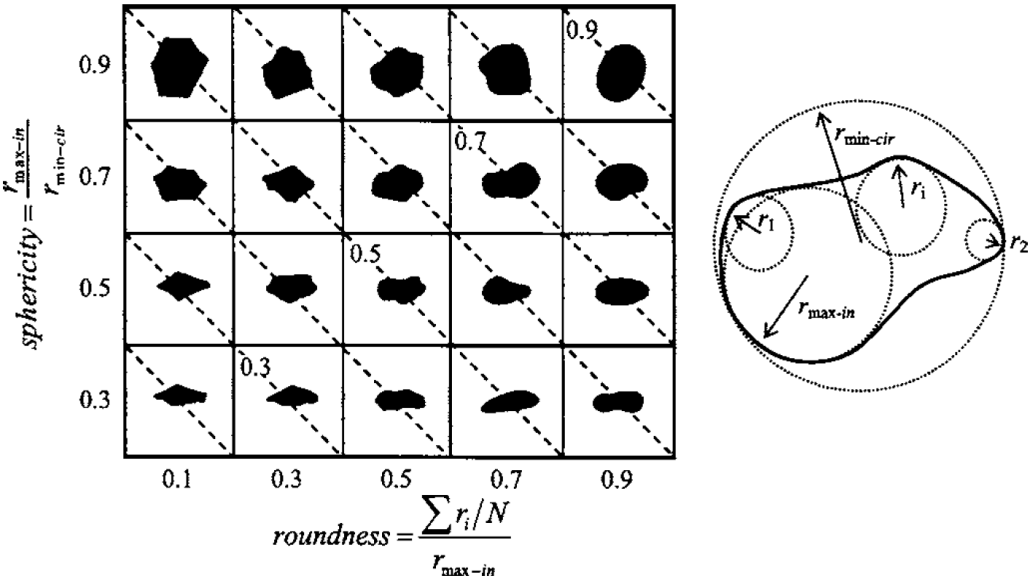

Figure 4. 17. A sketch for sphericity and roundness calculation parameters and particle shape determination chart (Cho et al. 2006)

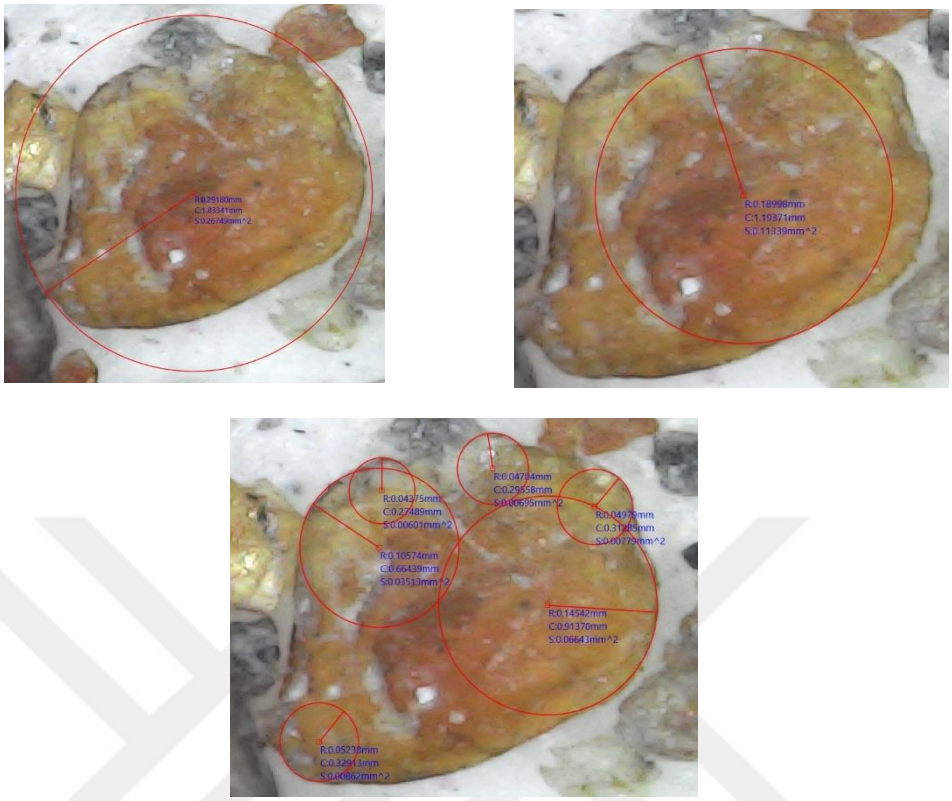

Figure 4. 18. Particle shape analysis test results for Aygaz Alluvial Sand (An example particle representation)

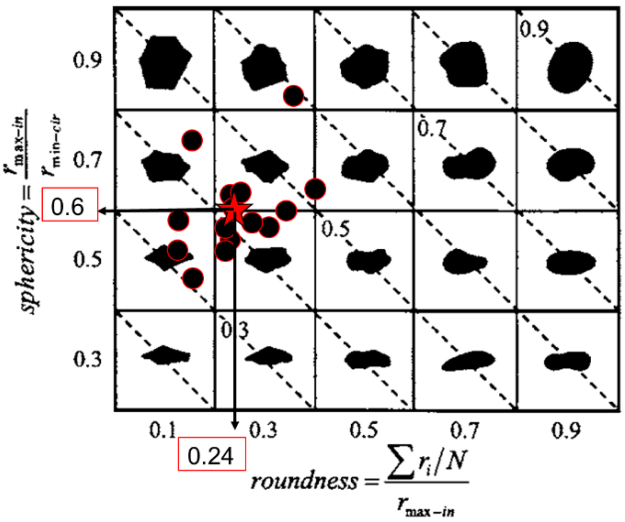

Figure 4. 19. Sphericity and roundness of the inspected Aygaz Alluvial Sand grains (after Cho *et al.*, 2006)

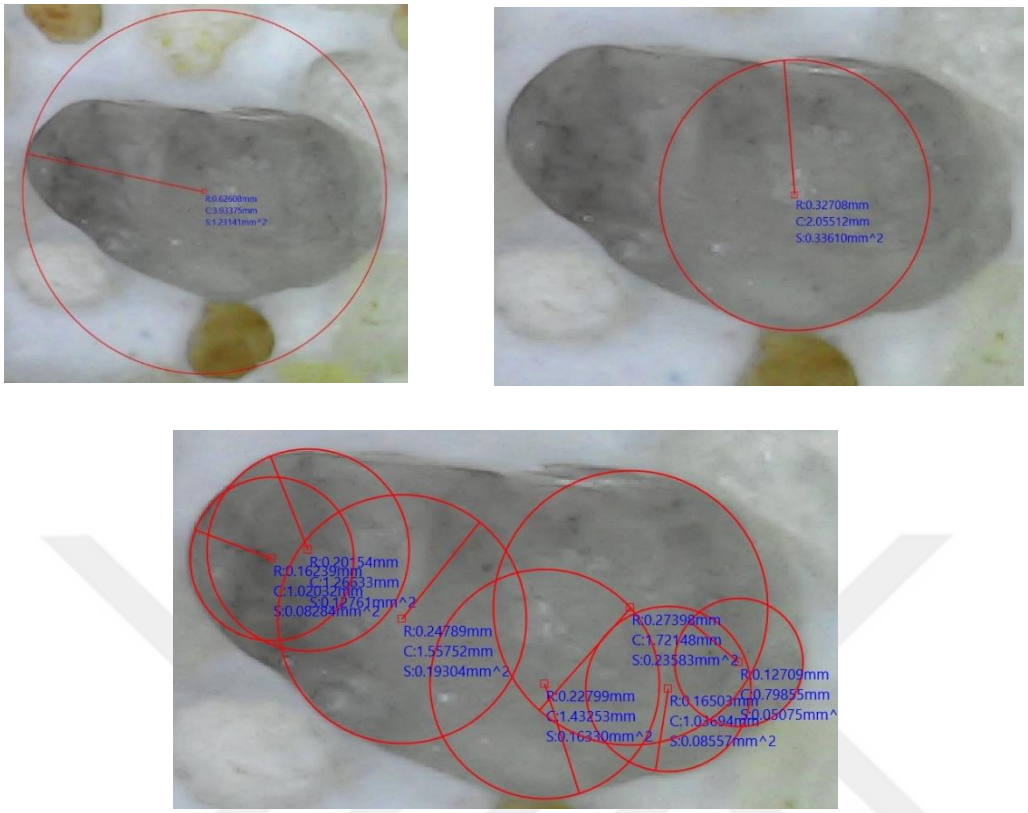

Figure 4. 20. Particle shape analysis test results for Sile Silica Sand – An example particle representation

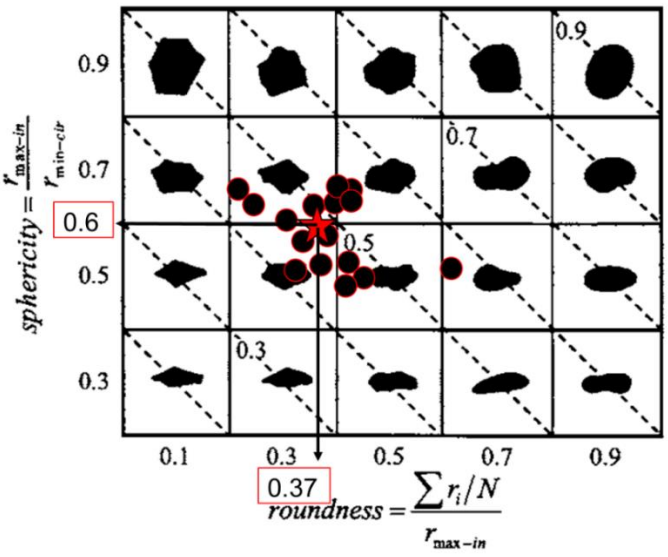

Figure 4. 21. Sphericity and roundness for Sile Silica Sand grains (after Cho et al., 2006)

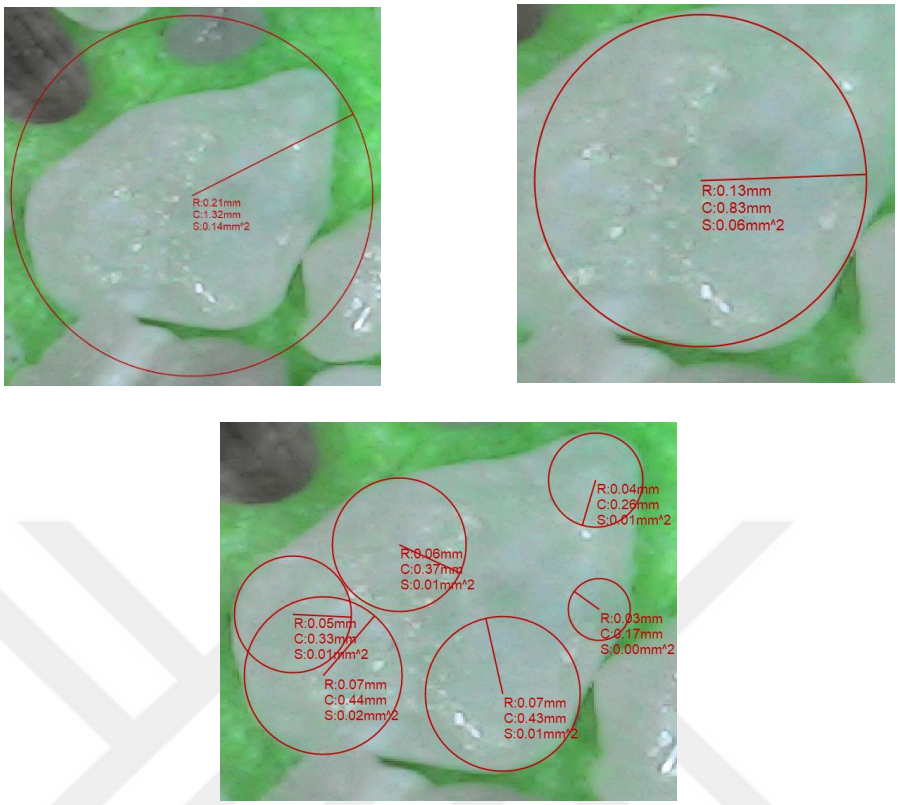

Figure 4. 22. Particle shape analysis test results for Sabratah Silt – An example particle representation

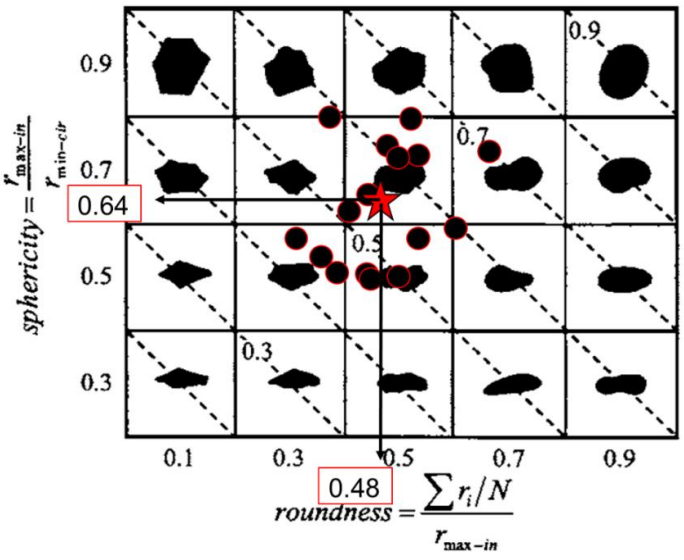

Figure 4. 23. Sphericity and roundness for Sabratah Silt grains (after Cho *et al.*, 2006)

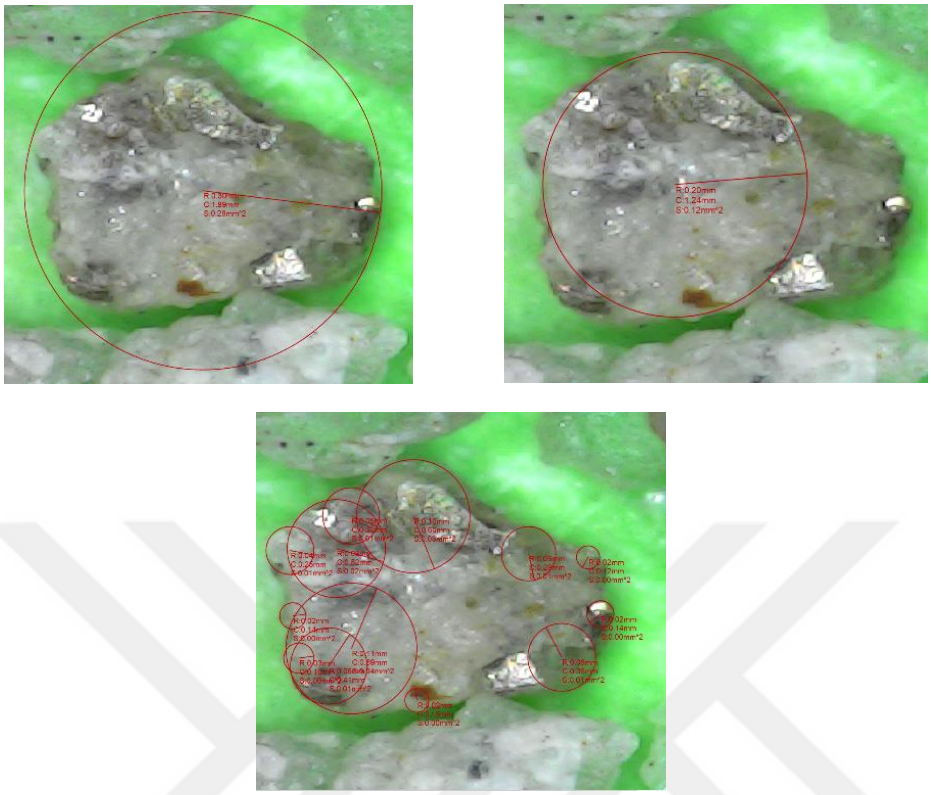

Figure 4. 24. Particle shape analysis test results for Cine Sand – An example particle representation

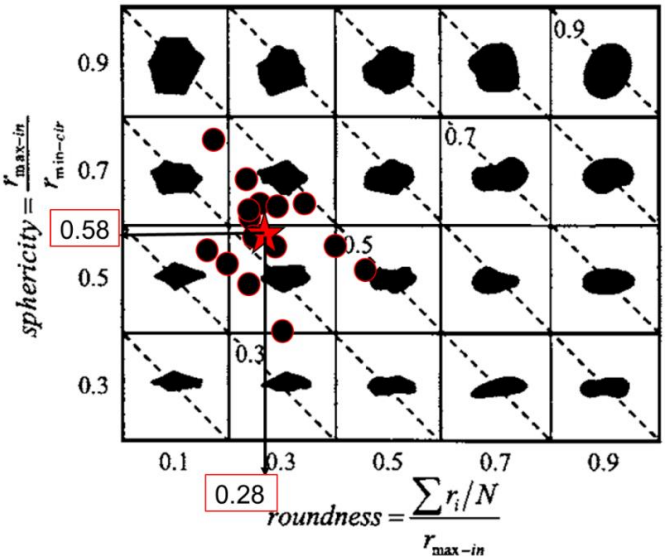

Figure 4. 25. Sphericity and roundness for Cine Sand grains (after Cho et al., 2006)

Figure 4. 26. Particle shape analysis test results for Tekirdag Silica Sand – An example particle representation

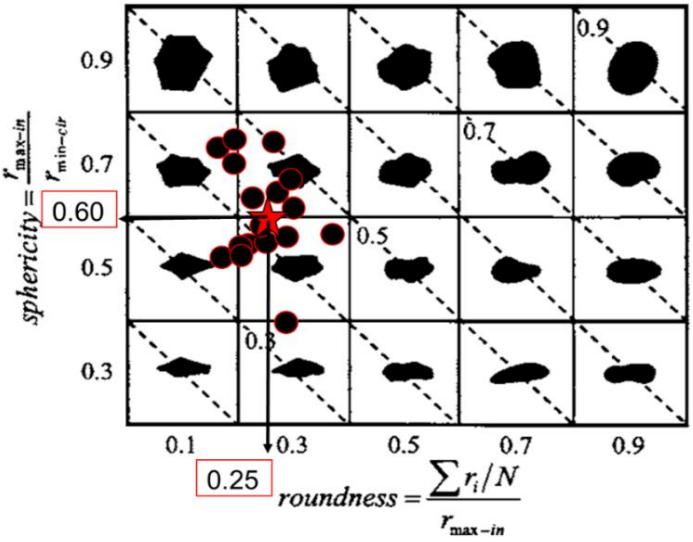

Figure 4. 27. Sphericity and roundness for Tekirdag Silica Sand grains (after Cho *et al.*, 2006)

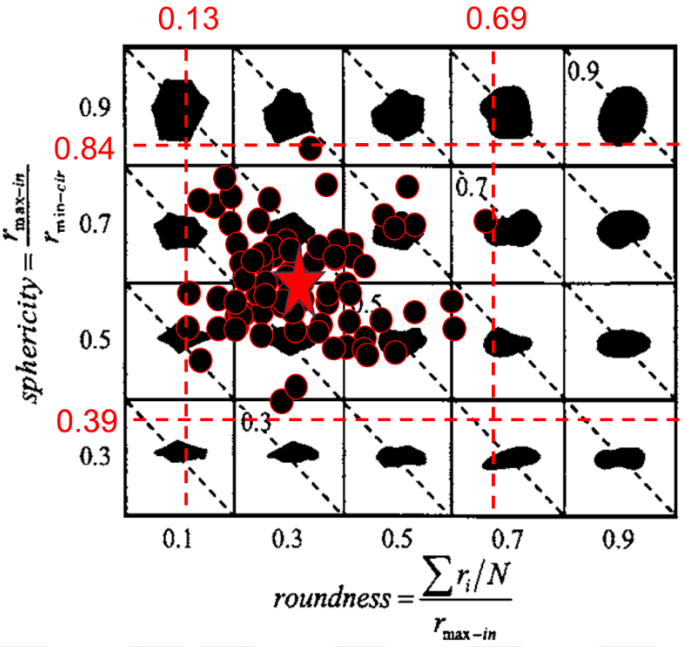

Figure 4. 28. Sphericity and roundness values on sketch for all tested samples

Table 4. 9. The results of tested particle sphericity and roundness

Sample Type	Sphercity, S	Roundness, R	Particle Shape Characteristics
Aygaz Alluvial Sand	0.60	0.24	High Sphericity - Angular
Cine Sand	0.60	0.37	High Sphericity - Sub-Angular
Sabratah Silt	0.64	0.48	High Sphericity - Sub-Angular
Sile Silica Sand	0.58	0.28	High Sphericity - Angular
Tekirdag Silica Sand	0.60	0.25	High Sphericity - Angular

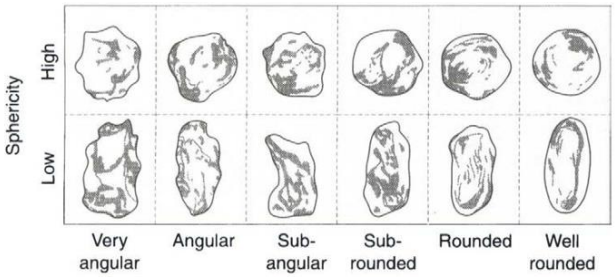

Figure 4. 29. Roundness and sphericity chart for visual assessment (after Powers 1953)

CHAPTER 5

LIMIT STATE MODELS

5.1. Introduction

Within the Critical State framework, the locus parameters, slope (λ_{10}) and intercept (Γ_1) should be regarded as intrinsic properties which do not vary with the state or the boundary conditions under which soil exists (Yang and Luo, 2015). However, the particle size, distribution and grain shape characteristics are expected to affect these parameters. An important question arises here: Do the particle size and shape parameters examined at the microscale affect the sample behavior at the macroscale? It is clear that, the critical state angle of shearing resistance decreases as the roundness increases, indicating an inverse relationship. More details on these relationships between particle shape, size and critical state parameters will be presented in this chapter, together with a summary of available correlations from literature.

5.2. Limit State Models For Critical State Parameters

The mathematical representation of a limit state function typically takes the form g(x, θ), where x denotes the set of defining (input) parameters, and θ represents the set of unknown model coefficients. Considering the previous studies and the observational behaviors determined in the compiled data set and experiments, the main parameters affecting the boundaries and ranges of λ_{10}, Γ_1 and ϕ'_{cs} were determined to be D_{50}, C_u, R, and S.

A total of 775 distinct datapoints were employed to develop the proposed model. The resulting database is given in appendix. To identify the variables which govern critical state characteristics, more specifically, to assess the correlations between dependent variables ϕ'_{cs}, Γ_1 and λ_{10} are plotted against independent variables of mean particle size (D_{50}), coefficient of uniformity (C_u), Roundness (R), and Sphericity (S). These plots are provided in figures 5.1 to 5.3.

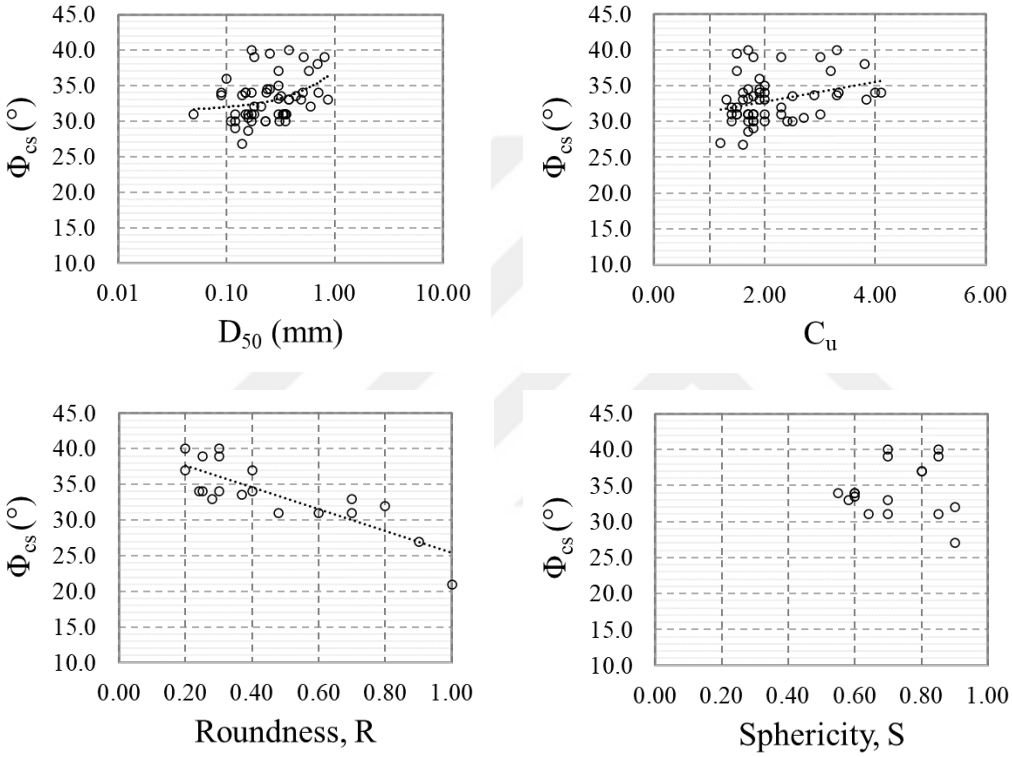

Figure 5. 1. Dependency of ϕ'_{cs} on D_{50}, C_u, R and S

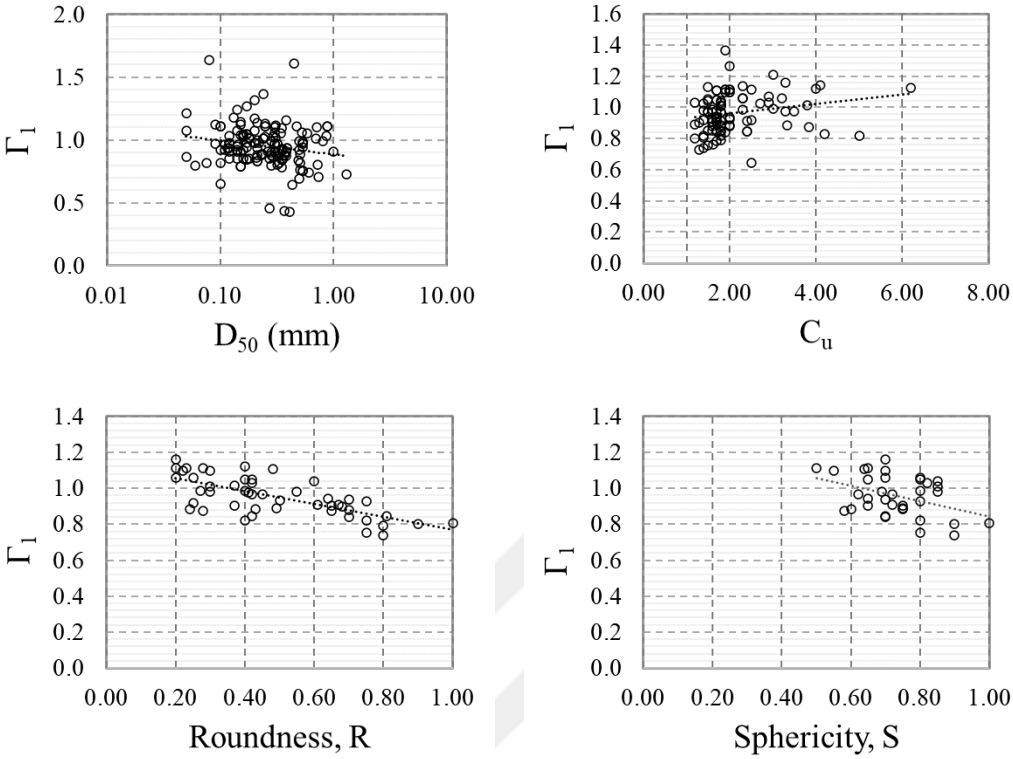

Figure 5. 2. Dependency of Γ_1 on D_{50}, C_u, R and S

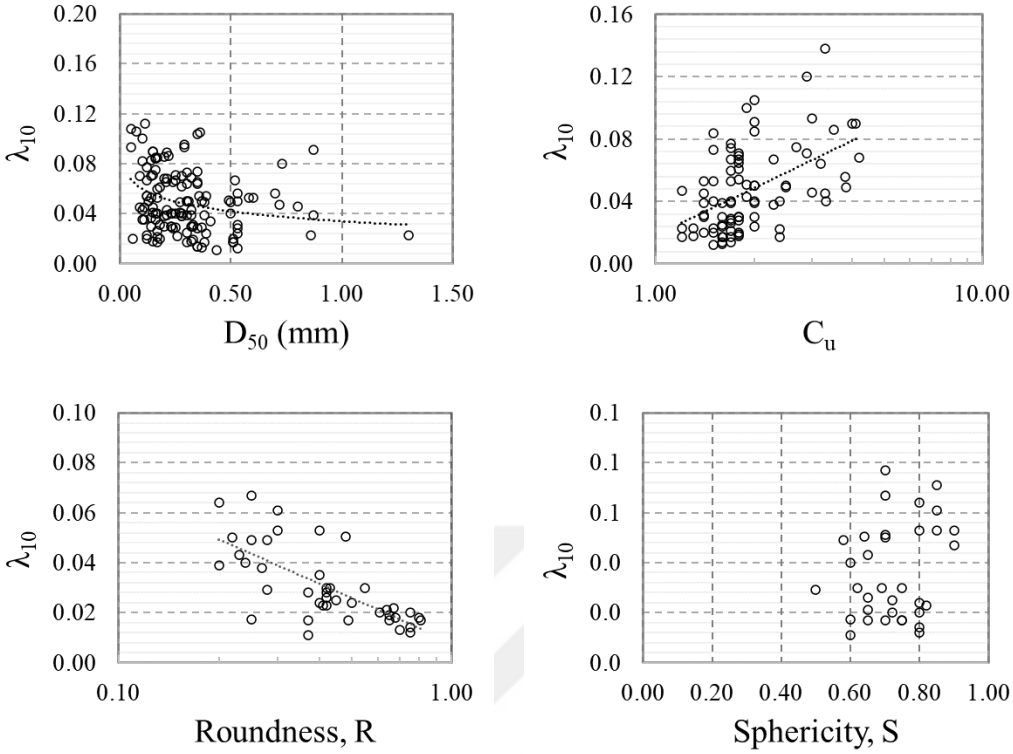

Figure 5. 3. Dependency of λ_{10} on D_{50}, C_u, R and S

Data from both literature and experiments were plotted against critical state parameters to establish a correlation with size and shape parameters. Among the resulting graphs, the model that provided the best fit—whether linear, logarithmic, or polynomial—was selected. The model with the highest correlation coefficient was ultimately preferred, ensuring the most accurate representation of the relationship.Visual inspection of these trends suggest the followings:

- There is log-linear correlation between ϕ'_{cs} and D_{50}, a linear correlation with C_u and R. No correlation was identified with S.
- There is log-linear correlation between Γ_1 and D_{50}, a linear positive correlation with C_u and a linear negative with R. This inverse relationship highlights the significance of particle shape on the parameter Γ_1. Moreover, a linear correlation with S is observed.

- A linear correlation between λ_{10} and D_{50} is observed. Moreover, a strong positive logarithmic correlation with C_u is identified, suggesting that λ_{10} increases as C_u increases. This indicates that as soil becomes more uniform λ_{10} increases. Conversely, a strong negative logarithmic correlation with R is noted, demonstrating that as the roundness of particles increases, λ_{10}

decreases. This highlights the significant impact of particle shape on λ_{10}. No distinct correlation is observed between S and λ_{10}.

Inspired from these observations, and after trying several functional forms, the limit state functions, g( ), given in Equations 5-1, 5-2, and 5-3 are selected as the most appropriate models for ϕ'_{cs}, Γ_1 and λ_{10},

$$g_1(\phi_{cs}, D_{50}, C_u, R, \theta_1) = \phi_{cs} - \ln(D_{50}) - C_u - R + \theta_1 \pm \varepsilon_1 = 0 \quad \text{Eqn. 5-1}$$

$$g_2(\Gamma_1, D_{50}, C_u, R, S, \theta_2) = \Gamma_1 - \ln(D_{50}) - C_u - R + S + \theta_2 \pm \varepsilon_2 = 0 \quad \text{Eqn. 5-2}$$

$$g_3(\lambda_{10}, D_{50}, C_u, R, \theta_3) = \lambda_{10} + D_{50} + \ln(C_u) - \ln(R) + \theta_3 \pm \varepsilon_3 = 0 \quad \text{Eqn. 5-3}$$

These forms not only exhibit the necessary functional flexibility to replicate observational trends but also demonstrate higher overall likelihood sums, signifying a statistically superior fit to the dataset. However, it is important to note that Equations 5-1 to 5-3 include a random model correction term (ε) that varies for each model. This term takes into account: i) the potential existence of unobserved explanatory variables and ii) the possibility that the mathematical expression adopted may not have an ideal functional form. It is both reasonable and appropriate to assume that ε follows a normal distribution with zero mean, because it aims to produce an unbiased model (Cetin, 2000).

By adopting maximum likelihood assessment framework, the detials of which are discussed elsewhere (Cetin, 2000, Bouanger and Idriss, 2012), the model coefficients are estimated. The resulting probabilistic predictive models are given in Equation 5-4 through 5-6.

$$\phi'_{cs} = -0.773 \cdot \ln(D_{50}) - 0.826 \cdot C_u - 16.868 \cdot R + 42.621 \pm 2.436 \quad \text{Eqn. 5-4}$$

$$\Gamma_1 = -0.062 \cdot \ln(D_{50}) - 0.002 \cdot C_u - 0.324 \cdot R + 0.038 \cdot S + 1.003 \pm 0.096 \quad \text{Eqn. 5-5}$$

$$\lambda_{10} = 0.140 \cdot D_{50} + 0.037 \cdot \ln(C_u) - 0.028 \cdot \ln(R) - 0.046 \pm 0.089 \quad \text{Eqn. 5-6}$$

The residuals of the models, which are defined as the difference between the predicted and measured value, are shown in figures 5.4 through 5.6. Mean residuals spreading around zero suggest that the models are unbiased. Also, the wide scatter in the difference between model and test values is indicative of highly variable critical state responses for D50, Cu, R and S.

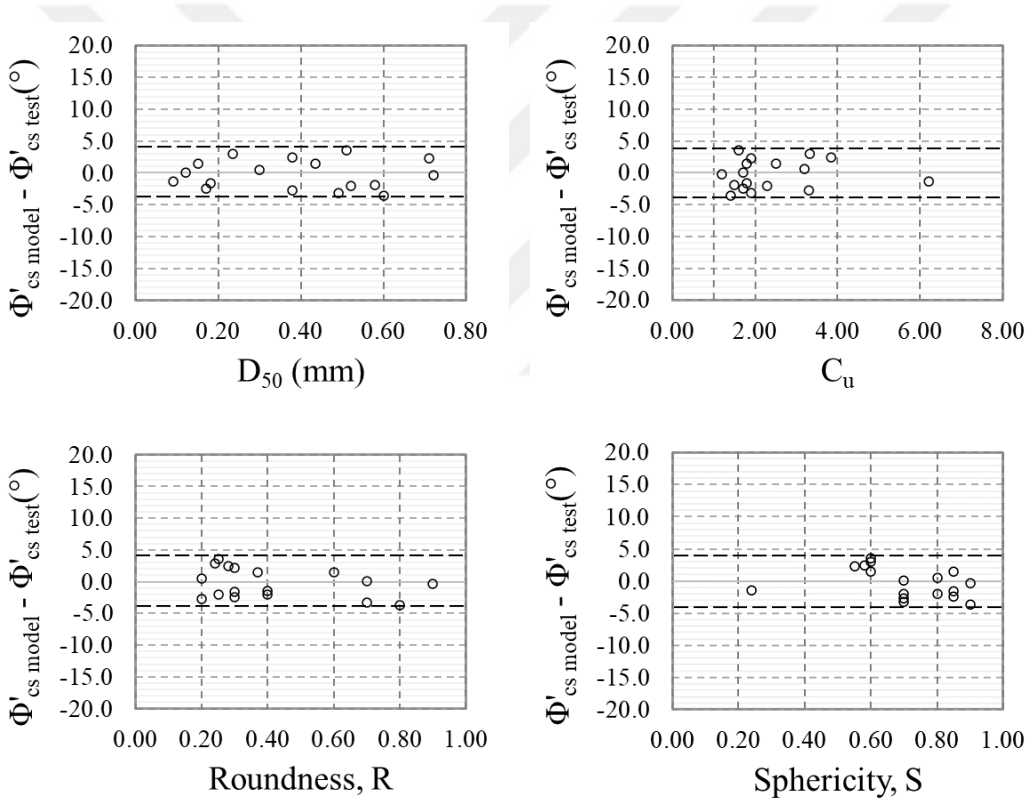

Figure 5. 4. Residuals of ϕ'_{cs} vs. D_{50}, C_u, R and S

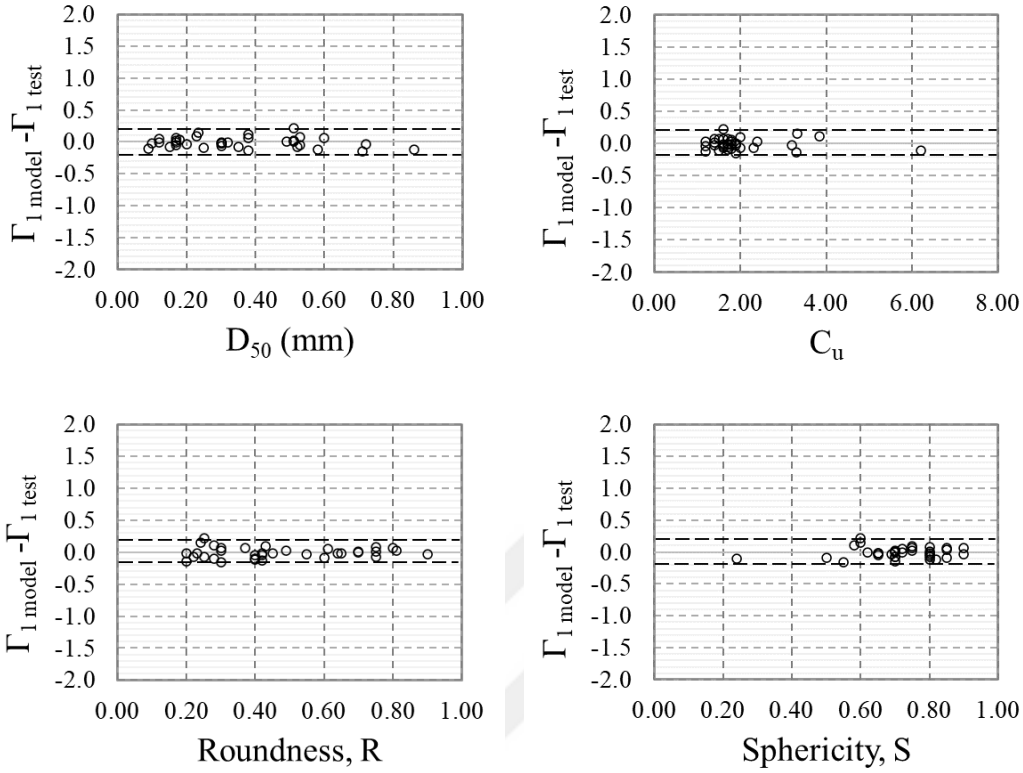

Figure 5. 5. Residuals of Γ_1 vs. D_{50}, C_u, R and S

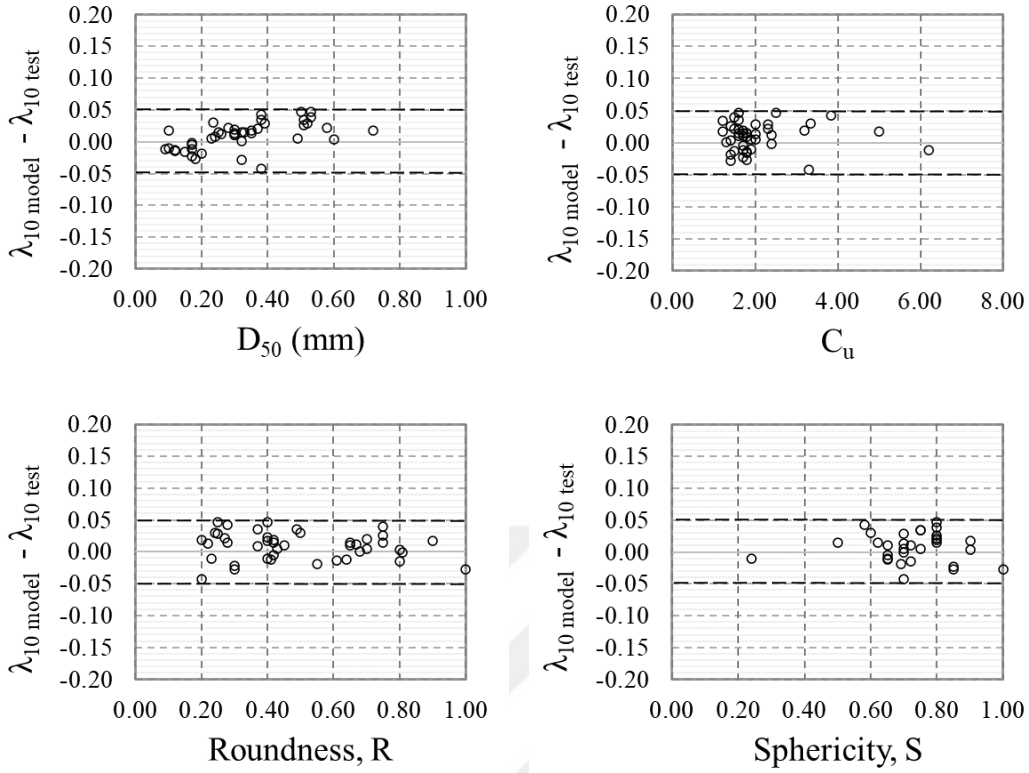

Figure 5. 6. Residuals of λ_{10} vs. D_{50}, C_u, R and S

Upon reviewing the data sets utilized in constructing the model, as well as the input parameters from the samples used in the experiments, it is evident that the model's applicability is confined to specific parameter ranges found in the literature. The model demonstrates validity within the following intervals:

D_{50}: 0.4 mm – 1 mm

C_u: 1 – 6.5

R: 0.2 – 1

S: 0.4 – 1

These ranges indicate the model's robustness in capturing the relevant characteristics of the system under study, and its accuracy may diminish when applied beyond these bounds. Consequently, the model should remain within these established limits to ensure reliable outcomes.

CHAPTER 6

SUMMARY AND CONCLUSIONS

6.1. Summary

In the scope of this study, the critical state characteristics of some silt and sands were evaluated. For this purpose, the simplified critical state test apparatus developed by Santamarina and Cho (2001) was employed. Due to various challenges encountered during the experimental procedures, the apparatus was modified by an innovative approach. This modification allowed for reasonably accurate determination of the critical state locus in the e-log(p') space, more specifically the slope (λ_{10}) and the intercept (Γ_1) parameters of it.

To comprehensively investigate the effects of grain size, distribution, and shape characteristics of soils and grains on the critical state locus, micro-level (granular) analyses were conducted on these silt and sand samples. These analyses employed a similarly innovative and practical method. An electronic microscope with a zoom capacity of 1600x was utilized to determine the grain shape parameters, following the methodology proposed by Cho, Dodds, and Santamarina (2006). This method provided detailed and accurate images essential for the analysis.

Furthermore, the method outlined by Santamarina and Cho (2001) was used to determine the angle of shearing resistance (ϕ'_{cs}) values. This approach ensured that the obtained values were consistent and reliable for further analysis.

Upon completing these experimental processes, the data from existing literature were also compiled. This comprehensive dataset was then analyzed to identify potential correlations between the grain shape and size parameters and the critical state parameters. Predictive models were developed employing the parameters that

exhibited significant correlation with λ_{10} and Γ_1 and ϕ'_{cs}. A probability-based model was developed benefitting from resulting limit state models. These models are shown to produce unbiased estimates of λ_{10} and Γ_1 and ϕ'_{cs} as functions of D_{50}, C_u, R and S, providing a robust framework for understanding the interactions between grain characteristics and critical state parameters.

6.2. Conclusion

Within the scope of this research study, an experimental assessment to explore the interconnections between critical state parameters and the morphological characteristics, size, and distribution properties of particles, aiming to deepen the fundamental comprehension of granular soil mechanics was employed. For this purpose, a series of tests was performed on five silt and sand samples, which are summarized again in Table 6.1

Table 6. 1. Experimental results for 5 silt and sand samples

Sample	**D_{50} (mm)**	**C_u**	**R**	**S**	**e_{max}**	**e_{min}**	**ϕ'_{cs} (°)**	**Γ_1**	**λ_{10}**
Sabratah Silt			0.48	0.64	1.339	0.74	31.0	1.108	0.0503
Cine Sand	0.38	3.83	0.28	0.58	0.889	0.516	33.0	0.876	0.0490
Sile Silica Sand	0.435	2.5	0.37	0.60	0.706	0.538	33.5	0.644	0.0109
Aygaz Alluvial Sand	0.235	3.33	0.24	0.60	0.934	0.544	31.2	0.884	0.0400
Tekirdag Silica Sand	0.51	1.61	0.25	0.60	0.818	0.580	34.0	0.763	0.0174

The principal outcomes and findings of this research are summarized as follows:

- The critical state angle of shearing resistance ϕ'_{cs} decreases with increasing particle roundness (R). This conclusion is consistent with the findings of Cho et al., 2006; Rouse et al., 2008.

- When compared to correlations established for the other shape parameter: sphericity, the roundness demonstrates a significantly stronger correlation.
- While not as robust a correlation as roundness, the coefficient of uniformity (C_u) and the mean grain size (D_{50}) also impact ϕ'_{cs}.
- An increase in C_u correlates with an increase in ϕ'_{cs}.
- The relationship between ϕ'_{cs} and particle shape suggests that the volumetric change of granular material under shearing is affected by both interparticle friction—largely governed by particle mineralogy and surface roughness—and particle rearrangement.
- As a result, particles that are regular and rounded with high roundness values (R) tend to move and slip more easily by rotation under shearing as compared to irregularly shaped angular particles with lower roundness values, thereby exhibiting lower shear resistances (Yang and Luo, 2015).
- The correlations between the intercept of the critical state line (Γ_1) and shape parameters, including mean grain size (D_{50}), coefficient of uniformity (C_u), roundness (R), and sphericity (S), were also examined.
- The findings indicate that Γ_1 exhibits a reasonably strong correlation with these shape parameters, showing a linear decrease as roundness (R) and sphericity (S) increase.
- Among these parameters, Γ_1 has the strongest correlation with roundness. The model equation for Γ_1 is presented in Equation 5-5. Within critical state theory, the intercept of the critical state line in the volumetric compression space signifies the maximum void ratio that the material can achieve under conditions of extremely low mean effective stress.
- The values of the CSL slope (λ_{10}) for the tested samples, along with those compiled from the literature, were plotted against the grain shape and size parameters. A reasonably strong correlation was found between λ_{10} and roundness, with a notable decrease in λ_{10} observed as roundness increased.
- The CSL slope indicates the material's compressibility; a higher slope suggests higher compressibility. Round particles, due to their ability to move

more efficiently under loading, tend to form a denser packing state, resulting in lower compressibility compared to irregular and angular particles. This trend explains why both Γ_1 and λ_{10} increase with increasing particle uniformity.

- Conversely, granular materials with irregular and angular particles exhibit higher compressibility (larger λ_{10}). These tests also demonstrate that the CSL slope (λ_{10}) is not significantly affected by changes in grain size but is directly related to the coefficient of uniformity (C_u). Additionally, no strong correlation was observed with another shape parameter, sphericity. The model equation for λ_{10} is provided in Equation 5-6.

Importantly, as the concluding remark, the findings of this study reveal that critical state parameters are highly sensitive to changes in particle shape, grain size, and distribution.

6.3. Future Studies

In this study, the results of modified simplified critical state tests were presesnted, including parameters related to grain shape, size, and distribution. To verify the uniqueness of these parameters, it is recommended to employ similar tests through conventional triaxial, simple shear, or torsional shear experiments, in conjunction with Scanning Electron Microscope (SEM) imaging for determination of grain shape parameters.

To enhance the consistency of the experimental outcomes and improve the model, increasing the number of tested samples is advisable. This approach would facilitate the creation of a database that is internally consistent, eliminating the need for integrating disparate datasets.

Additionally, the utilization of more advanced equipment, such as high-resolution cameras, could significantly improve the accuracy of the results. Also, developing

an algorithm for the image processing method could enable the simultaneous analysis of multiple grains from a single photograph in a systematic manner. This would increase the number of grains analyzed concurrently, yielding results that more accurately reflect real-world conditions.

REFERENCES

Santamarina, J. C., & Cho, G. C. (2001). Determination of critical state parameters in sandy soils—simple procedure. *Geotechnical testing journal*, *24*(2), 185-192.

Jefferies, M., & Been, K. (2015). Soil liquefaction: a critical state approach. CRC press.

Cho, G. C., Dodds, J., & Santamarina, C. J. (2006). Particle shape effects on packing density, stiffness, and strength: natural and crushed sands. J Geotech Geoenviron 132 (5): 591–602.

Santana, T., & Candeias, M. (2018). Effect of void ratio on K 0 of a sand by means of triaxial stress-path testing. *Geotechnical and Geological Engineering*, *36*, 257-266.

Been, K., Jefferies, M. G., & Hachey, J. (1991). The critical state of sands. *Geotechnique*, *41*(3), 365-381.

Jerves, A. X., Kawamoto, R. Y., & Andrade, J. E. (2016). Effects of grain morphology on critical state: a computational analysis. *Acta Geotechnica*, *11*(3), 493-503.

Zheng, J., & Hryciw, R. D. (2016). Roundness and sphericity of soil particles in assemblies by computational geometry. *Journal of Computing in Civil Engineering*, *30*(6), 04016021.

Salvatore, E., Modoni, G., Andò, E., Albano, M., & Viggiani, G. (2017). Determination of the critical state of granular materials with triaxial tests. *Soils and Foundations*, *57*(5), 733-744.

Cho, G. C., Dodds, J., & Santamarina, J. C. (2007). Closure to “particle shape effects on packing density, stiffness, and strength: natural and crushed sands” by Gye-Chun

Cho, Jake Dodds, and J. Carlos Santamarina. *Journal of geotechnical and geoenvironmental engineering*, *133*(11), 1474-1474.

Chu, J. (1995). An experimental examination of the critical state and other similar concepts for granular soils. *Canadian Geotechnical Journal*, *32*(6), 1065-1075.

Cubrinovski, M., & Ishihara, K. (2002). Maximum and minimum void ratio characteristics of sands. *Soils and foundations*, *42*(6), 65-78.

Yang, J., & Luo, X. D. (2015). Exploring the relationship between critical state and particle shape for granular materials. *Journal of the Mechanics and Physics of Solids*, *84*, 196-213.

Yang, J., & Luo, X. D. (2018). The critical state friction angle of granular materials: does it depend on grading?. *Acta Geotechnica*, *13*, 535-547.

Jia, J., Zheng, J., & Sun, X. (2021). The critical state parameters of sands from their image-based intrinsic properties. *Acta Geotechnica*, *16*, 4081-4092.

Sadrekarimi, A., & Olson, S. M. (2011). Critical state friction angle of sands. *Géotechnique*, *61*(9), 771-783.

Santamarina, J. C., & Cho, G. C. (2004). Soil behaviour: The role of particle shape. In *Advances in geotechnical engineering: The Skempton conference: Proceedings of a three day conference on advances in geotechnical engineering, organised by the Institution of Civil Engineers and held at the Royal Geographical Society, London, UK, on 29–31 March 2004* (pp. 604-617). Thomas Telford Publishing.

Shen, C., Liu, S., Xu, S., & Wang, L. (2019). Rapid estimation of maximum and minimum void ratios of granular soils. *Acta Geotechnica*, *14*, 991-1001.

Mooney, M. A., Finno, R. J., & Viggiani, M. G. (1998). A unique critical state for sand?. *Journal of Geotechnical and Geoenvironmental Engineering*, *124*(11), 1100-1108.

Cetin, K. O., & Ilgac, M. (2021). Probabilistic assessments of void ratio limits and their range for cohesionless soils. Soil Dynamics and Earthquake Engineering, 142, 106481.

Cetin, K. O., Der Kiureghian, A., & Seed, R. B. (2002). Probabilistic models for the initiation of seismic soil liquefaction. *Structural safety*, *24*(1), 67-82.

Boulanger, R. W., & Idriss, I. M. (2012). Probabilistic standard penetration test–based liquefaction–triggering procedure. *Journal of Geotechnical and Geoenvironmental Engineering*, *138*(10), 1185-1195.

Lea's Chemistry of Cement and Concrete (Fourth Edition): Sims and Brown (1998, Chapter 16, p. 907-1015)

Powers MC. A new roundness scale for sedimentary particles. Journal of Sedimentary Petrology 1953; 23(2): 117-9.

Szeliski, R. (2022). *Computer vision: algorithms and applications*. Springer Nature

APPENDICES

A. Appendix A

Sample	D_{50}	C_u	R	S	e_{max}	e_{min}	Φ_{cs}	Γ_1	λ_{10}	References
Nevada sand	0.15	1.8	0.6	0.85	0.85	0.57	31	1.04	0.071	Cho et al. (2006)
Ticino sand	0.58	1.5	0.4	0.8	0.99	0.57	37	1.05	0.053	
Margaret river sand	0.49	1.9	0.7	0.7	0.87		33	0.84	0.051	
ASTM 20/30 sand	0.6	1.4	0.8	0.9	0.69		32	0.74	0.053	
Ponte Vedra sand	0.18	1.8	0.3	0.85	1.07		39	1.01	0.061	
8M8 crushed sand	0.38	3.3	0.2	0.7	0.97		40	1.16	0.138	
9C1 crushed sand	0.52	2.3	0.25	0.7	0.91		39	1.06	0.067	
Jekyll Island sand	0.17	1.7	0.3	0.85	1.04		40	0.98	0.053	
Blasting sand	0.71	1.9	0.3	0.55	1.025	0.70	34	1.099	0.69	
Glass beads	0.32	1.4	1	1	0.72	0.54	21	0.807	0.039	
Granite powder	0.09	6.2	0.4	0.24	1.296	0.48	34	1.124	0.07	
Ottawa #20/30 sand	0.72	1.2	0.9	0.9	0.742	0.50	27	0.802	0.047	
Ottawa F-110 sand	0.12	1.7	0.7	0.7	0.848	0.54	31	0.937	0.077	
7U7-crushed sand	0.3	3.2	0.2	0.8	0.79		37	1.06	0.064	
Brasted sand	0.26	2.4	0.67		0.79	0.48		0.91	0.022	Cornforth DH (1964)
Sand B	0.15	1.8	0.8		0.84	0.50		0.791	0.018	Castro G (1969)
Sand C	0.28	2.3	0.27		0.99	0.66		0.988	0.038	
Leighton Buzzard sand	0.12	1.5	0.41		1.02	0.67		0.975	0.023	Been and Jefferies (1991)
Erksak sand	0.33	1.8	0.65		0.81	0.61		0.875	0.019	

Sample	D_{50}	C_u	R	S	e_{max}	e_{min}	Φ_{cs}	Γ_1	λ_{10}	References
Masonry sand	0.32	1.3	0.68		0.88	0.60		0.9	0.018	Zhang et al. 1997)
Ottawa C109	0.35	1.6	0.75	0.8	0.82	0.50		0.926	0.014	Robertson et al. (1995)
Toyoura sand	0.17	1.7	0.42	0.65	0.97	0.64		1.048	0.026	
Lornex	0.3	2	0.22	0.7	1.08	0.68		1.1	0.05	
Brenda	0.1	1.9	0.23	0.65	1.06	0.69		1.112	0.043	
Syncrude	0.17	2.4	0.81	0.7	0.93	0.55		0.847	0.017	
Kogyuk sand	0.35	1.7	0.42		0.78	0.52		0.845	0.028	Been and Jefferies (1991)
Nerkerk	0.23	2	0.43	0.75	0.94	0.62		0.885	0.03	Sladen et al. 1985)
Leighton Buzard sand	0.86	1.2	0.42	0.82	0.82	0.54		1.03	0.023	
Reid Bedford sand	0.24	1.8	0.37		0.87	0.55		1.014	0.028	Been and Jefferies (2004
Nevada	0.12	1.8	0.61	0.72	0.89	0.51		0.91	0.02	
Fraser River Sand	0.25	1.7	0.28	0.5	1	0.60		1.11	0.029	Ghafghazi et al. 20214)
Toyoura sand	0.17	1.7	0.64	0.65	0.98	0.60		0.941	0.021	Verdugo and Ishihara (1996)
Hostun sand	0.32	1.8	0.42	0.62	1	0.66		0.969	0.03	Wood (1999)
Monterey sand	0.38	1.6	0.37	0.75	0.86	0.53		0.905	0.017	Reimer et al. (1990)
Crushed Unimin 2010	0.87	2	0.2		1.03	0.65		1.112	0.039	Zhang and Garga (1999)
Sydney sand	0.3	1.6	0.45	0.72	0.86	0.57		0.969	0.025	Chu et al. (1993)
Ottawa 20/40 sand	0.51	1.4	0.75	0.8	0.68	0.39		0.82	0.02	Sadrekarimi and Olson (2010)
Illinois River sand	0.5	2.5	0.25		0.76	0.46		0.92	0.049	
Mississippi River sand	0.1	5	0.4		1.04	0.56		0.82	0.035	
Ticino sand	0.53	1.6	0.4	0.8	0.89	0.60		0.986	0.024	Maki et al. (2014)
Ottawa sand	0.53	1.5	0.75	0.8	0.79	0.49		0.754	0.012	
Hokksund sand	0.39	2	0.5		0.91	0.55		0.934	0.024	
Monterey sand	0.37	1.6	0.7		0.82	0.54		0.878	0.013	

Sample	D_{50}	C_u	R	S	e_{max}	e_{min}	Φ_{cs}	Γ_1	λ_{10}	References
Fontainebleau sand	0.2	1.4	0.55	0.69	0.87	0.54		0.98	0.03	Tsomokos and Georgiannou (2010)
Sacramento sand	0.3	1.7	0.65	0.65	0.87	0.53		0.905	0.017	Riemer and Seed (1997)
Fujian sand	0.51	1.2	0.49	0.75				0.89	0.017	Yang and Luo (2015)
Daytona beach sand	0.23	1.4	0.62	0.7	1	0.64				Sukumaran and Ashmawy (2001)
Ottawa #20/70 sand	0.53	2.4	0.76	0.81	0.78	0.47				
Ottawa #45 sand	0.57	2.1	0.45	0.68	1.11	0.75				
Ottawa #60/80 sand	0.21	2.4	0.65	0.78	0.85	0.55				
Ottawa #90 sand	0.27	2.2	0.4	0.6	1.1	0.73				
Syncrude tailings	0.18	2.5	0.47	0.62	0.91	0.59				
Ottawa 20–30	0.72	1.2	0.65	0.75	0.77	0.46				Zelasko et al. (1975)
Ottawa 35 -45	0.42	1.2	0.6	0.75	0.82	0.48				
Ottawa 50–70	0.25	1.2	0.52	0.74	0.89	0.53				
Ottawa 70–100	0.18	1.2	0.5	0.73	0.92	0.54				
Ottawa 100–140	0.12	1.2	0.5	0.72	0.92	0.54				
Evanston beach 20–30	0.72	1.2	0.44	0.71	0.92	0.55				
Evanston beach 35–45	0.42	1.2	0.43	0.73	0.9	0.52				
Evanston beach 50–70	0.25	1.2	0.41	0.73	0.92	0.54				
Evanston beach 70–100	0.18	1.2	0.42	0.72	0.93	0.53				
Franklin falls 20–30	0.72	1.2	0.36	0.52	1.01	0.62				
Franklin falls 35–45	0.42	1.2	0.35	0.52	1.09	0.63				

Sample	D_{50}	C_u	R	S	e_{max}	e_{min}	Φ_{cs}	Γ_1	λ_{10}	References
Franklin falls 50–70	0.25	1.2	0.34	0.52	1.1	0.64				
Brown mortar	0.6	2.1	0.79	0.76	0.91	0.58				Cerato and Lutenegger (2006)
Ottawa	0.5	1	0.63	0.72	0.69	0.46				
Morie sand	1.3	1.8	0.24	0.75	0.78	0.59				
Gravel pack	2.8	2.1	0.29	0.73	0.83	0.67				
Ottawa 20	0.7	1.2	0.75	0.72	0.73	0.50				Cox and Budhu (2008)
Rillito river	0.56	2	0.5	0.65	0.73	0.42				
Silica 40	0.52	1.4	0.4	0.72	0.8	0.40				
Santa Cruz river	0.34	2.7	0.5	0.71	0.8	0.40				
Sabratah Soil			0.48	0.64	1.339	0.74	31	1.108	0.05	Ahmet
Cine Sand	0.38	3.8	0.28	0.58	0.889	0.52	33	0.876	0.049	Ahmet
Sile Silis Sand	0.44	2.5	0.37	0.6	0.706	0.54	33.5	0.644	0.011	Ahmet
Aygaz Sand	0.24	3.3	0.24	0.6	0.934	0.54	34	0.884	0.04	Ahmet
Tekirdag Silis Sand	0.51	1.6	0.25	0.6	0.818	0.58	34	0.7626	0.017	Ahmet
Castro Sand B	0.15				0.84	0.50		0.791	0.041	Castro (1969)
Castro Sand C	0.28				0.99	0.66		0.988	0.038	Castro (1969)
Hokksund	0.39				0.91	0.55		0.934	0.054	Golder project files
Leighton Buzzard	0.12				1.023	0.67		0.972	0.054	Golder project files
Leighton Buzzard	0.5				0.79	0.52		0.69	0.04	Hird and Hassona (1990)
Leighton Buzzard: 10% Mica	0.5				1.07	0.59		0.99	0.145	Hird and Hassona (1990)
Leighton Buzzard: 17% Mica	0.47				1.32	0.62		1.11	0.16	Hird and Hassona (1990)
Leighton Buzzard: 30% Mica	0.45				1.789	0.82		1.61	0.385	Hird and Hassona (1990)
Monterey	0.37				0.82	0.54		0.878	0.029	Golder project files
Nevada	0.15				0.887	0.51		0.91	0.045	Velacs project

Sample	D_{50}	C_u	R	S	e_{max}	e_{min}	Φ_{cs}	Γ_1	λ_{10}	References
Ottawa	0.53				0.79	0.49		0.754	0.028	Golder project files
Reid Bedford	0.24				0.87	0.55		1.014	0.065	Golder project files
Ticino-4	0.53				0.89	0.60		0.986	0.056	Golder project files
Ticino-8	0.53							0.943	0.031	Golder project files
Ticino-9	0.53							0.97	0.05	Golder project files
Toyoura	0.21				0.873	0.66		1	0.039	Golder project files
Toyoura	0.16				0.981	0.61		1.043	0.085	Golder project files
Amauligak F-24	0.14							0.946	0.083	Golder project files
Amauligak F-24	0.14							0.966	0.124	Golder project files
Amauligak I-65	0.08							1.634	0.358	Golder project files
Amauligak I-65	0.31							1.018	0.153	Golder project files
Amauligak I-65	0.29							1.023	0.095	Golder project files
Erksak	0.32				0.808	0.64		0.875	0.043	Golder project files
Erksak	0.36				0.963	0.53		0.848	0.054	Golder project files
Erksak	0.33				0.747	0.52		0.816	0.031	Golder project files
Isserk	0.21				0.76	0.52		0.833	0.043	Golder project files
Isserk	0.21				0.83	0.55		0.879	0.089	Golder project files
Isserk	0.21				0.86	0.44		0.933	0.123	Golder project files
Kogyuk	0.35				0.83	0.47		0.844	0.064	Golder project files
Kogyuk	0.35				0.87	0.49		0.924	0.104	Golder project files

Sample	D_{50}	C_u	R	S	e_{max}	e_{min}	Φ_{cs}	Γ_1	λ_{10}	References
Kogyuk	0.35				0.93	0.46		1.095	0.205	Golder project files
Kogyuk	0.28				0.87	0.56		0.902	0.062	Golder project files
Nerlerk	0.27				0.812	0.54		0.849	0.049	Golder project files
Nerlerk	0.28				0.94	0.62		0.88	0.04	Sladen et al. (1985)
Nerlerk	0.28				0.96	0.43		0.8	0.07	Sladen et al. (1985)
Alaskan Beaufort	0.14				0.856	0.57		0.91	0.037	Golder project files
Alaskan Beaufort	0.14				0.837	0.53		0.92	0.053	Golder project files
West Kowloon Sand	0.73				0.685	0.44		0.71	0.08	Golder project files
Chek Lap Kok	1				0.682	0.41		0.905	0.13	Golder project files
Fraser River (Massey)	0.2				1.1	0.70		1.071	0.038	Robertson et al. (2000)
Duncan Dam	0.2				1.15	0.76		1.17	0.085	Robertson et al. (2000)
San Fernando 3	0.29							0.869	0.093	Seed et al. (1988)
San Fernando 7	0.08							0.815	0.106	Seed et al. (1988)
Bennett silty sand (a)	0.27				0.678	0.18		0.457	0.041	Golder project files
Bennett silty sand (b)	0.37				0.524	0.33		0.435	0.05	Golder project files
Bennett silty sand (c)	0.41				0.509	0.34		0.43	0.034	Golder project files
Hilton Mines	0.2				1.05	0.62		1.315	0.17	Golder project files
Highland Valley Copper	0.2				1.055	0.54		0.98	0.068	Robertson et al. (2000)
Faro Lead-Zinc	0.1				0.99	0.56		0.921	0.082	Golder project files
Faro Lead-Zinc	0.05				2.017	0.84		1.076	0.159	Golder project files

Sample	D_{50}	C_u	R	S	e_{max}	e_{min}	Φ_{cs}	Γ_1	λ_{10}	References
Sudbury (nickel)	0.12				1.032	0.54		0.938	0.112	Golder project files
Sudbury (nickel)	0.05							0.868	0.108	Golder project files
Syncrude Oil Sand Tailings	0.21				0.898	0.54		0.86	0.065	Golder project files
Syncrude (Mildred Lake)	0.16				0.958	0.52		0.919	0.035	Robertson et al. (2000)
Yatesville Silty Sand	0.1							0.653	0.164	Brandon et al. (1991)
Merriespruit gold tailings	0.14				1.221	0.74		1.24	0.07	Fourie & Papageorgiou (2001)
Merriespruit gold tailings	0.13				1.326	0.70		1.18	0.05	Fourie & Papageorgiou (2001)
Merriespruit gold tailings	0.11				1.331	0.58		0.96	0.035	Fourie & Papageorgiou (2001)
Merriespruit gold tailings	0.06				1.827	0.66		0.8	0.02	Fourie & Papageorgiou (2001)
Banding 1 0%	0.18	1.5			0.82	0.54	32	0.85	0.02	Castro et al. 1982
Banding 5 0%	0.11	1.4			0.87	0.55	30	0.92	0.045	Sladen et al. 1985
Banding 6 0%	0.16	1.7			0.82	0.52	28.6	0.85	0.04	
Banding 9 0%	0.14	1.6			0.8	0.53	26.8	0.85	0.03	
Brenda 0%	0.1	1.9			1.06	0.69	36	1.112	0.1	Robertson et al. 1995
Chiba 3%	0.17	2			1.271	0.84	34	1.265	0.085	Ishihara 1993
Chiba 18%	0.15	4			1.307	0.69	34	1.12	0.09	
Chonan Silty 18%	0.15	4.1			1.31	0.69	34	1.144	0.09	
Dune 6%	0.21	2.3			1.08	0.59	32	1.139	0.159	Konrad 1990
Erksak 330 0.7%	0.33	1.8			0.753	0.53	31	0.82	0.03	Konrad and Watts 1995
Fort Peck 2%a					1.01		32	0.879	0.087	Been et al. 1991
Fraser River 0%	0.25	1.7			1	0.60	34.5	1.11	0.067	Chillarige et al. 1997

Sample	D_{50}	C_u	R	S	e_{max}	e_{min}	Φ_{cs}	Γ_1	λ_{10}	References
Hostun RF 0%	0.32	1.8			1	0.66	33.5	0.969	0.069	Thevanayagam et al. 1996
Kiyosu 0%	0.31	2.5			1.206	0.75	30	1.115	0.05	Ishihara 1993
Kogyuk 350 0%	0.35	1.7			0.783	0.52	31	0.784	0.014	Been and Jefferies 1985
Kogyuk 350 2%	0.35	1.8			0.829	0.47	31	0.845	0.065	
Kogyuk 350 5%	0.36	2			0.866	0.49	31	0.925	0.105	
Kogyuk 350 10%	0.34	2.3			0.927	0.47	31	1.056	0.175	
Lagunillas 70%	0.05	3			1.389	0.77	31	1.21	0.093	Ishihara 1993
Leighton Buzzard 5%	0.12	1.8			1.023	0.67	30	1.03	0.054	Been et al. 1991.
Likan 0%	0.24	1.9			1.239	0.76	34.5	1.364	0.148	Lee 1995
Lornex 0%	0.3	2			1.08	0.68	35	1.1	0.05	Castro et al. 1982
Mailiao 5%	0.25	2.9			1.279	0.74		1.029	0.071	Chen and Liao 1999
Mailiao 10%	0.22	3.5			1.151	0.60		0.975	0.086	
Mailiao 15%	0.21	4.2			1.031	0.44		0.83	0.068	Chen and Liao 1999
Massey tunnel 3%	0.25	1.5			1.102	0.71	39.5	1.129	0.04	Konrad 1997
Monterey 0%	0.38	1.6			0.86	0.53	33	0.905	0.039	Riemer et al. 1990
Monterey 16%	1.3	1.3			0.71	0.49	33	0.73	0.023	Riemer and Seed 1997
Nerlerk 0%	0.23	1.8			0.89	0.66	30	0.885	0.03	Sladen et al. 1985
Nerlerk 2%	0.23	2			0.94	0.62	30	0.88	0.04	
Nevada fine 5%	0.12	1.8			0.87	0.57	29	0.85	0.067	Arulanandan et al. 1993
Ottawa 5%							29.5	0.809	0.067	Cunning et al. 1995
Ottawa C109 0%	0.35	1.7			0.82	0.50	30	0.926	0.074	Sasitharan et al. 1994
S 2%	0.8	3			1.133	0.60	39	0.992	0.046	Verdugo et al. 1995

Sample	D_{50}	C_u	R	S	e_{max}	e_{min}	Φ_{cs}	Γ_1	λ_{10}	References
S 20%	0.7	3.8			1.111	0.55	38	1.012	0.056	
Sacramento 0%	0.3	1.7			0.87	0.53	33.2	0.905	0.039	Riemer et al. 1990
Sand A 13%	0.14	2.9					33.7	1.071	0.12	Dobry et al. 1985
Sand B 32%	0.09	3.3					33.7	0.972	0.045	
Sydney 0%	0.3	1.5			0.855	0.57	31	0.969	0.073	Chu and Lo 1993
Syncrude 12%	0.17	2.4			0.93	0.55	30	0.847	0.04	Sladen and Hanford 1987
Tar Island Dyke 5%					1.005			0.885	0.057	Konrad and Watts 1995
Tia Juana Silty 12%	0.16	2.7			1.099	0.62	30.5	1.026	0.075	Ishihara 1993
Toyoura 0%	0.17	1.7			0.977	0.60	31	1.048	0.06	Ishihara 1993
Toyoura 0%	0.16	1.5			0.981	0.61	31	1.041	0.084	Been et al. 1991
Unimin 2010 0%	0.87	2			1.027	0.65	33	1.112	0.091	Zhang and Garga 1997
Well rounded 1%	0.18	1.4			1.06	0.67	31	1.022	0.031	Konrad 1990
Silty Soils (30<FC<70%)	0.04									Cubrinovski and Ishiara (2002)
Silty Soils (30<FC<70%)	0.04									Cubrinovski and Ishiara (2002)
Silty Soils (30<FC<70%)	0.05									Cubrinovski and Ishiara (2002)
Nevada Fines	0.05	1.7			1.18	0.75				Cubrinovski and Ishiara (2002), Lade et al. (1998)
Faro Lead-Zinc	0.05				2.02	0.84				Jefferies and Been (2006), Golder Project Files
Sudbury (nickel)	0.05									Jefferies and Been (2006), Golder Project Files
Silty Soils (30<FC<70%)	0.05									Cubrinovski and Ishiara (2002)

Sample	D_{50}	C_u	R	S	e_{max}	e_{min}	Φ_{cs}	Γ_1	λ_{10}	References
Merriespruit Gold Tailings	0.06				1.83	0.66				Jefferies and Been (2006), Fourie & Papageorgiou (2001)
Silty Soils (30<FC<70%)	0.06									Cubrinovski and Ishiara (2002)
Silty Soils (30<FC<70%)	0.06									Cubrinovski and Ishiara (2002)
Silty Soils (30<FC<70%)	0.07									Cubrinovski and Ishiara (2002)
Silty Soils (30<FC<70%)	0.07									Cubrinovski and Ishiara (2002)
Silty Soils (30<FC<70%)	0.08									Cubrinovski and Ishiara (2002)
San Fernando 7	0.08									Jefferies and Been (2006), Seed et al. (1988)
Silty Soils (30<FC<70%)	0.08									Cubrinovski and Ishiara (2002)
Amauligak I-65	0.08									Jefferies and Been (2006), Golder Project Files
Silty Soils (30<FC<70%)	0.08									Cubrinovski and Ishiara (2002)
Silty Soils (30<FC<70%)	0.09									Cubrinovski and Ishiara (2002)
Granite Powder	0.09	6.2			1.3	0.48				Santamarina and Cho (2001), Santamarina and Cho (2001)
Granite Powder	0.09	6.2	0.4	0.24	1.3					Zheng and Hryciw (2016), Cho et al. (2006)
Silty Soils (30<FC<70%)	0.09									Cubrinovski and Ishiara (2002)
Silty Soils (30<FC<70%)	0.1									Cubrinovski and Ishiara (2002)

Sample	D_{50}	C_u	R	S	e_{max}	e_{min}	Φ_{cs}	Γ_1	λ_{10}	References
Del Monte white Sand	0.1	1.4			1.2	0.63				Youd (1973)
Crushed Basalt	0.1	1.4			1.42	0.80				Youd (1973)
Faro Lead-Zinc	0.1				0.99	0.56				Jefferies and Been (2006), Golder Project Files
Silty Soils (30<FC<70%)	0.1									Cubrinovski and Ishiara (2002)
Silty Soils (30<FC<70%)	0.1									Cubrinovski and Ishiara (2002)
Yatesville Silty Sand	0.1									Jefferies and Been (2006), Brandon et al. (1991)
Silty Soils (30<FC<70%)	0.11									Cubrinovski and Ishiara (2002)
Merriespruit Gold Tailings	0.11				1.33	0.58				Jefferies and Been (2006), Fourie & Papageorgiou (2001)
Sudbury (nickel)	0.12				1.03	0.54				Jefferies and Been (2006), Golder Project Files
Silty Soils (30<FC<70%)	0.12									Cubrinovski and Ishiara (2002)
Silty Soils (30<FC<70%)	0.12									Cubrinovski and Ishiara (2002)
Ottawa F-110 Sand	0.12	1.6			0.85	0.54				Santamarina and Cho (2001)
Ottawa F-110 Sand	0.12	1.7	0.7	0.7	0.85	0.54				Zheng and Hryciw (2016), Cho et al. (2006)
Ottawa 100–140	0.12	1.2	0.5	0.9	0.92	0.54				Zheng and Hryciw (2016), Zelasko et al. (1975)

Sample	D_{50}	C_u	R	S	e_{max}	e_{min}	Φ_{cs}	Γ_1	λ_{10}	References
Nevada Sand 80/200	0.12	1.6			0.94	0.62				Cubrinovski and Ishiara (2002), Lade et al. (1998)
Leighton Buzzard	0.12				1.02	0.67				Jefferies and Been (2006), Golder Project Files
Sands with Clay (15<FC<30 %)	0.12									Cubrinovski and Ishiara (2002)
Silty Soils (30<FC<70%)	0.13									Cubrinovski and Ishiara (2002)
Silty Soils (30<FC<70%)	0.13									Cubrinovski and Ishiara (2002)
Ottawa 100–200	0.13	1.9	0.6	0.6	0.9	0.59				Zheng and Hryciw (2016), Thomann (1990)
Jamuna Sand	0.13	1.9	0.1	0.68	1.14	0.72				Zheng and Hryciw (2016), Yasin and Safiullah (2003)
Merriespruit Gold Tailings	0.13				1.33	0.70				Jefferies and Been (2006), Fourie & Papageorgiou (2001)
Silty Soils (30<FC<70%)	0.13									Cubrinovski and Ishiara (2002), Cubrinovski and Ishiara (2002)
Alaskan Beaufort	0.14				0.84	0.53				Jefferies and Been (2006), Golder Project Files
Alaskan Beaufort	0.14				0.86	0.57				Jefferies and Been (2006), Golder Project Files
Merriespruit Gold Tailings	0.14				1.22	0.74				Jefferies and Been (2006),

Sample	D_{50}	C_u	R	S	e_{max}	e_{min}	Φ_{cs}	Γ_1	λ_{10}	References
										Fourie & Papageorgiou (2001)
Amauligak F-24	0.14									Jefferies and Been (2006), Golder Project Files
Sands with Clay (15<FC<30 %)	0.14									Cubrinovski and Ishiara (2002)
Amauligak F-24	0.14									Jefferies and Been (2006), Golder Project Files
Clean Sands (FC=0-5%)	0.15									Cubrinovski and Ishiara (2002)
Castro Sand B	0.15				0.84	0.50				Jefferies and Been (2006), Castro (1969)
Nevada Sand	0.15	1.8	0.6	0.85	0.85	0.57				Zheng and Hryciw (2016), Cho et al (2006)
P2-S7	0.15	3.2	0.22		0.86	0.52				Zheng and Hryciw (2016), Bareither et al. (2008)
Nevada	0.15				0.89	0.51				Jefferies and Been (2006), Velacs Project
Toyoura Sand	0.15				0.99	0.61				Cubrinovski and Ishiara (2002), Shamoto et al. (1996)
Longstone Sand	0.15	1.3	0.3	0.65	1	0.61				Zheng and Hryciw (2016), Tsomokos and Georgiannou (2010)
TKS Sand	0.15	1.9			1.02	0.60				Kokusho and Yoshida (1997)

Sample	D_{50}	C_u	R	S	e_{max}	e_{min}	Φ_{cs}	Γ_1	λ_{10}	References
Sands with Fines (5<FC<15%)	0.15									Cubrinovski and Ishiara (2002)
Sands with Clay (15<FC<30 %)	0.16									Cubrinovski and Ishiara (2002)
Sands with Clay (15<FC<30 %)	0.16									Cubrinovski and Ishiara (2002)
Sands with Clay (15<FC<30 %)	0.16									Cubrinovski and Ishiara (2002)
Nevada Sand	0.16	1.3	0.61	0.72	0.88	0.58				Zheng and Hryciw (2016)
Syncrude (Mildred Lake)	0.16				0.96	0.52				Jefferies and Been (2006), Robertson et al. (2000)
P2-S3	0.16	2.3	0.24		0.96	0.58				Zheng and Hryciw (2016), Bareither et al. (2008)
Toyoura Sand	0.16	1.5	0.35	0.65	0.97	0.61				Zheng and Hryciw (2016), Bolton (1987)
Toyoura Sand	0.16	1.5			0.97	0.61				Cubrinovski and Ishiara (2002), Hoque and Tatsuoka (1998)
Toyoura Sand	0.16	1.5			0.98	0.61				Cubrinovski and Ishiara (2002), Goto et al. (1993)
Toyoura Sand	0.16				0.98	0.61				Cubrinovski and Ishiara (2002), Sakai and Tanaka (1998)
Toyoura Sand	0.16	1.5	0.3		0.98	0.61				Zheng and Hryciw (2016), Herle and Gudehus (1999)

Sample	D_{50}	C_u	R	S	e_{max}	e_{min}	Φ_{cs}	Γ_1	λ_{10}	References
Toyoura	0.16				0.98	0.61				Jefferies and Been (2006), Golder Project Files
Sands with Fines (5<FC<15%)	0.16									Cubrinovski and Ishiara (2002)
Sands with Fines (5<FC<15%)	0.16									Cubrinovski and Ishiara (2002)
Ottawa Sand F-95	0.16	1.8			0.87	0.58				Cubrinovski and Ishiara (2002), Lade and Yamamuro (1997)
Sands with Fines (5<FC<15%)	0.16									Cubrinovski and Ishiara (2002)
Sands with Clay (15<FC<30 %)	0.17									Cubrinovski and Ishiara (2002)
Clean Sands (FC=0-5%)	0.17									Cubrinovski and Ishiara (2002)
Ooestershelde	0.17	1.8			0.89	0.56				Mayne and Kulhawy (1991), Greeuw et al. (1988)
S. Oakleigh Fine	0.17	1.6			0.93	0.57				Mayne and Kulhawy (1991), Veismanis (1974)
Toyoura Sand	0.17				0.98	0.60				Cubrinovski and Ishiara (2002), Gutierrez et al. (1991)
Toyoura Sand	0.17	1.6			0.99	0.62				Cubrinovski and Ishiara (2002), Zlatovic (1994)
Jekyll Island Sand	0.17	1.7	0.3	0.85	1.04					Zheng and Hryciw (2016), Cho et al. (2006)

Sample	D_{50}	C_u	R	S	e_{max}	e_{min}	Φ_{cs}	Γ_1	λ_{10}	References
Sands with Clay (15<FC<30 %)	0.18									Cubrinovski and Ishiara (2002)
Silty Soils (30<FC<70%)	0.18									Cubrinovski and Ishiara (2002)
Ottawa 70–100	0.18	1.2	0.5	0.9	0.92	0.54				Zheng and Hryciw (2016), Zelasko et al. (1975)
Evanston Beach 70–100	0.18	1.2	0.42	0.72	0.93	0.53				Zheng and Hryciw (2016), Zelasko et al. (1975)
Toyoura Sand	0.18	1.5			0.97	0.62				Cubrinovski and Ishiara (2002), Yamashita and Toki (1993)
Toyoura Sand	0.18	1.2			0.97	0.64				Cubrinovski and Ishiara (2002), Hyodo et al. (1991)
Toyoura Sand	0.18				0.97	0.64				Cubrinovski and Ishiara (2002), Zhang et al. (1997)
Toyoura Sand	0.18	1.3			0.98	0.61				Cubrinovski and Ishiara (2002), Miura and Kawamura (1996)
Toyoura Sand	0.18	1.8			0.99	0.62				Cubrinovski and Ishiara (2002), Zen and Yamazaki (1990)
Ponte Vedra Sand	0.18	1.8	0.3	0.85	1.07					Zheng and Hryciw (2016), Cho et al. (2006)
Syncrude Tailings	0.18	2.5	0.2	0.62	1.14	0.59				Zheng and Hryciw (2016), Sukumaran and Ashmawy (2001)

Sample	D_{50}	C_u	R	S	e_{max}	e_{min}	Φ_{cs}	Γ_1	λ_{10}	References
Niigata LD3-S2	0.18	1.8			1.26	0.66				Ishiara et al (1978), Ishiara et al (1978)
Sands with Clay (15<FC<30 %)	0.18									Cubrinovski and Ishiara (2002)
Clean Sands (FC=0-5%)	0.18									Cubrinovski and Ishiara (2002)
Sands with Clay (15<FC<30 %)	0.18									Cubrinovski and Ishiara (2002)
Ottowa Sand	0.19	1.4			0.82	0.45				Youd (1973)
Crushed Basalt	0.19	1.4			1.34	0.74				Youd (1973)
Del Monte white Sand	0.19	1.4			1.07	0.55				Youd (1973)
Clean Sands (FC=0-5%)	0.19									Cubrinovski and Ishiara (2002)
Clean Sands (FC=0-5%)	0.19									Cubrinovski and Ishiara (2002)
Sands with Fines (5<FC<15%)	0.19									Cubrinovski and Ishiara (2002)
Mol Sand	0.19	1.5	0.65	0.65	0.89	0.56				Zheng and Hryciw (2016), DeBeer (1963)
Toyoura Sand	0.19	1.7			0.99	0.62				Cubrinovski and Ishiara (2002), Cubrinovski and Ishiara (1998)
Clean Sands (FC=0-5%)	0.19									Cubrinovski and Ishiara (2002)
P2-S10	0.2	2.3	0.31		0.75	0.46				Zheng and Hryciw (2016), Bareither et al. (2008)
P2-S2	0.2	2.1	0.29		0.83	0.56				Zheng and Hryciw (2016), Bareither et al. (2008)

Sample	D_{50}	C_u	R	S	e_{max}	e_{min}	Φ_{cs}	Γ_1	λ_{10}	References
Sizewell	0.2	2			0.94	0.50				Skempton (1986)
Hochstetten Sand	0.2	1.6	0.3		0.95	0.55				Zheng and Hryciw (2016), Herle and Gudehus (1999)
Hilton Mines	0.2	2	0.23	0.72	1.05	0.62				Mayne and Kulhawy (1991), Schmertmann (1978)
Highland Valley Copper	0.2				1.06	0.54				Jefferies and Been (2006), Robertson et al. (2000)
Fraser River	0.2				1.1	0.70				Jefferies and Been (2006), Robertson et al. (2000)
Duncan Dam	0.2				1.15	0.76				Jefferies and Been (2006), Robertson et al. (2000)
Sands with Clay (15<FC<30 %)	0.2									Cubrinovski and Ishiara (2002)
Ottawa Sand 50/200	0.2	1.9			0.81	0.55				Cubrinovski and Ishiara (2002), Lade and Yamamuro (1997)
Sands with Fines (5<FC<15%)	0.2									Cubrinovski and Ishiara (2002)
Syncrude Oil Sand Tailings	0.21				0.9	0.54				Jefferies and Been (2006), Golder Project Files
Isserk	0.21				0.76	0.52				Jefferies and Been (2006), Golder Project Files

Sample	D_{50}	C_u	R	S	e_{max}	e_{min}	Φ_{cs}	Γ_1	λ_{10}	References
1O6 Crushed Sand	0.21	2.8	0.3	0.7	0.77					Zheng and Hryciw (2016), Cho et al. (2006)
Isserk	0.21				0.83	0.55				Jefferies and Been (2006), Golder Project Files
Ottawa #60/80 Sand	0.21	2.4	0.65	0.78	0.85	0.55				Zheng and Hryciw (2016), Sukumaran and Ashmawy (2001)
Isserk	0.21				0.86	0.44				Jefferies and Been (2006), Golder Project Files
Class IIA, Michigan	0.21	1.9	0.62	0.69	0.86	0.56				Zheng and Hryciw (2016)
Fontainebleau Sand	0.21	1.2	0.65	0.71	0.87	0.54				Zheng and Hryciw (2016), Tsomokos and Georgiannou (2010)
Toyoura	0.21				0.87	0.66				Jefferies and Been (2006), Golder Project Files
Fontainebleau Sand	0.21	1.5	0.45	0.75	0.9	0.51				Zheng and Hryciw (2016), Yang et al. (2010)
Nevada Sand 50/80	0.21	1.2			0.86	0.58				Cubrinovski and Ishiara (2002), Lade et al. (1998)
Sands with Fines (5<FC<15%)	0.21									Cubrinovski and Ishiara (2002)
Clean Sands (FC=0-5%)	0.22									Cubrinovski and Ishiara (2002)

Sample	D_{50}	C_u	R	S	e_{max}	e_{min}	Φ_{cs}	Γ_1	λ_{10}	References
Sands with Clay (15<FC<30 %)	0.22									Cubrinovski and Ishiara (2002)
Clean Sands (FC=0-5%)	0.22									Cubrinovski and Ishiara (2002)
Ottawa 90	0.22	1.9			0.79	0.49				Mayne and Kulhawy (1991), Schmertmann (1978)
P3-S7	0.22	1.8	0.46		0.8	0.51				Zheng and Hryciw (2016), Bareither et al. (2008)
Ottawa 50–70	0.22	1.1	0.7	0.8	0.84	0.57				Zheng and Hryciw (2016), Thomann (1990)
Sands with Clay (15<FC<30 %)	0.22									Cubrinovski and Ishiara (2002)
Sands with Clay (15<FC<30 %)	0.22									Cubrinovski and Ishiara (2002)
Clean Sands (FC=0-5%)	0.23									Cubrinovski and Ishiara (2002)
Douglas Lake Sand	0.23	2.4	0.45	0.75	0.83	0.54				Zheng and Hryciw (2016), Thomann (1990)
Meghna Sand	0.23	1.9	0.2	0.74	0.97	0.66				Zheng and Hryciw (2016), Yasin and Safiullah (2003)
Daytona Beach Sand	0.23	1.4	0.3	0.7	1	0.64				Zheng and Hryciw (2016), Sukumaran and Ashmawy (2001)
Osterberg B3-S2	0.23	2.5			1.22	0.61				Ishiara et al (1979)
Sands with Fines (5<FC<15%)	0.23									Cubrinovski and Ishiara (2002)

Sample	D_{50}	C_u	R	S	e_{max}	e_{min}	Φ_{cs}	Γ_1	λ_{10}	References
Sands with Clay (15<FC<30 %)	0.24									Cubrinovski and Ishiara (2002)
Clean Sands (FC=0-5%)	0.24									Cubrinovski and Ishiara (2002)
Reid Bedford	0.24				0.87	0.55				Jefferies and Been (2006), Golder Project Files
Reid Bedford	0.24	1.7	0.29	0.76	0.87	0.55				Mayne and Kulhawy (1991), Schmertmann (1978)
Kawagishi-cho S-4	0.24	2.1			1.16	0.63				Ishiara and Koga (1981), Ishiara and Koga (1981)
Sands with Clay (15<FC<30 %)	0.24									Cubrinovski and Ishiara (2002)
Clean Sands (FC=0-5%)	0.25									Cubrinovski and Ishiara (2002)
1O2 Crushed Sand	0.25	2.9	0.25	0.8	0.83					Zheng and Hryciw (2016), Cho et al. (2006)
Lausitz Sand	0.25	3.1	0.51		0.85	0.44				Zheng and Hryciw (2016), Herle and Gudehus (1999)
Treasure Island, California	0.25	1.8	0.56	0.72	0.85	0.57				Zheng and Hryciw (2016), Zheng and Hryciw (2016)
Ottawa 50–70	0.25	1.2	0.52	0.9	0.89	0.53				Zheng and Hryciw (2016), Zelasko et al. (1975)
6F5 Crushed Sand	0.25	3.3	0.25	0.8	0.91					Zheng and Hryciw (2016), Cho et al. (2006)
Evanston Beach 50–70	0.25	1.2	0.41	0.73	0.92	0.54				Zheng and Hryciw (2016),

Sample	D_{50}	C_u	R	S	e_{max}	e_{min}	Φ_{cs}	Γ_1	λ_{10}	References
										Zelasko et al. (1975)
Host Sand A2	0.25	1.6			0.98	0.60				Cubrinovski and Ishiara (2002), Thevanayagam (1998)
Franklin Falls 50–70	0.25	1.2	0.34	0.52	1.1	0.64				Zheng and Hryciw (2016), Zelasko et al. (1975)
Kawagishi-cho S-8	0.25	2.2			1.13	0.67				Ishiara and Koga (1981), Ishiara and Koga (1981)
Agsco 50–80	0.25	1.3	0.2	0.5	1.24	0.79				Zheng and Hryciw (2016), Thomann (1990)
Clean Sands (FC=0-5%)	0.25									Cubrinovski and Ishiara (2002)
3C7 Crushed Sand	0.26	3.2	0.25	0.8	0.85					Zheng and Hryciw (2016), Cho et al. (2006)
Chesterton, Indiana Dunes	0.26	1.3	0.64	0.76	0.87	0.57				Zheng and Hryciw (2016)
Kawagishi-cho S-6	0.26	2			1.09	0.66				Ishiara and Koga (1981)
Sands with Clay (15<FC<30 %)	0.26									Cubrinovski and Ishiara (2002)
Clean Sands (FC=0-5%)	0.26									Cubrinovski and Ishiara (2002)
Clean Sands (FC=0-5%)	0.26									Cubrinovski and Ishiara (2002)
Sands with Clay (15<FC<30 %)	0.26									Cubrinovski and Ishiara (2002)
Sands with Clay (15<FC<30 %)	0.27									Cubrinovski and Ishiara (2002)
Bennett Silty Sand a	0.27				0.68	0.18				Jefferies and Been (2006),

Sample	D_{50}	C_u	R	S	e_{max}	e_{min}	Φ_{cs}	Γ_1	λ_{10}	References
										Golder Project Files
P2-S6	0.27	3.8	0.25		0.76	0.46				Zheng and Hryciw (2016), Bareither et al. (2008)
Nerlerk	0.27				0.81	0.54				Jefferies and Been (2006), Golder Project Files
3P3 Crushed Sand	0.27	2.2	0.2	0.7	0.95					Zheng and Hryciw (2016), Cho et al. (2006)
Ottawa #90 Sand	0.27	2.2	0.16	0.6	1.1	0.73				Zheng and Hryciw (2016), Sukumaran and Ashmawy (2001)
Clean Sands (FC=0-5%)	0.27									Cubrinovski and Ishiara (2002)
Sands with Clay (15<FC<30 %)	0.27									Cubrinovski and Ishiara (2002)
Sands with Fines (5<FC<15%)	0.28									Cubrinovski and Ishiara (2002)
Sands with Clay (15<FC<30 %)	0.28									Cubrinovski and Ishiara (2002)
2L6 Crushed Sand	0.28	3.5	0.25	0.8	0.84					Zheng and Hryciw (2016), Cho et al. (2006)
Ottawa	0.28	1.1			0.87	0.55				Mayne and Kulhawy (1991), Lambrechts and Leonards (1978)
Kogyuk	0.28				0.87	0.56				Jefferies and Been (2006), Golder Project Files
Ham River	0.28	1.6	0.45	0.65	0.92	0.59				Zheng and Hryciw (2016),

Sample	D_{50}	C_u	R	S	e_{max}	e_{min}	Φ_{cs}	Γ_1	λ_{10}	References
										Coop and Lee (1993)
Nerlerk	0.28				0.94	0.62				Jefferies and Been (2006), Sladen et al. (1985)
Nerlerk	0.28	2	0.43	0.75	0.94	0.62				Zheng and Hryciw (2016), Sladen et al. (1985)
Nerlerk	0.28				0.96	0.43				Jefferies and Been (2006), Sladen et al. (1985)
Castro Sand C	0.28				0.99	0.66				Jefferies and Been (2006), Castro (1969)
Showa Bridge S-1	0.28	2.4			1.1	0.65				Ishiara and Koga (1981)
Niigata South Bank	0.28	2.4			1.1	0.65				Skempton (1986)
Osterberg O-4	0.28	4.1			1.11	0.59				Ishiara and Koga (1981)
Osterberg O-7	0.28	2.4			1.14	0.67				Ishiara and Koga (1981)
Kawagishi-cho S-9	0.28	1.9			1.14	0.71				Ishiara and Koga (1981)
Osterberg B3-S4/2	0.28	1.6			1.15	0.61				Ishiara et al (1979)
Niigata Road Site D=8.4 m/2	0.28	1.6			1.15	0.61				Skempton (1986)
Niigata Station D=9.6 m	0.28				1.2	0.75				Skempton (1986)
P3-S6	0.29	2.1	0.36		0.77	0.50				Zheng and Hryciw (2016), Bareither et al. (2008)
P1-S7	0.29	2	0.42		0.81	0.52				Zheng and Hryciw (2016),

Sample	D_{50}	C_u	R	S	e_{max}	e_{min}	Φ_{cs}	Γ_1	λ_{10}	References
										Bareither et al. (2008)
Showa Bridge O-1	0.29	1.5			1.07	0.63				Ishiara and Koga (1981)
Niigata South Bank/2	0.29	1.5			1.08	0.64				Skempton (1986)
Showa Bridge O-2	0.29	1.4			1.08	0.63				Ishiara and Koga (1981)
Showa Bridge O-3	0.29	1.4			1.09	0.66				Ishiara and Koga (1981)
Niigata Station D=9.5 m	0.29				1.21	0.76				Skempton (1986)
Niigata Station D=9.25 m	0.29				1.22	0.76				Skempton (1986)
Amauligak I-65	0.29									Jefferies and Been (2006), Golder Project Files
San Fernando 3	0.29									Jefferies and Been (2006), Seed et al. (1988)
Clean Sands (FC=0-5%)	0.29									Cubrinovski and Ishiara (2002)
Clean Sands (FC=0-5%)	0.3									Cubrinovski and Ishiara (2002)
P1-S4	0.3	2.7	0.59		0.7	0.40				Zheng and Hryciw (2016), Bareither et al. (2008)
Evanston Beach Sand	0.3	1.8	0.75	0.8	0.79	0.50				Zheng and Hryciw (2016), Baxter and Mitchell (2004)
7U7 Crushed Sand	0.3	3.2	0.2	0.8	0.79					Zheng and Hryciw (2016), Cho et al. (2006)
P2-S1	0.3	1.9	0.31		0.8	0.51				Zheng and Hryciw (2016), Bareither et al. (2008)

Sample	D_{50}	C_u	R	S	e_{max}	e_{min}	Φ_{cs}	Γ_1	λ_{10}	References
Michigan Dunes	0.3	1.5	0.62	0.72	0.85	0.56				Zheng and Hryciw (2016)
Sydney Sand	0.3	1.5			0.86	0.57				Bobei et al. (2009)
Ham River Sand	0.3	1.3	0.55	0.75	0.87	0.53				Zheng and Hryciw (2016), Tsomokos and Georgiannou (2010)
M31 Sand	0.3	1.3	0.75	0.7	0.87	0.53				Zheng and Hryciw (2016), Tsomokos and Georgiannou (2010)
M31 Sand	0.3	1.6	0.62	0.7	0.87	0.53				Zheng and Hryciw (2016), Georgiannou and Konstadinou (2013)
Lone Star 60	0.3	1.5			0.91	0.57				Mayne and Kulhawy (1991), Villet and Mitchell (1981)
Ogishima Island	0.3	4			1.08	0.57				Skempton (1986)
Fraser River Sand	0.3	1.9	0.43	0.5	1.13	0.78				Zheng and Hryciw (2016), Sukumaran and Ashmawy (2001)
Niigata Road Site D=8.4 m	0.3	1.8			1.15	0.59				Skempton (1986)
Osterberg B3-S4	0.3	1.8			1.16	0.59				Ishiara et al (1979)
Niigata Road Site	0.3	1.7			1.16	0.64				Skempton (1986)
1K9 Crushed Sand	0.3	3.4	0.2	0.4	1.16					Zheng and Hryciw (2016), Cho et al. (2006)
Niigata Road Site D=9.3 m	0.3	1.8			1.18	0.68				Skempton (1986)

Sample	D_{50}	C_u	R	S	e_{max}	e_{min}	Φ_{cs}	Γ_1	λ_{10}	References
Osterberg B3-S5/2	0.3	1.8			1.18	0.68				Ishiara et al (1979)
Niigata Station D=9.8 m	0.3				1.2	0.78				Skempton (1986)
Clean Sands (FC=0-5%)	0.31									Cubrinovski and Ishiara (2002)
P1-S1	0.31	1.9	0.5		0.76	0.48				Zheng and Hryciw (2016), Bareither et al. (2008)
Frankston	0.31	2.1			0.79	0.46				Mayne and Kulhawy (1991), Chapman and Donald (1981)
P1-S3	0.31	2.3	0.4		0.83	0.50				Zheng and Hryciw (2016), Bareither et al. (2008)
Oakland County, Michigan	0.31	1.6	0.65	0.72	0.86	0.53				Zheng and Hryciw (2016)
Amauligak I-65	0.31									Jefferies and Been (2006), Golder Project Files
P2-S4	0.32	5.3	0.4		0.68	0.39				Zheng and Hryciw (2016), Bareither et al. (2008)
Glass Beads	0.32	1.4			0.72	0.54				Santamarina and Cho (2001)
Glass Beads	0.32	1.4	1	1	0.72	0.54				Zheng and Hryciw (2016), Cho et al. (2006)
S. Oakleigh Medium	0.32	2.2			0.75	0.41				Mayne and Kulhawy (1991), Veismanis (1974)
Erksak	0.32				0.81	0.61				Jefferies and Been (2006),

Sample	D_{50}	C_u	R	S	e_{max}	e_{min}	Φ_{cs}	Γ_1	λ_{10}	References
										Golder Project Files
New Madrid, Missouri	0.32	2.2	0.57	0.73	0.81	0.52				Zheng and Hryciw (2016)
5U1 Crushed Sand	0.32	3.5	0.15	0.7	0.84					Zheng and Hryciw (2016), Cho et al. (2006)
8B8 Crushed Sand	0.32	3.7	0.25	0.8	0.85					Zheng and Hryciw (2016), Cho et al. (2006)
Kawagishi-cho S-1	0.32	3.3			1.08	0.64				Ishiara and Koga (1981)
Clean Sands (FC=0-5%)	0.33									Cubrinovski and Ishiara (2002)
Clean Sands (FC=0-5%)	0.33									Cubrinovski and Ishiara (2002)
Earlston	0.33	2.6			0.73	0.40				Mayne and Kulhawy (1991), Veismanis (1974)
Erksak	0.33				0.75	0.52				Jefferies and Been (2006), Golder Project Files
9F1 Crushed Sand	0.33	3.5	0.2	0.8	0.9					Zheng and Hryciw (2016), Cho et al. (2006)
6A2 Crushed Sand	0.33	5.5	0.2	0.75	0.93					Zheng and Hryciw (2016), Cho et al. (2006)
Scotts Valley, California	0.33	1.5	0.4	0.73	0.94	0.60				Zheng and Hryciw (2016)
6H1 Crushed Sand	0.33	3.8	0.2	0.8	0.97					Zheng and Hryciw (2016), Cho et al. (2006)
Sands with Fines (5<FC<15%)	0.33									Cubrinovski and Ishiara (2002)
P1-S6	0.34	2.4	0.62		0.69	0.43				Zheng and Hryciw (2016),

Sample	D_{50}	C_u	R	S	e_{max}	e_{min}	Φ_{cs}	Γ_1	λ_{10}	References
										Bareither et al. (2008)
Ackerman Lake Sand	0.34	2.5	0.6	0.8	0.72	0.48				Zheng and Hryciw (2016), Thomann (1990)
Kogyuk Sand	0.34	2.3			0.93	0.47				Been and Jefferies (1985)
TS Sand	0.34	2			0.97	0.58				Kokusho and Yoshida (1997)
Osterberg B3-S1/2	0.34	1.8			1.1	0.66				Ishiara et al (1979)
Niigata Road Site D=9.2 m	0.34	1.4			1.16	0.67				Skempton (1986)
Osterberg B3-S5	0.34	1.4			1.16	0.67				Ishiara et al (1979)
Clean Sands (FC=0-5%)	0.35									Cubrinovski and Ishiara (2002)
Clean Sands (FC=0-5%)	0.35									Cubrinovski and Ishiara (2002)
Sands with Fines (5<FC<15%)	0.35									Cubrinovski and Ishiara (2002)
Kogyuk Sand	0.35	1.7			0.78	0.52				Been and Jefferies (1985)
ASTM graded Sand	0.35	1.7			0.82	0.50				Santamarina and Cho (2001)
ASTM graded Sand	0.35	1.7	0.8	0.9	0.82	0.50				Zheng and Hryciw (2016), Cho et al. (2006)
Kogyuk Sand	0.35	1.8			0.83	0.47				Been and Jefferies (1985)
Kogyuk	0.35				0.83	0.47				Jefferies and Been (2006), Golder Project Files
Sydney Sand	0.35	1.7			0.84	0.56				Rix and Stokoe (1991)
Kogyuk	0.35				0.87	0.49				Jefferies and Been (2006), Golder Project Files

Sample	D_{50}	C_u	R	S	e_{max}	e_{min}	Φ_{cs}	Γ_1	λ_{10}	References
Capitola, California	0.35	1.6	0.48	0.72	0.89	0.57				Zheng and Hryciw (2016)
Kogyuk	0.35				0.93	0.46				Jefferies and Been (2006), Golder Project Files
Erksak	0.35	2.2			0.96	0.53				Mayne and Kulhawy (1991), Been et al. (1987)
Hostun RF Sand	0.35	1.7	0.3		0.98	0.61				Zheng and Hryciw (2016), Herle and Gudehus (1999)
Hostun Fine	0.35	2.2			1	0.65				Mayne and Kulhawy (1991), Canou et al. (1988)
Kawagishi-cho S-3	0.35	2.8			1.07	0.65				Ishiara and Koga (1981)
Niigata LD3-S3	0.35	2			1.07	0.57				Ishiara et al (1978)
Kawagishi-cho S-5	0.35	2.1			1.07	0.66				Ishiara and Koga (1981)
Osterberg O-6	0.35	2.4			1.08	0.65				Ishiara and Koga (1981)
Kawagishi-cho	0.35	2.4			1.08	0.63				Skempton (1986)
Osterberg B3-S6/2	0.35	1.5			1.08	0.63				Ishiara et al (1979)
Clean Sands (FC=0-5%)	0.35									Cubrinovski and Ishiara (2002)
Erksak Sand	0.36				0.96	0.53				Jefferies and Been (2006), Golder Project Files
Sands with Fines (5<FC<15%)	0.36									Cubrinovski and Ishiara (2002)
Sandboil Sand	0.36	2.4			0.79	0.51				Santamarina and Cho (2001)

Sample	D_{50}	C_u	R	S	e_{max}	e_{min}	Φ_{cs}	Γ_1	λ_{10}	References
Sandboil Sand	0.36	2.4	0.55	0.7	0.79	0.51				Zheng and Hryciw (2016), Cho et al. (2006)
Rincon, New Mexico	0.36	3	0.55	0.82	0.8	0.51				Zheng and Hryciw (2016)
Kogyuk Sand	0.36	2			0.87	0.49				Been and Jefferies (1985)
Niigata LD4-S2	0.36	2.7			1.02	0.65				Ishiara et al (1978)
Osterberg B3-S6	0.36	1.5			1.07	0.62				Ishiara et al (1979)
Osterberg B3-S3	0.36	1.5			1.08	0.57				Ishiara et al (1979)
Bennett Silty Sand b	0.37				0.52	0.33				Jefferies and Been (2006), Golder Project Files
Leighton Buzzard	0.37	1.5			0.82	0.49				Mayne and Kulhawy (1991), Chong (1988)
Monterey 0	0.37	1.6	0.35	0.8	0.82	0.54				Mayne and Kulhawy (1991), Huntsman et al. (1986)
Monterey Sand	0.37				0.82	0.54				Jefferies and Been (2006), Golder Project Files
Niigata LD4-S3	0.37	2.5			1.07	0.62				Ishiara et al (1978)
Ottowa Sand	0.37	1.4			0.76	0.40				Youd (1973)
Crushed Basalt	0.38	1.4			1.3	0.68				Youd (1973)
Del Monte white Sand	0.38	1.4			0.95	0.50				Youd (1973)
P1-S2	0.38	2.2	0.61		0.67	0.42				Zheng and Hryciw (2016), Bareither et al. (2008)
Sand O	0.38	1.8	0.41	0.93	0.81	0.50				Zheng and Hryciw (2016),

Sample	D_{50}	C_u	R	S	e_{max}	e_{min}	Φ_{cs}	Γ_1	λ_{10}	References
										Guo and Su (2007)
8M8 Crushed Sand	0.38	3.3	0.2	0.7	0.97					Zheng and Hryciw (2016), Cho et al. (2006)
Osterberg B3-S3/2	0.38	1.6			1.06	0.57				Ishiara et al (1979)
Clean Sands (FC=0-5%)	0.39									Cubrinovski and Ishiara (2002)
Sands with Fines (5<FC<15%)	0.39									Cubrinovski and Ishiara (2002)
Ottawa Sand	0.39	1.6			0.78	0.48				Cubrinovski and Ishiara (2002), Salgado et al. (2000)
Lone Star 30	0.39	1.9			0.82	0.54				Mayne and Kulhawy (1991), Villet and Mitchell (1981)
Ottawa Sand C-109	0.39	2			0.83	0.50				Cubrinovski and Ishiara (2002), Pitman et al. (1994)
Hokksund	0.39	2.2			0.88	0.54				Mayne and Kulhawy (1991), Baldi et al. (1981)
Hokksund Sand	0.39	2.1			0.89	0.55				Huang Report (1991), Borden (1991)
Hokksund	0.39				0.91	0.55				Jefferies and Been (2006), Golder Project Files
Osterberg B1-S7	0.39	1.7			0.93	0.51				Ishiara et al (1979)
Osterberg O-1	0.39	3.3			1.05	0.62				Ishiara and Koga (1981)
Niigata Road Site D=13.8 m	0.39	1.8			1.07	0.58				Skempton (1986)

Sample	D_{50}	C_u	R	S	e_{max}	e_{min}	Φ_{cs}	Γ_1	λ_{10}	References
Osterberg B3-S8	0.39	1.8			1.07	0.58				Ishiara et al (1979)
Clean Sands (FC=0-5%)	0.39									Cubrinovski and Ishiara (2002)
Lanchester 25/52	0.4	1.4			0.82	0.56				Mayne and Kulhawy (1991), Thomas (1968)
Karlsruhe Sand	0.4	1.9	0.45		0.84	0.53				Zheng and Hryciw (2016), Herle and Gudehus (1999)
Muskegon, Michigan	0.4	1.6	0.55	0.74	0.84	0.56				Zheng and Hryciw (2016)
5Z9 Crushed Sand	0.4	3.6	0.3	0.9	0.89					Zheng and Hryciw (2016), Cho et al. (2006)
Osterberg B1-S3	0.4	2.1			1	0.61				Ishiara et al (1979)
Osterberg B1-S4	0.4	1.6			1.01	0.62				Ishiara et al (1979)
Osterberg LD3-S10/2	0.4	2			1.02	0.62				Ishiara et al (1979)
Clean Sands (FC=0-5%)	0.4									Cubrinovski and Ishiara (2002)
Bennett Silty Sand c	0.41				0.51	0.34				Jefferies and Been (2006), Golder Project Files
Osterberg LD3-S10	0.41	1.8			1.02	0.55				Ishiara et al (1979)
Clean Sands (FC=0-5%)	0.42									Cubrinovski and Ishiara (2002)
P2-S12	0.42	3.1	0.42		0.64	0.39				Zheng and Hryciw (2016), Bareither et al. (2008)
Ottawa 35–45	0.42	1.2	0.6	0.9	0.82	0.48				Zheng and Hryciw (2016), Zelasko et al. (1975)

Sample	D_{50}	C_u	R	S	e_{max}	e_{min}	Φ_{cs}	Γ_1	λ_{10}	References
Evanston Beach 35–45	0.42	1.2	0.43	0.73	0.9	0.52				Zheng and Hryciw (2016), Zelasko et al. (1975)
Franklin Falls 35–45	0.42	1.2	0.35	0.52	1.04	0.63				Zheng and Hryciw (2016), Zelasko et al. (1975)
Osterberg O-2	0.42	2.1			1.05	0.64				Ishiara and Koga (1981)
Kawagishi-cho S-2	0.42	2			1.08	0.65				Ishiara and Koga (1981)
Clean Sands (FC=0-5%)	0.42									Cubrinovski and Ishiara (2002)
Gravelly Sands (FC<6 %)	0.42									Cubrinovski and Ishiara (2002)
Sands with Fines (5<FC<15%)	0.42									Cubrinovski and Ishiara (2002)
Hormuz Island	0.43	3.2	0.2	0.5	1.05	0.72				Zheng and Hryciw (2016), Shahnazari and Rezvai (2013)
Clean Sands (FC=0-5%)	0.43									Cubrinovski and Ishiara (2002)
P1-S5	0.44	2.6	0.62		0.76	0.43				Zheng and Hryciw (2016), Bareither et al. (2008)
Fort Davis, Texas	0.44	8.6	0.41	0.68	0.85	0.51				Zheng and Hryciw (2016)
Hokksund	0.44	2.2			0.91	0.54				Mayne and Kulhawy (1991), Lunne and Christoffersen (1985) & Parkin et al. (1980)
Clean Sands (FC=0-5%)	0.45									Cubrinovski and Ishiara (2002)

Sample	D_{50}	C_u	R	S	e_{max}	e_{min}	Φ_{cs}	Γ_1	λ_{10}	References
Monterey 0/30	0.45	1.4			0.8	0.56				Mayne and Kulhawy (1991), Sweenay (1987)
Edgar	0.45	1.8			0.92	0.54				Mayne and Kulhawy (1991), Veismanis (1974) & Holden (1976)
Niigata River Site D=7.5 m	0.45	2.1			0.97	0.55				Skempton (1986)
Niigata LD4-S7	0.45	2.1			0.97	0.55				Ishiara et al (1978)
Niigata Road Site/2	0.45	1.8			1.03	0.56				Skempton (1986)
Osterberg B3-S8/2	0.45	1.9			1.05	0.56				Ishiara et al (1979)
Leighton Buzzard 30%Mica	0.45				1.79	0.82				Jefferies and Been (2006), Hird and Hassona (1990)
Niigata River Site D=7.5 m/2	0.46	2			1.02	0.54				Skempton (1986)
Niigata, River Site	0.46	2			1.02	0.57				Skempton (1986)
Osterberg B1-S6	0.46	1.9			1.05	0.54				Ishiara et al (1979)
Niigata LD3-S4	0.46	2			1.06	0.53				Ishiara et al (1978)
Niigata River Site D=6.5 m	0.46	2			1.06	0.53				Skempton (1986)
Osterberg O-3	0.47	2.1			1.02	0.62				Ishiara and Koga (1981)
Hoston Sand	0.47	1.4	0.3	0.6	1.04	0.64				Zheng and Hryciw (2016), Ezaoui and Benedetto (2009)
Leighton Buzzard 17%Mica	0.47				1.32	0.62				Jefferies and Been (2006),

Sample	D_{50}	C_u	R	S	e_{max}	e_{min}	Φ_{cs}	Γ_1	λ_{10}	References
										Hird and Hassona (1990)
P3-S5	0.48	3	0.56		0.62	0.38				Zheng and Hryciw (2016), Bareither et al. (2008)
P3-S2	0.48	4.8	0.48		0.7	0.39				Zheng and Hryciw (2016), Bareither et al. (2008)
P4-S2	0.48	2.9	0.31		0.72	0.44				Zheng and Hryciw (2016), Bareither et al. (2008)
2Z8 Crushed Sand	0.48	5	0.1	0.6	0.86					Zheng and Hryciw (2016), Cho et al. (2006)
Osterberg B3-S7	0.48	1.7			0.99	0.55				Ishiara et al (1979)
Niigata Road Site D=12.8 m	0.48	1.7			0.99	0.55				Skempton (1986)
Osterberg B3-S7/2	0.48	1.8			1.01	0.56				Ishiara et al (1979)
Niigata Road Site D=12.8 m/2	0.48	1.8			1.01	0.56				Skempton (1986)
Margaret River Sand	0.49	1.9	0.7	0.7	0.87					Zheng and Hryciw (2016), Cho et al. (2006)
Gravelly Sands (FC<6 %)	0.5									Cubrinovski and Ishiara (2002)
P2-S9	0.5	4.2	0.43		0.56	0.33				Zheng and Hryciw (2016), Bareither et al. (2008)
P2-S8	0.5	3.1	0.37		0.64	0.40				Zheng and Hryciw (2016), Bareither et al. (2008)

Sample	D_{50}	C_u	R	S	e_{max}	e_{min}	Φ_{cs}	Γ_1	λ_{10}	References
Density Sand	0.5	1.9	0.8	0.9	0.72	0.48				Zheng and Hryciw (2016), Baxter and Mitchell (2004)
Leighton Buzzard	0.5				0.79	0.52				Jefferies and Been (2006), Hird and Hassona (1990)
Michigan 2NS	0.5	2.3	0.53	0.67	0.82	0.54				Zheng and Hryciw (2016)
Zbraslav Sand	0.5	2.6	0.3		0.82	0.52				Zheng and Hryciw (2016), Herle and Gudehus (1999)
Ticino	0.5	1.6	0.38	0.79	0.92	0.57				Mayne and Kulhawy (1991), Baldi et al. (1981), Baldi et al. (1986), Bellotti et al. (1979) & Canou et al. (1988)
Teesta Sand	0.5	2.5	0.4	0.65	0.92	0.57				Zheng and Hryciw (2016), Yasin and Safiullah (2003)
Leighton Buzzard 10%Mica	0.5				1.07	0.59				Jefferies and Been (2006), Hird and Hassona (1990)
9C1 Crushed Sand	0.52	2.3	0.25	0.7	0.91					Zheng and Hryciw (2016), Cho et al. (2006)
Osterberg O-5	0.52	2.1			1.05	0.65				Ishiara and Koga (1981)
Ottawa #20/70 Sand	0.53	2.4	0.32	0.81	0.78	0.47				Zheng and Hryciw (2016), Sukumaran and Ashmawy (2001)
Ottawa	0.53				0.79	0.49				Jefferies and Been (2006),

Sample	D_{50}	C_u	R	S	e_{max}	e_{min}	Φ_{cs}	Γ_1	λ_{10}	References
										Golder Project Files
Ticino-4	0.53				0.89	0.60				Jefferies and Been (2006), Golder Project Files
Ticino-9	0.53									Jefferies and Been (2006), Golder Project Files
Ticino Sand	0.53	1.6			0.93	0.58				Borden (1991)
Ticino-8	0.53									Jefferies and Been (2006), Golder Project Files
P3-S3	0.54	2.5	0.59		0.64	0.37				Zheng and Hryciw (2016), Bareither et al. (2008)
Clean Sands (FC=0-5%)	0.55									Cubrinovski and Ishiara (2002)
Gravelly Sands (FC<6 %)	0.55									Cubrinovski and Ishiara (2002)
Niigata LD2-S7	0.55	2.7			0.99	0.55				Ishiara et al (1978)
Niigata River Site D=8.5 m	0.55	2.7			0.99	0.55				Skempton (1986)
Clean Sands (FC=0-5%)	0.56									Cubrinovski and Ishiara (2002)
Osterberg B1-S7/2	0.57	2.1			0.94	0.60				Ishiara et al (1979)
Ottawa #45 Sand	0.57	2.1	0.24	0.68	1.11	0.75				Zheng and Hryciw (2016), Sukumaran and Ashmawy (2001)
P4-S1	0.58	2	0.42		0.84	0.56				Zheng and Hryciw (2016), Bareither et al. (2008)

Sample	D_{50}	C_u	R	S	e_{max}	e_{min}	Φ_{cs}	Γ_1	λ_{10}	References
Michigan 30A	0.58	7	0.15	0.69	0.92	0.55				Zheng and Hryciw (2016)
Ticino Sand	0.58	1.4			0.94	0.57				Santamarina and Cho (2001)
Ticino Sand	0.58	1.5	0.4	0.8	0.99	0.57				Zheng and Hryciw (2016), Cho et al. (2006)
Daedalus Sand	0.6	4.7	0.75	0.9	0.61	0.36				Zheng and Hryciw (2016), Thomann (1990)
ASTM 20/30 Sand	0.6	1.4	0.8	0.9	0.69					Zheng and Hryciw (2016), Cho et al. (2006)
Hawaiian Sand	0.6	1.5	0.6	0.75	0.86	0.52				Zheng and Hryciw (2016), Roberts (1964)
Brady, Texas	0.61	1.4	0.68	0.76	0.84	0.57				Zheng and Hryciw (2016)
P3-S1	0.63	3.2	0.5		0.58	0.35				Zheng and Hryciw (2016), Bareither et al. (2008)
Niigata River Site D=9.5 m/2	0.63	2.8			0.99	0.51				Skempton (1986)
Osterberg B3-S1	0.63	2.2			1.07	0.66				Ishiara et al (1979)
P2-S5	0.64	2.8	0.33		0.69	0.44				Zheng and Hryciw (2016), Bareither et al. (2008)
Chesterton, Indiana Beach	0.64	2.9	0.64	0.66	0.85	0.54				Zheng and Hryciw (2016)
Osterberg B1-S6/2	0.65	3			0.93	0.49				Ishiara et al (1979)
Niigata Road Site D=13.8 m/2	0.65	1.9			1.05	0.56				Skempton (1986)
Clean Sands (FC=0-5%)	0.66									Cubrinovski and Ishiara (2002)

Sample	D_{50}	C_u	R	S	e_{max}	e_{min}	Φ_{cs}	Γ_1	λ_{10}	References
Gravelly Sands (FC<6 %)	0.66									Cubrinovski and Ishiara (2002)
Niigata LD2-S10	0.68	3			1.02	0.54				Ishiara et al (1978)
Gravelly Sands (FC<6 %)	0.68									Cubrinovski and Ishiara (2002)
P5-S1	0.69	5.3	0.38		0.55	0.31				Zheng and Hryciw (2016), Bareither et al. (2008)
Cape Fear Sand	0.69	2.8			0.8	0.53				Borden (1991)
P3-S4	0.7	2.9	0.52		0.6	0.37				Zheng and Hryciw (2016), Bareither et al. (2008)
Small glass Beads	0.7	1.1	1	1	0.75	0.50				Zheng and Hryciw (2016)
Niigata LD2-S8	0.7	3			1	0.48				Ishiara et al (1978)
Niigata River Site D=9.5 m	0.7	3			1	0.48				Skempton (1986)
Ottawa 20–30	0.71	1.4	0.75	0.82	0.74	0.49				Zheng and Hryciw (2016)
Blasting Sand	0.71	1.9			1.03	0.70				Santamarina and Cho (2001)
Blasting Sand	0.71	1.9	0.3	0.55	1.03	0.70				Zheng and Hryciw (2016), Cho et al. (2006)
Gravelly Sands (FC<6 %)	0.72									Cubrinovski and Ishiara (2002)
Trakya	0.72	6.3	0.35	0.65	0.7	0.49				Zheng and Hryciw (2016), Cabalar et al. (2013)
Ottawa #20/30 Sand	0.72	1.2	0.9	0.9	0.74	0.50				Zheng and Hryciw (2016), Cho et al. (2006)

Sample	D_{50}	C_u	R	S	e_{max}	e_{min}	Φ_{cs}	Γ_1	λ_{10}	References
Ottawa Sand	0.72	1.4	0.8	0.9	0.74	0.50				Zheng and Hryciw (2016), Georgiannou and Konstadinou (2013)
Ottawa 20–30	0.72	1.2			0.74	0.50				Santamarina and Cho (2001)
Ottawa 20–30	0.72	1.2	0.65	0.87	0.78	0.46				Zheng and Hryciw (2016), Zelasko et al. (1975)
Evanston Beach 20–30	0.72	1.2	0.44	0.71	0.92	0.55				Zheng and Hryciw (2016), Zelasko et al. (1975)
Franklin Falls 20–30	0.72	1.2	0.36	0.52	1.08	0.62				Zheng and Hryciw (2016), Zelasko et al. (1975)
West Kowloon Sand	0.73				0.69	0.44				Jefferies and Been (2006), Golder Project Files
Gravelly Sands (FC<6 %)	0.73									Cubrinovski and Ishiara (2002)
Sands with Fines (5<FC<15%)	0.73									Cubrinovski and Ishiara (2002)
Ottawa 20–30	0.74	1.1	0.78	0.9	0.74	0.51				Zheng and Hryciw (2016), DeJong and Christoph (2009)
Griffin, Indiana	0.74	4.3	0.6	0.69	0.79	0.51				Zheng and Hryciw (2016)
Ottawa 20–30	0.75	1.2	0.75	0.9	0.72	0.51				Zheng and Hryciw (2016), Thomann (1990)

Sample	D_{50}	C_u	R	S	e_{max}	e_{min}	Φ_{cs}	Γ_1	λ_{10}	References
Clean Sand	0.75	3.8	0.4	0.68	0.9	0.48				Zheng and Hryciw (2016), Kumar and Madhusudhan (2012)
Q-Rok	0.75	1.5	0.2	0.5	1.14	0.70				Zheng and Hryciw (2016), DeJong and Christoph (2009)
Ottowa Sand	0.75	1.4			0.69	0.39				Youd (1973)
Monterey Sand	0.75	1.4			0.77	0.44				Youd (1973)
Crushed Basalt	0.75	1.4			1.24	0.69				Youd (1973)
Abraded Leighton Buzzard	0.76	1.3	0.75	0.8	0.8	0.51				Zheng and Hryciw (2016), Lings and Dietz (2004)
P4-S3	0.77	6.5	0.35		0.62	0.33				Zheng and Hryciw (2016), Bareither et al. (2008)
Bushehr Port	0.78	4.5	0.35	0.6	0.91	0.63				Zheng and Hryciw (2016), Shahnazari and Rezvai (2013)
Crushed gabbro	0.8	5.5	0.23	0.56	0.96	0.60				Zheng and Hryciw (2016)
Clean Sands (FC=0-5%)	0.82									Cubrinovski and Ishiara (2002)
Gravelly Sands (FC<6 %)	0.85									Cubrinovski and Ishiara (2002)
Gravelly Sands (FC<6 %)	0.85									Cubrinovski and Ishiara (2002)
Leighton Buzzard	0.85	1.3			0.79	0.49				Mayne and Kulhawy (1991), Houlsby and

Sample	D_{50}	C_u	R	S	e_{max}	e_{min}	Φ_{cs}	Γ_1	λ_{10}	References
										Hitchman (1988)
Birecik	0.86	3.3	0.65	0.72	0.8	0.55				Zheng and Hryciw (2016), Cabalar et al. (2013)
Leighton Buzzard	0.86	1.2	0.5	0.82	0.82	0.54				Zheng and Hryciw (2016), Sladen et al. (1985)
Gravelly Sands (FC<6 %)	0.91									Cubrinovski and Ishiara (2002)
Gravelly Sands (FC<6 %)	0.95									Cubrinovski and Ishiara (2002)
Gravelly Sands (FC<6 %)	0.96									Cubrinovski and Ishiara (2002)
Large glass Beads	0.97	1.1	1	1	0.74	0.50				Zheng and Hryciw (2016)
Chek Lap Kok	1				0.68	0.41				Jefferies and Been (2006), Golder Project Files
Lone Star 2	1	2			0.77	0.48				Mayne and Kulhawy (1991), Villet and Mitchell (1981)
Narli	1	3.7	0.75	0.65	0.83	0.52				Zheng and Hryciw (2016), Cabalar et al. (2013)
Gravels	1.06									Cubrinovski and Ishiara (2002)
G25 Gravel	1.13	5.7			0.57	0.33				Kokusho and Yoshida (1997)
Crushed stone Sand	1.4	2.5	0.45	0.61	0.93	0.62				Zheng and Hryciw (2016), Cabalar et al. (2013)

Sample	D_{50}	C_u	R	S	e_{max}	e_{min}	Φ_{cs}	Γ_1	λ_{10}	References
Monterey Sand	1.5	1.4			0.75	0.45				Youd (1973)
Cambria Sand	1.5	1.3			0.77	0.54				Cubrinovski and Ishiara (2002), Lade et al. (1998)
Long-grain rice	1.51	1.1	0.62	0.4	1.08	0.85				Zheng and Hryciw (2016)
Crushed Basalt	1.52	1.4			1.23	0.70				Youd (1973)
Sand L	1.64	2	0.14	0.57	1.2	0.62				Zheng and Hryciw (2016), Guo and Su (2007)
Fused aluminum oxide	1.8	1.6	0.3	0.69	0.92	0.63				Zheng and Hryciw (2016)
Short-grain rice	1.91	1.1	0.54	0.55	0.97	0.65				Zheng and Hryciw (2016)
Gravels	2.15									Cubrinovski and Ishiara (2002)
G50 Gravel	2.28	11			0.43	0.24				Kokusho and Yoshida (1997)
Lapis Lustre Sand	3.02	1.4			0.73	0.44				Youd (1973)
Crushed Basalt	3.02	1.4			1.16	0.68				Youd (1973)
Gravels	3.47									Cubrinovski and Ishiara (2002)
Gravels	3.47									Cubrinovski and Ishiara (2002)
P2-S11	3.5	3.4	0.52		0.43	0.26				Zheng and Hryciw (2016), Bareither et al. (2008)
Gravels	3.53									Cubrinovski and Ishiara (2002)
Gravels	4.9									Cubrinovski and Ishiara (2002)
Gravels	5.89									Cubrinovski and Ishiara (2002)

Sample	D_{50}	C_u	R	S	e_{max}	e_{min}	Φ_{cs}	Γ_1	λ_{10}	References
Gravels	6									Cubrinovski and Ishiara (2002)
Gravels	6.45									Cubrinovski and Ishiara (2002)
Gravels	7.07									Cubrinovski and Ishiara (2002)
Gravels	7.2									Cubrinovski and Ishiara (2002)
G75 Gravel	7.3	31			0.35	0.18				Kokusho and Yoshida (1997)
Gravels	7.6									Cubrinovski and Ishiara (2002)
Gravels	8.03									Cubrinovski and Ishiara (2002)
Gravels	8.48									Cubrinovski and Ishiara (2002)
Gravels	9.13									Cubrinovski and Ishiara (2002)
Gravels	9.13									Cubrinovski and Ishiara (2002)
Gravels	10.2									Cubrinovski and Ishiara (2002)
Gravels	10.6									Cubrinovski and Ishiara (2002)
Gravels	12.2									Cubrinovski and Ishiara (2002)
Gravels	12.5									Cubrinovski and Ishiara (2002)
Gravels	12.5									Cubrinovski and Ishiara (2002)
Gravels	13.4									Cubrinovski and Ishiara (2002)
Gravels	14.7									Cubrinovski and Ishiara (2002)
Gravels	16.4									Cubrinovski and Ishiara (2002)
Gravels	19									Cubrinovski and Ishiara (2002)
Mix4	0.74	8	0.37		0.49	0.27				Youd (1973)
Mix3	0.74	4.3	0.37		0.58	0.30				Youd (1973)

Sample	D_{50}	C_u	R	S	e_{max}	e_{min}	Φ_{cs}	Γ_1	λ_{10}	References
Mix5	0.74	4.3	0.37		0.64	0.34				Youd (1973)
Mix2	0.74	2.5	0.35		0.69	0.37				Youd (1973)
Mix1	0.74	1.4	0.34		0.8	0.46				Youd (1973)
CB-4	0.74	8	0.19		0.8	0.44				Youd (1973)
CB-3	0.74	4.3	0.19		0.99	0.48				Youd (1973)
CB-2	0.74	2.5	0.19		1.1	0.59				Youd (1973)
CB-1	0.74	1.4	0.19		1.26	0.71				Youd (1973)
Aged Sand	0.09	1.5			1.05	0.63				Chen and Kulhawy (2014)
Aged Sand	0.11	2			1.1	0.63				Chen and Kulhawy (2014)
Aged Sand	0.13	2.1			1.03	0.60				Chen and Kulhawy (2014)
Aged Sand	0.15	2.3			0.99	0.61				Chen and Kulhawy (2014)
Quaternary Sand	0.25	1.4			1.05	0.67				Chen and Kulhawy (2014)
Quaternary Sand	0.29	1.5			1.08	0.64				Chen and Kulhawy (2014)
Quaternary Sand	0.2	1.6			1.06	0.70				Chen and Kulhawy (2014)
Quaternary Sand	0.23	1.6			0.91	0.62				Chen and Kulhawy (2014)
Quaternary Sand	0.16	1.7			1.15	0.65				Chen and Kulhawy (2014)
Quaternary Sand	0.29	1.8			1.1	0.70				Chen and Kulhawy (2014)
Quaternary Sand	0.16	1.8			1.21	0.76				Chen and Kulhawy (2014)
Quaternary Sand	0.46	1.8			1.03	0.68				Chen and Kulhawy (2014)
Quaternary Sand	0.2	1.8			1.13	0.56				Chen and Kulhawy (2014)
Quaternary Sand	0.2	2			0.84	0.57				Chen and Kulhawy (2014)
Quaternary Sand	0.46	2			1.02	0.50				Chen and Kulhawy (2014)
Quaternary Sand	0.56	2.1			1.19	0.78				Chen and Kulhawy (2014)

Sample	D_{50}	C_u	R	S	e_{max}	e_{min}	Φ_{cs}	Γ_1	λ_{10}	References
Quaternary Sand	0.16	2.2			0.94	0.65				Chen and Kulhawy (2014)
Quaternary Sand	0.18	2.2			1.13	0.75				Chen and Kulhawy (2014)
Quaternary Sand	0.2	2.4			0.94	0.65				Chen and Kulhawy (2014)
Quaternary Sand	0.28	2.4			1.11	0.53				Chen and Kulhawy (2014)
Quaternary Sand	0.3	2.5			1.15	0.76				Chen and Kulhawy (2014)
Quaternary Sand	0.63	2.8			0.99	0.51				Chen and Kulhawy (2014)
Sand Fill	0.25	1.2			0.84	0.52				Chen and Kulhawy (2014)
Sand Fill	0.32	1.7			1	0.63				Chen and Kulhawy (2014)
Sand Fill	0.21	2			1.41	0.90				Chen and Kulhawy (2014)
Sand Fill	0.21	2.1			1.15	0.72				Chen and Kulhawy (2014)
Sand Fill	0.23	2.1			1.22	0.72				Chen and Kulhawy (2014)
Sand Fill	0.3	4			1.08	0.57				Chen and Kulhawy (2014)
Tailing Sand	0.16	2.2			0.96	0.52				Chen and Kulhawy (2014)
Tailing Sand	0.17	2.5			0.99	0.46				Chen and Kulhawy (2014)
Tailing Sand	0.2	2.8			1.06	0.54				Chen and Kulhawy (2014)
Tailing Sand	0.25	3.9			1.01	0.51				Chen and Kulhawy (2014)
Volcanic Sand	0.53	3.5			1.71	1.08				Chen and Kulhawy (2014)
Volcanic Sand	0.38	11			2.38	1.45				Chen and Kulhawy (2014)
Volcanic Sand	0.45	12			1.71	0.96				Chen and Kulhawy (2014)
Volcanic Sand	0.37	14			1.59	0.96				Chen and Kulhawy (2014)

Sample	D_{50}	C_u	R	S	e_{max}	e_{min}	Φ_{cs}	Γ_1	λ_{10}	References
Quaternary Gravel	0.32	3.2			0.62	0.35				Chen and Kulhawy (2014)
Quaternary Gravel	1.67	5.1			0.54	0.28				Chen and Kulhawy (2014)
Quaternary Gravel	1.21	5.7			0.68	0.37				Chen and Kulhawy (2014)
Quaternary Gravel	1.8	8.6			0.62	0.31				Chen and Kulhawy (2014)
Quaternary Gravel	2.84	10			0.63	0.35				Chen and Kulhawy (2014)
Quaternary Gravel	4.51	12			0.53	0.29				Chen and Kulhawy (2014)
Quaternary Gravel	10.3	14			0.41	0.20				Chen and Kulhawy (2014)
Quaternary Gravel	25	14			0.7	0.42				Chen and Kulhawy (2014)
Quaternary Gravel	25	14			0.55	0.35				Chen and Kulhawy (2014)
Quaternary Gravel	7.05	15			0.59	0.43				Chen and Kulhawy (2014)
Quaternary Gravel	8.82	15			0.67	0.39				Chen and Kulhawy (2014)
Quaternary Gravel	13.8	17			0.59	0.38				Chen and Kulhawy (2014)
Quaternary Gravel	4.27	20			0.6	0.40				Chen and Kulhawy (2014)
Quaternary Gravel	3.26	20			0.48	0.22				Chen and Kulhawy (2014)
Quaternary Gravel	10.1	21			0.58	0.33				Chen and Kulhawy (2014)
Quaternary Gravel	10.6	21			0.61	0.44				Chen and Kulhawy (2014)
Quaternary Gravel	2.93	22			0.62	0.44				Chen and Kulhawy (2014)
Quaternary Gravel	17	22			0.57	0.36				Chen and Kulhawy (2014)
Quaternary Gravel	5.51	23			0.7	0.47				Chen and Kulhawy (2014)
Quaternary Gravel	11.5	25			0.6	0.40				Chen and Kulhawy (2014)

Sample	D_{50}	C_u	R	S	e_{max}	e_{min}	Φ_{cs}	Γ_1	λ_{10}	References
Quaternary Gravel	13.1	38			0.67	0.39				Chen and Kulhawy (2014)
Quaternary Gravel	11.4	40			0.54	0.30				Chen and Kulhawy (2014)
Quaternary Gravel	12	42			0.66	0.42				Chen and Kulhawy (2014)
Quaternary Gravel	11.9	44			0.6	0.38				Chen and Kulhawy (2014)
Quaternary Gravel	14.1	50			0.69	0.41				Chen and Kulhawy (2014)
Quaternary Gravel	9.45	57			0.68	0.40				Chen and Kulhawy (2014)
Quaternary Gravel	5.73	60			0.45	0.23				Chen and Kulhawy (2014)
Quaternary Gravel	14.6	64			0.43	0.22				Chen and Kulhawy (2014)
Quaternary Gravel	19.5	68			0.41	0.20				Chen and Kulhawy (2014)
Quaternary Gravel	8.75	70			0.44	0.23				Chen and Kulhawy (2014)
Quaternary Gravel	5.6	122			0.45	0.26				Chen and Kulhawy (2014)
Gravel Fill	2.09	12			0.86	0.53				Chen and Kulhawy (2014)
Gravel Fill	2.51	26			0.75	0.40				Chen and Kulhawy (2014)
Gravel Fill	2.71	29			0.78	0.46				Chen and Kulhawy (2014)
Volcanic Gravel	3.99	137			0.41	0.21				Chen and Kulhawy (2014)
Volcanic Gravel	5.14	187			0.41	0.21				Chen and Kulhawy (2014)
Volcanic Gravel	5.1	200			0.41	0.21				Chen and Kulhawy (2014)
Volcanic Gravel	16.2	262			0.41	0.21				Chen and Kulhawy (2014)
Volcanic Gravel	9.09	325			0.41	0.21				Chen and Kulhawy (2014)
Clean Ahmedabad Sand	0.38				0.68	0.42				Zuo and Baudet (2015), Dash et al. (2010)

Sample	D_{50}	C_u	R	S	e_{max}	e_{min}	Φ_{cs}	Γ_1	λ_{10}	References
Sand from Stava Tailings	0.21				1.07	0.62				Zuo and Baudet (2015), Carrera et al (2011)
F55 Foundry Sand	0.25				0.8	0.61				Zuo and Baudet (2015), Thevanayagam et al. (2002)
Hokksund Sand	0.44				0.95	0.57				Zuo and Baudet (2015), Yang et al.(2006)
Monterey no.0/30 Sand	0.43				0.82	0.63				Zuo and Baudet (2015), Polito and Martin(2001)
Clean Sand M31 from Assyros in Greece	0.3				0.84	0.58				Zuo and Baudet (2015), PapadopoulouandTika (2008)
Sxinias-Marathon Sand	0.12				1.04	0.66				Zuo and Baudet (2015), Xenaki and Athanasopoulos (2003)
Leighton Buzzard Sand	0.9				0.79	0.52				Zuo and Baudet (2015), Cabalar (2010)
Non-plastic quarry dust around Bangalore	0.04				1.63	0.65				Zuo and Baudet (2015), Dash etal.(2010)
Non-plastic Crushed silica fines	0.01				2.1	0.63				Zuo and Baudet (2015), Thevanayagam et al. (2002)
Chengbeinon-plastic silt	0.03				1.41	0.73				Zuo and Baudet (2015), Yang etal.(2006)
Fine-grained portion of Yatesville Silty Sand	0.03				1.72	0.73				Zuo and Baudet (2015), Polito andMartin(2001)

Sample	D_{50}	C_u	R	S	e_{max}	e_{min}	Φ_{cs}	Γ_1	λ_{10}	References
Non-plastic silt from Assyrosin	0.02				1.66	0.66				Zuo and Baudet (2015), Papadopoulou andTika (2008)
Sxinias-Marathon fines	0.02				1.71	0.66				Zuo and Baudet (2015), Xenaki and Athanasopoulos (2003)
Mica	0.13				3	2.20				Zuo and Baudet (2015), Cabalar (2010)
Upper Peninsula, Michigan	0.6	2.8	0.51	0.69	0.85	0.54				Zheng and Hryciw (2016)
Kızılırmak Sand	1.13	8.2			0.8	0.45				Personel Communication

B. Appendix B

Cine Sand

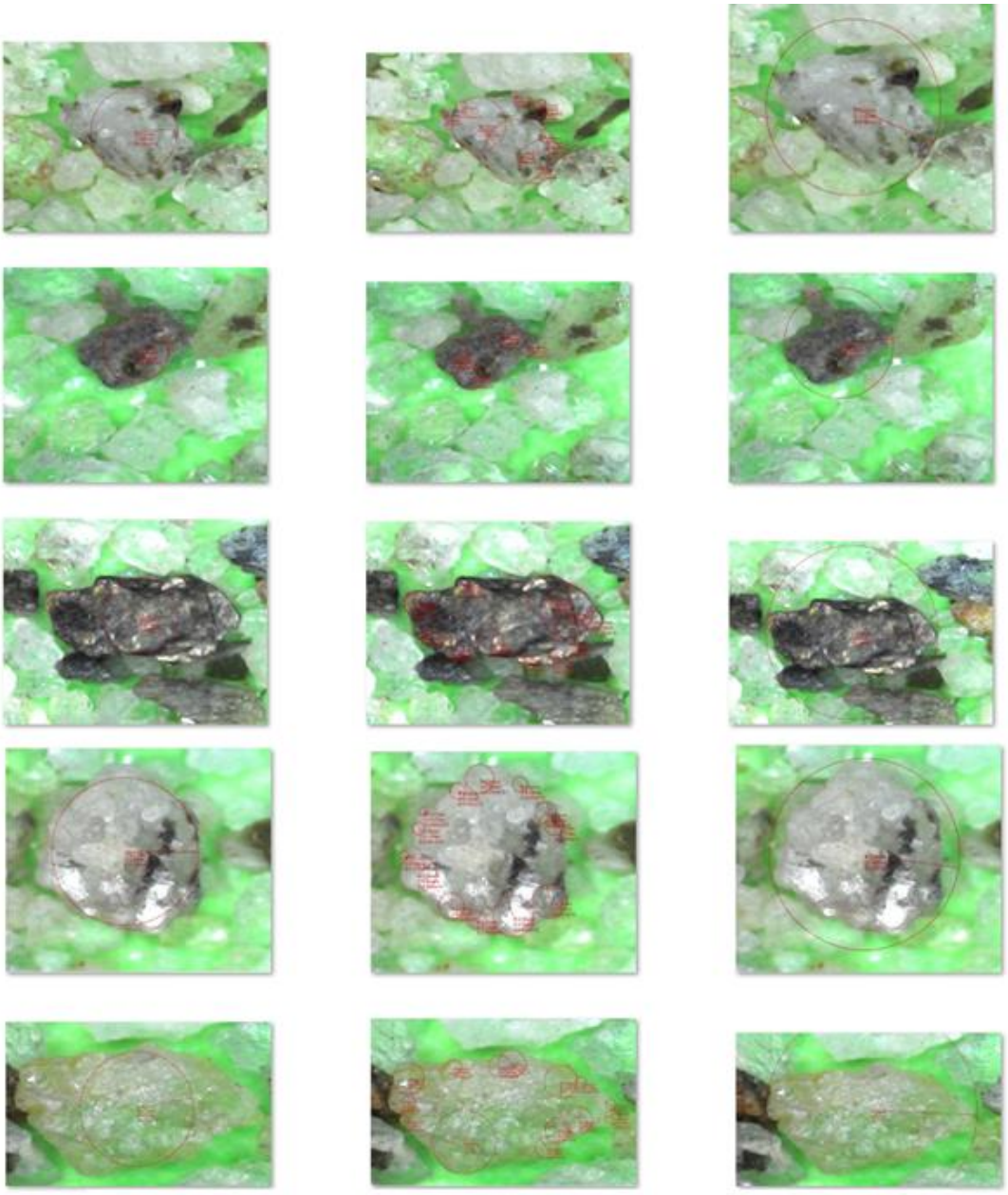

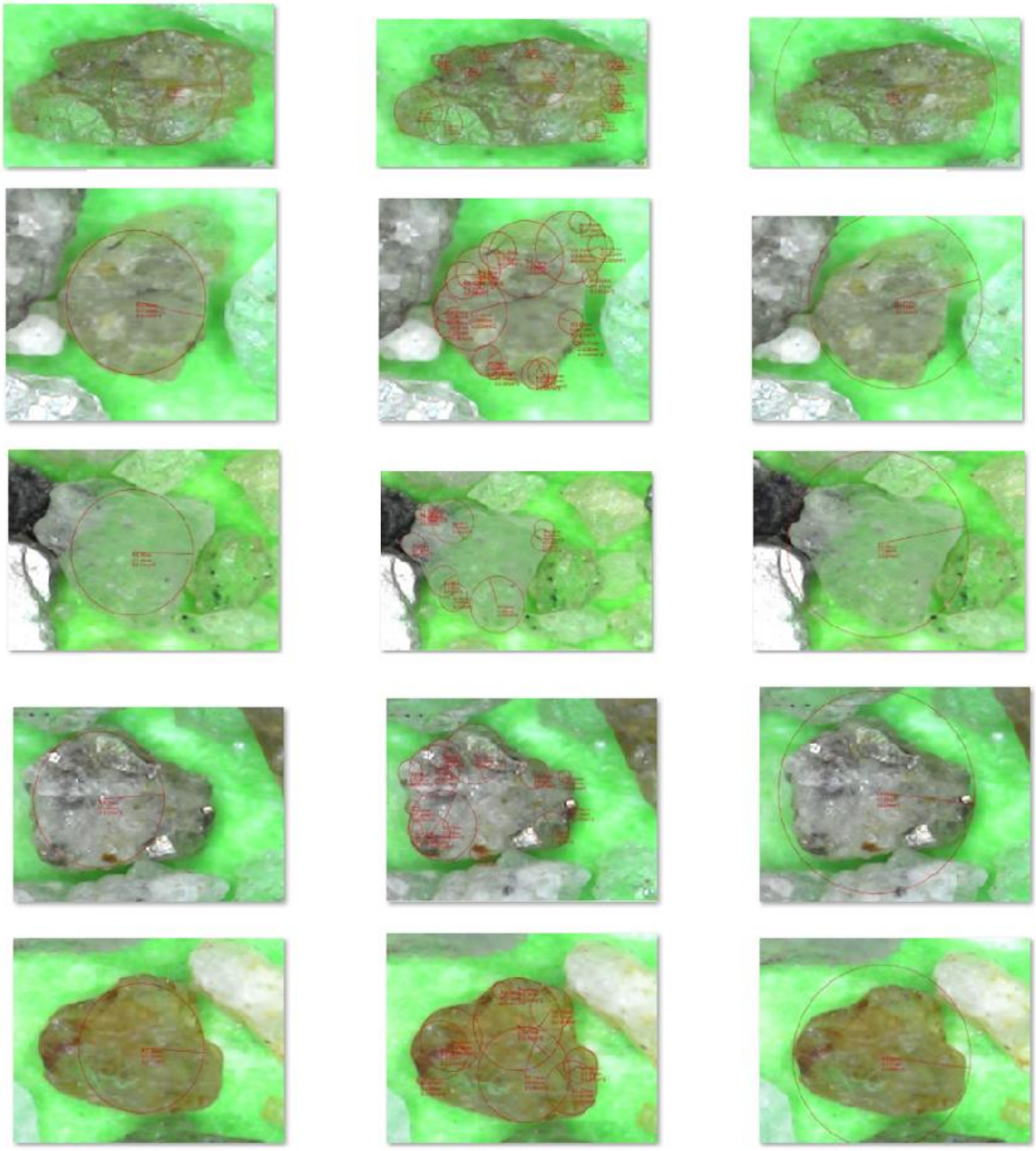

Aygaz Sand

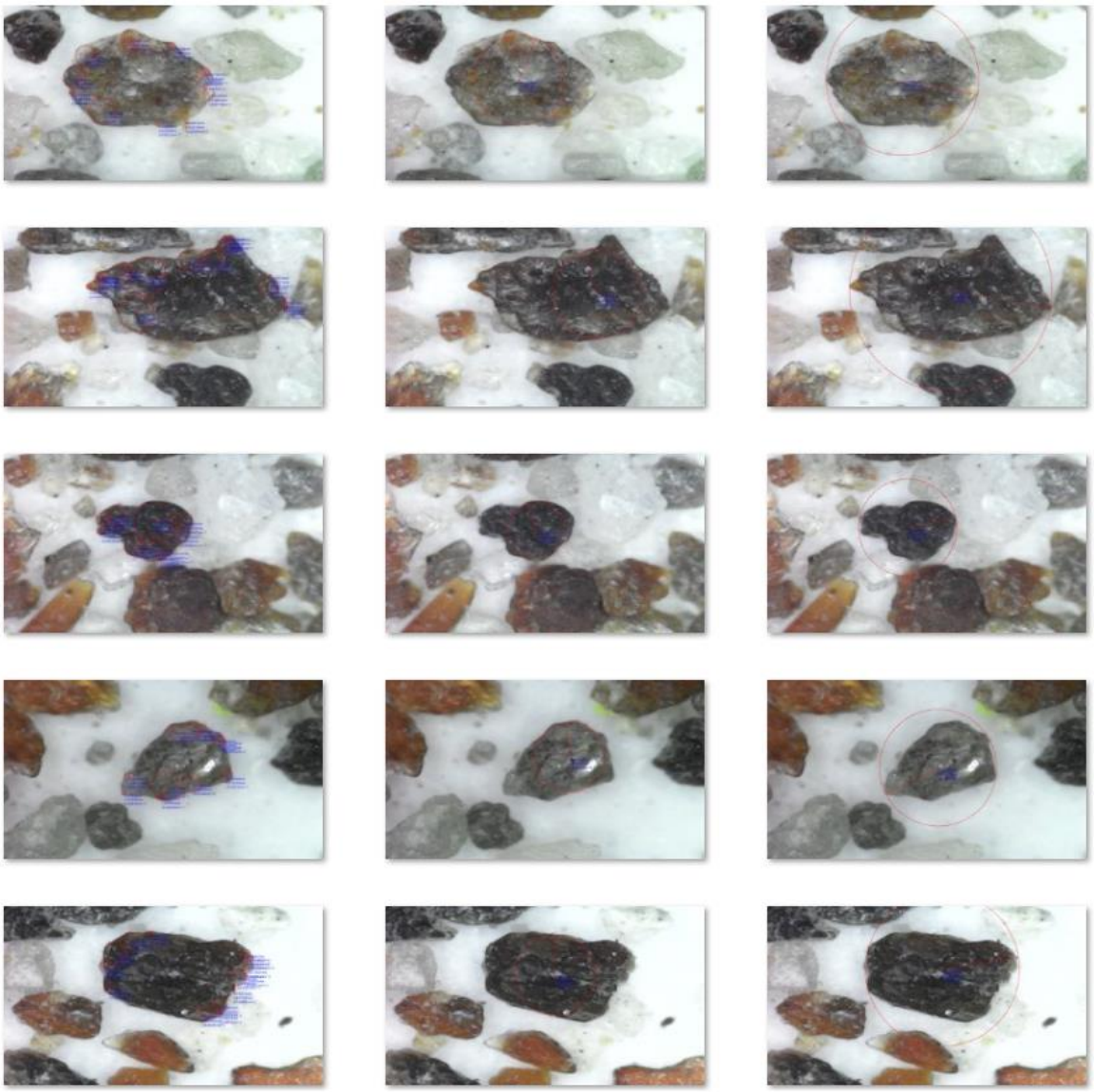

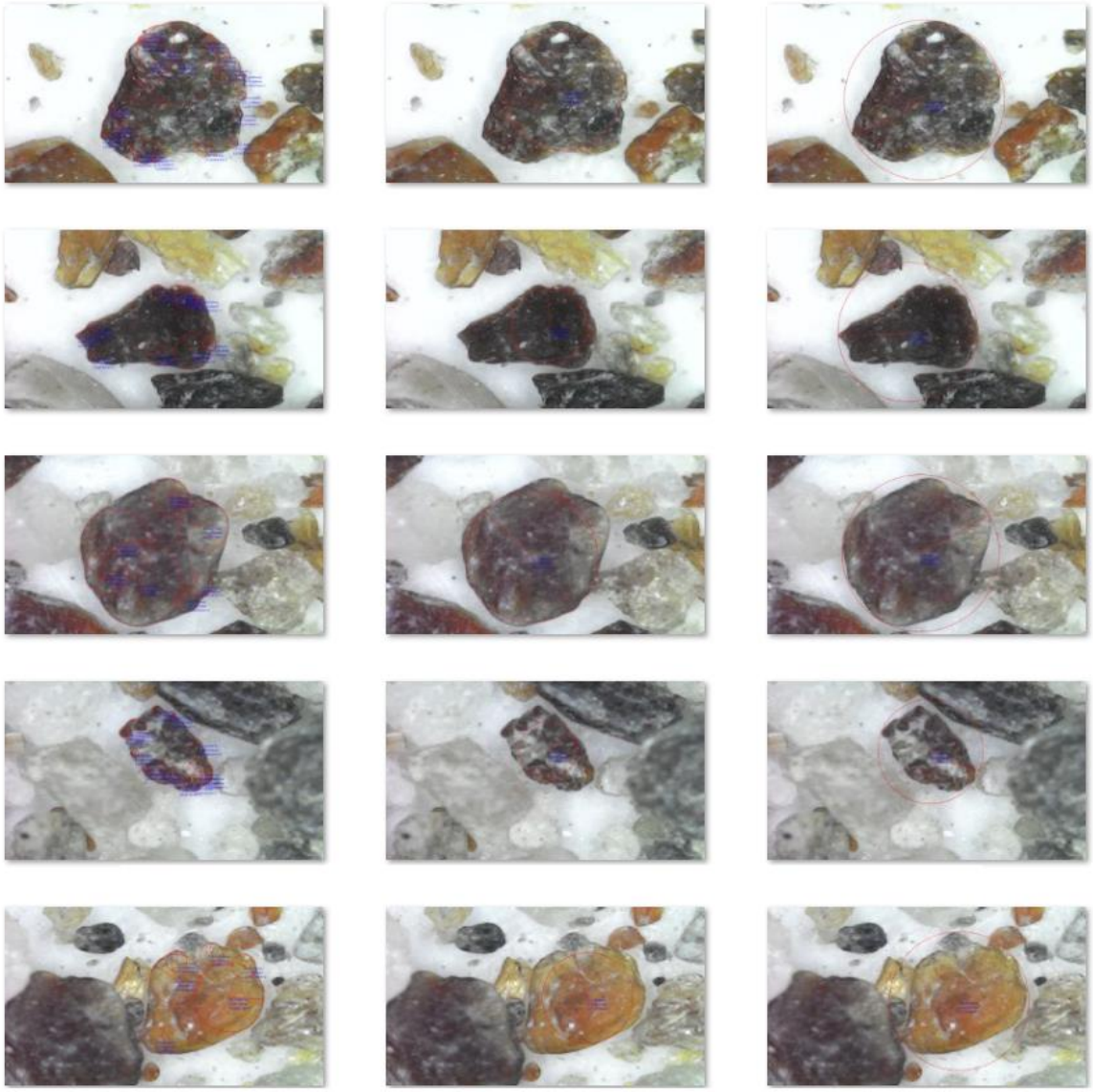

Sile Silica Sand

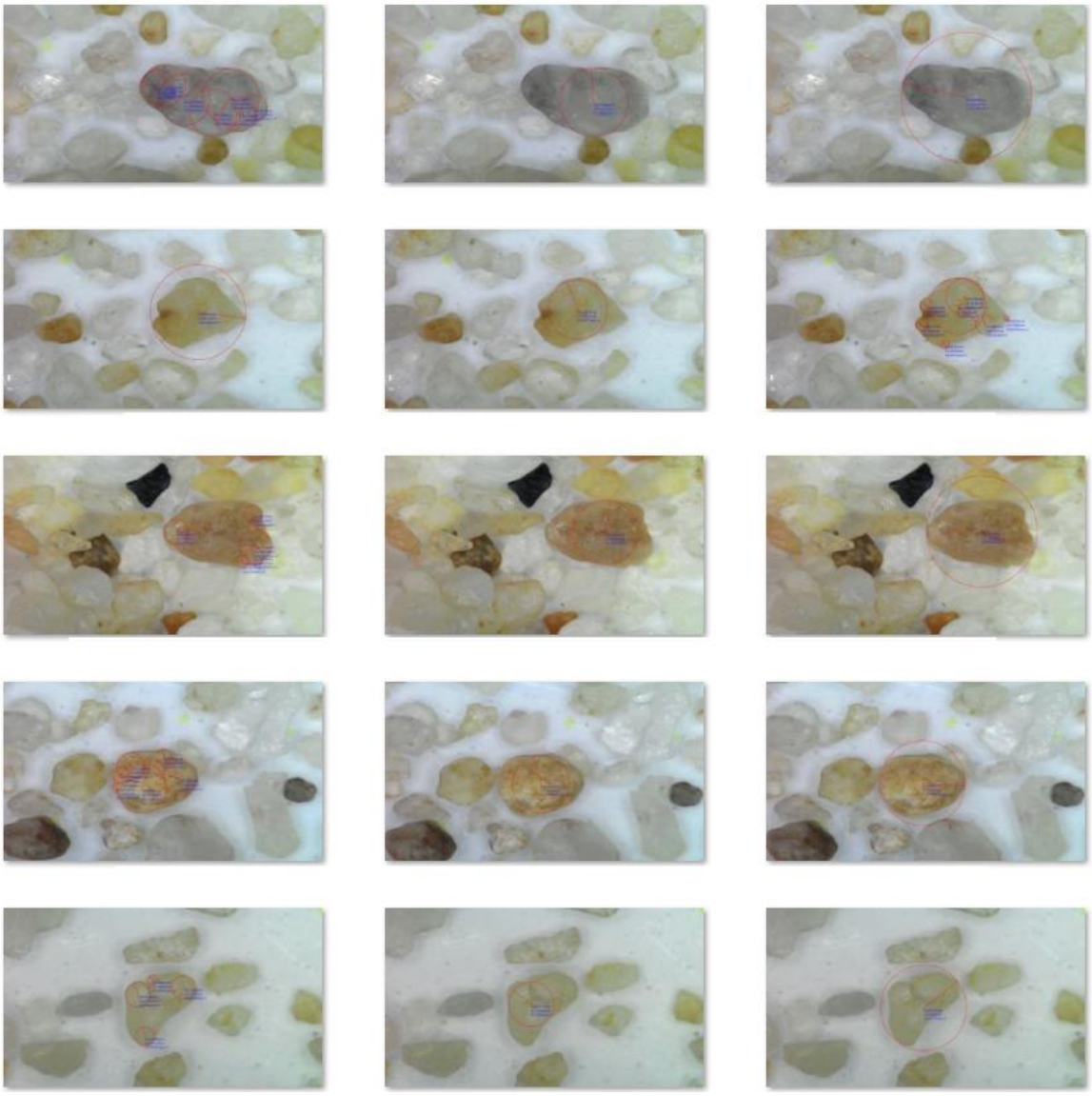

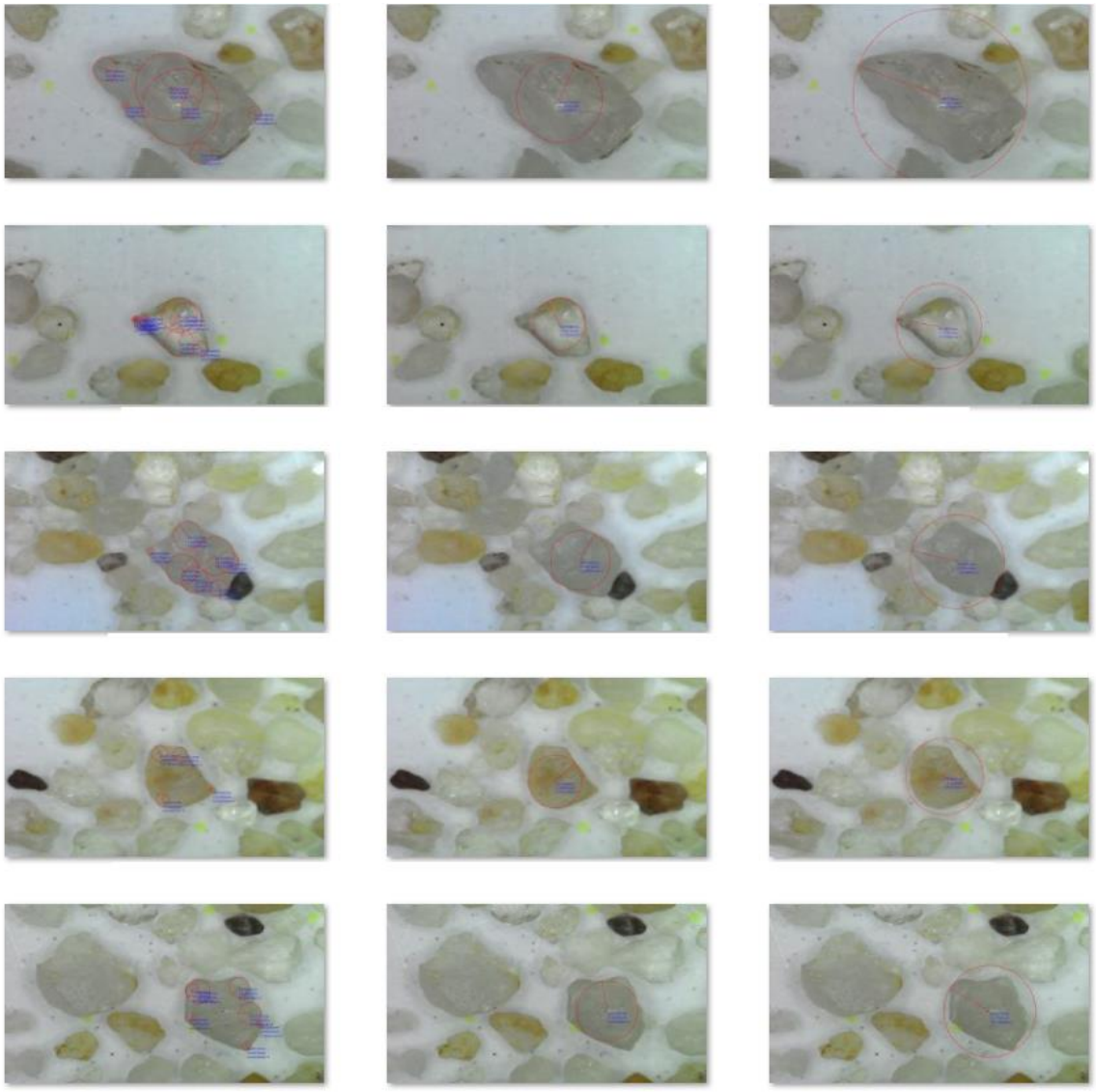

Tekirdag Silica Sand

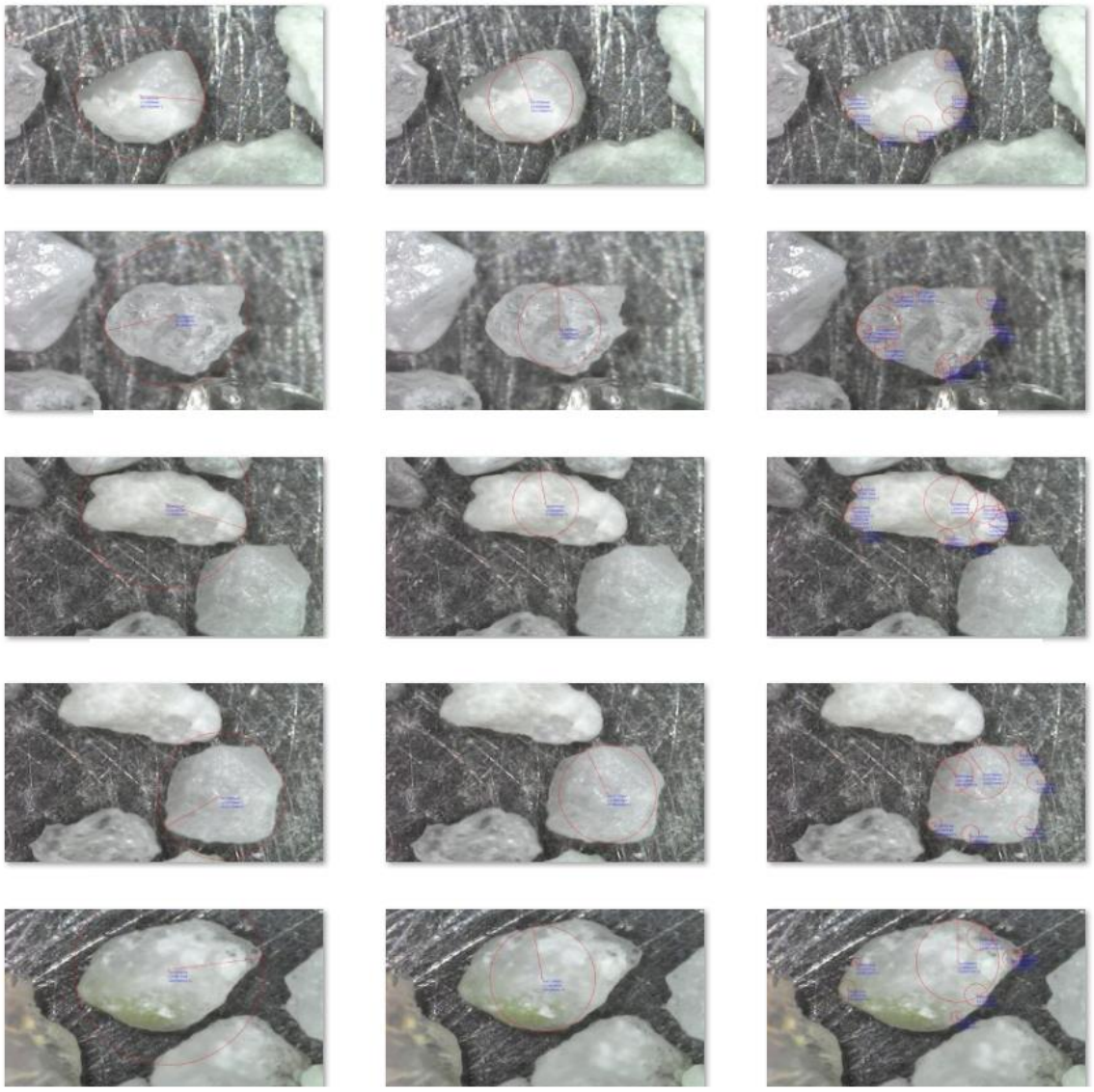

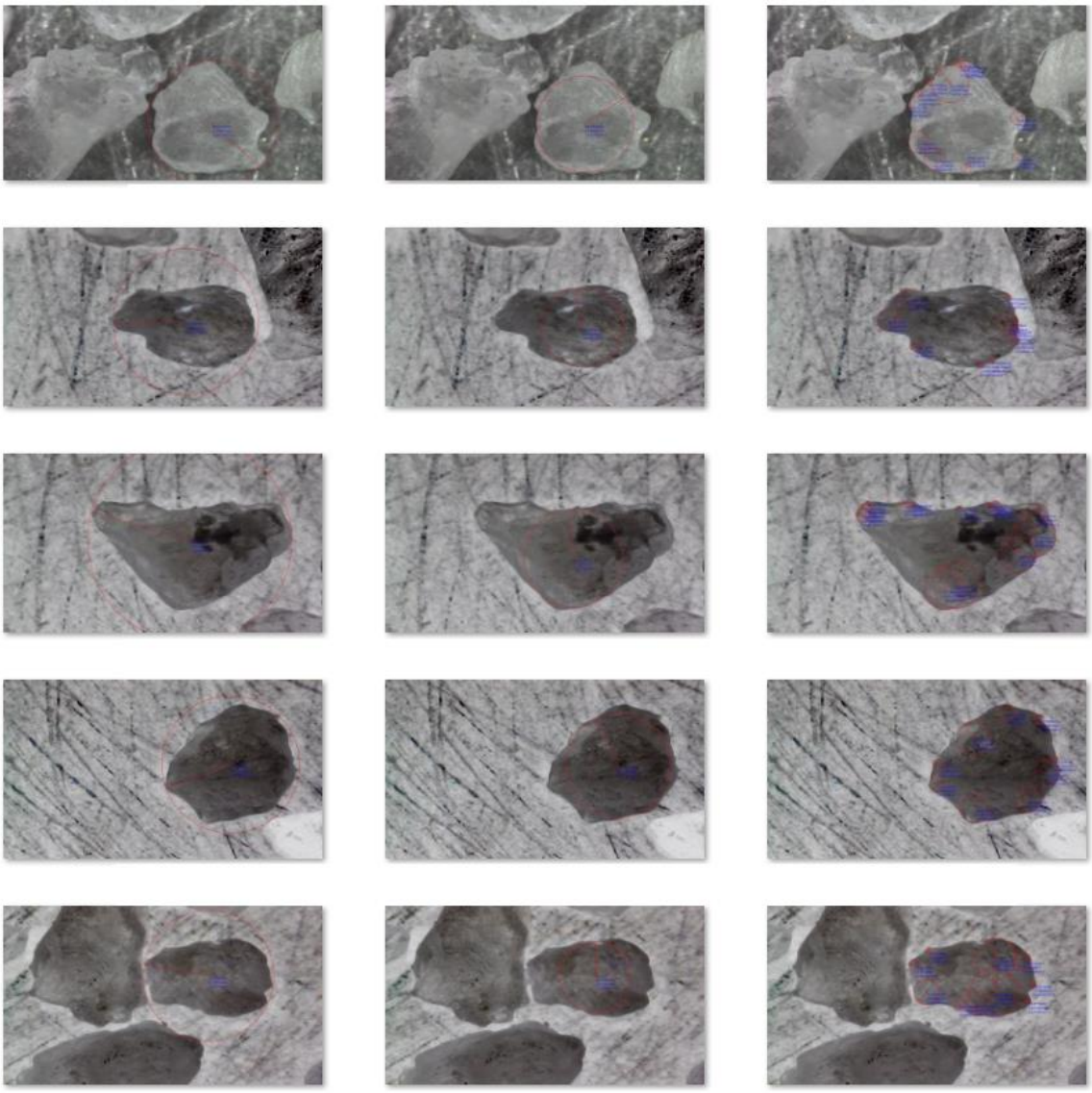

Sabratah Silt